

Doctorate Program in Molecular  
Oncology and Endocrinology  
Doctorate School in Molecular  
Medicine

XXV cycle - 2009–2012  
Coordinator: Prof. Massimo Santoro

**“Identification of targets of  
Twist1 transcription factor in  
anaplastic thyroid cancer”**

Gennaro Di Maro

Università degli Studi di Napoli Federico II  
Dipartimento di Medicina Molecolare e Biotecnologie  
Mediche

## **Administrative Location**

Università degli Studi di Napoli Federico II  
Dipartimento di Medicina Molecolare e Biotecnologie Mediche

### **Partner Institutions**

#### **Italian Institutions**

Università degli Studi di Napoli “Federico II”, Naples, Italy  
Istituto di Endocrinologia ed Oncologia Sperimentale “G. Salvatore”, CNR, Naples, Italy  
Seconda Università di Napoli, Naples, Italy  
Università degli Studi di Napoli “Parthenope”, Naples, Italy  
Università degli Studi del Sannio, Benevento, Italy  
Università degli Studi di Genova, Genova, Italy  
Università degli Studi di Padova, Padova, Italy  
Università degli Studi “Magna Graecia”, Catanzaro, Italy  
Università degli Studi di Udine, Udine, Italy

#### **Foreign Institutions**

Université Libre de Bruxelles, Bruxelles, Belgium  
Universidade Federal de Sao Paulo, Brazil  
University of Turku, Turku, Finland  
Université Paris Sud XI, Paris, France  
University of Madras, Chennai, India  
University Pavol Jozef Šafárik, Kosice, Slovakia  
Universidad Autonoma de Madrid, Centro de Investigaciones Oncologicas (CNIO), Spain  
Johns Hopkins School of Medicine, Baltimore, MD, USA  
Johns Hopkins Krieger School of Arts and Sciences, Baltimore, MD, USA  
National Institutes of Health, Bethesda, MD, USA  
Ohio State University, Columbus, OH, USA  
Albert Einstein College of Medicine of Yeshiwa University, N.Y., USA

#### **Supporting Institutions**

Dipartimento di Biologia e Patologia Cellulare e Molecolare “L. Califano”,  
Università degli Studi di Napoli “Federico II”, Naples, Italy  
Istituto di Endocrinologia ed Oncologia Sperimentale “G. Salvatore”, CNR,  
Naples, Italy  
Istituto Superiore di Oncologia, Italy

## Italian Faculty

Salvatore Maria Aloj

Francesco Saverio Ambesi

Impiombato

Francesco Beguinot

Maria Teresa Berlingieri

Bernadette Biondi

Francesca Carlomagno

Gabriella Castoria

Maria Domenica Castellone

Angela Celetti

Lorenzo Chiariotti

Annamaria Cirafici

Annamaria Colao

Sabino De Placido

Gabriella De Vita

Monica Fedele

Pietro Formisano

Alfredo Fusco

Domenico Grieco

Michele Grieco

Maddalena Illario

Paolo Laccetti

Antonio Leonardi

Paolo Emidio Macchia

Barbara Majello

Rosa Marina Melillo

Claudia Miele

Nunzia Montuori

Roberto Pacelli

Giuseppe Palumbo

Maria Giovanna Pierantoni

Rosario Pivonello

Giuseppe Portella

Maria Fiammetta Romano

Giuliana Salvatore

Massimo Santoro

Giampaolo Tortora

Donatella Tramontano

Giancarlo Troncone

Giancarlo Vecchio,

Giuseppe Viglietto

Mario Vitale

**“Identification of targets of  
Twist1 transcription factor in  
anaplastic thyroid cancer”**

## TABLE OF CONTENTS

<b>LIST OF PUBLICATIONS .....</b>	<b>4</b>
<b>ABBREVIATIONS .....</b>	<b>5</b>
<b>ABSTRACT .....</b>	<b>7</b>
<b>1. Background .....</b>	<b>8</b>
1.1 Thyroid tumors .....	8
1.1.1 Morphological and clinical characteristics of thyroid tumors .....	8
1.1.2 Genetics alterations in follicular thyroid cell derived tumors .....	11
1.2 The transcription factor Twist1 .....	16
1.2.1 Structures of the Twist1 gene and protein .....	16
1.2.2 Twist1 protein phosphorylation .....	19
1.2.3 Physiological functions of Twist1 protein .....	20
1.2.4 Role of Twist1 in human cancer .....	21
1.2.5 Mechanisms of overexpression of Twist1 in human cancer .....	22
1.2.6 Twist1 target genes .....	23
<b>2. AIM OF THE STUDY .....</b>	<b>25</b>
<b>3. MATERIALS AND METHODS .....</b>	<b>26</b>
3.1 Cell lines .....	26
3.2 Tissue samples .....	26
3.3 Immunohistochemistry .....	26
3.4 Microarray analysis .....	27
3.5 Network and gene ontology analysis .....	27
3.6 RNA extraction, cDNA synthesis, and quantitative real-time PCR .....	28
3.7 RNA silencing .....	28
3.8 Trypan-Blue assay .....	29
3.9 Wound Closure Assay .....	29
3.10 Transwell migration and Matrigel assay .....	29
3.11 Collagen Migration and Invasion Assay .....	30
3.12 Transendothelial Cell Migration Assay .....	30
3.13 Statistical analysis .....	30
<b>4. RESULTS .....</b>	<b>31</b>
4.1 Up-regulation of Twist1 in ATC .....	31
4.2 Identification of Twist1 target genes .....	33
4.3 Down-regulation of the Twist1 target genes in CAL62-shTwist1 cells .....	39
4.4 Silencing of Twist1 positive targets in TPC-Twist1 cells impairs cell viability .....	40

4.5 Silencing of HS6ST2, THRB, ID4, RHOB and PDZK1IP1 in TPC-Twist1 cells impairs cell migration.....	42
4.6 Silencing of HS6ST2, THRB, ID4, RHOB and PDZK1IP1 in TPC-Twist1 cells impairs cell invasion .....	47
4.7 Silencing of HS6ST2, THRB, ID4, RHOB and PDZK1IP1 in TPC-Twist1 cells impairs transendothelial cell migration .....	50
<b>5. DISCUSSION .....</b>	<b>52</b>
<b>6. ACKNOWLEDGEMENTS .....</b>	<b>55</b>
<b>7. REFERENCES .....</b>	<b>56</b>

## LIST OF PUBLICATIONS

This dissertation is based upon the following publications:

- I. **Di Maro G** et al. Identification of targets of Twist1 transcription factor in anaplastic thyroid cancer. (Main body of the dissertation).
- II. Salerno P, Garcia-Rostan G, Piccinin S, Bencivenga TC, **Di Maro G**, Doglioni C, Basolo F, Maestro R, Fusco A, Santoro M, Salvatore G. TWIST1 plays a pleiotropic role in determining the anaplastic thyroid cancer phenotype. *J Clin Endocrinol Metab.* 2011; 96(5): E772-81.
- III. **Di Maro G** et al. Anterior gradient protein 2 promotes survival, migration and invasion of papillary thyroid carcinoma cells. (Manuscript in preparation).
- IV. Mancini M, Greco A, Salvatore G, Liuzzi R, **Di Maro G**, Vergara E, Chiappetta G, Pasquinelli R, Brunetti A, Salvatore M. Ultrasound imaging of thyroid tumor angiogenesis with microbubbles targeted to vascular endothelial growth factor receptor type 2 in mice (Manuscript in preparation).

## ABBREVIATIONS

AKAP9	A Kinase (PRKA) Anchor Protein (yotiao) 9
AKT	v-Akt murine Thymoma viral oncogene
ALK	Anaplastic Lymphoma Kinase
ATC	Anaplastic Thyroid carcinoma
bHLH	basic Helix-Loop-Helix
BRAF	B-type RAF family kinase
CBP	CREB-binding protein
CCDC6	Coiled-Coil Domain Containing 6
CCH	C-cell hyperplasia
CLA	Cutaneous Lichen Amyloidosis
CREB	cAMP-response element binding protein
CTNNB1	Catenin Beta 1 (cadherin-associated protein)
DMEM	Dulbecco's modified Eagle's medium
DOCK3	Dedicator of Cytokinesis 3
EBM	Endothelial cell Basal Medium
EBV	Epstein-Barr Virus
EMT	Epithelial Mesenchymal Transition
ERK	Extracellular signal-Regulated Kinase
FBS	Fetal Bovine Serum
FMTC	Familial Medullary Thyroid carcinoma
FTC	Follicular Thyroid carcinoma
HIF1 $\alpha$	Hypoxia Inducible Factor 1, alpha
HMG A2	High Mobility Group A2
IPA	Ingenuity Pathway Analysis
LMP1	Latent Membrane Protein 1
MAPK	Mitogen-Activated Protein Kinases
MEN2	Multiple Endocrine Neoplasia type 2
miRNA	microRNA
MMP	Metalloproteinase
MTC	Medullary Thyroid carcinoma
NCOA4	Nuclear Receptor Coactivator 4
NEDD9	Neural precursor cell Expressed, Developmentally Down-regulated 9
NF- $\kappa$ B	Nuclear Factor-Kappa B
NLS	Nuclear Localization Signal
NTRK1	Neurotrophic Tyrosine Kinase Receptor type 1
PAX8	Paired box 8
PCAF	p300/CBP associated factor

PDGFR $\alpha$	Platelet-derived Growth Factor Receptor $\alpha$
PDC	Poorly Differentiated Carcinoma
PIK3CA	Phosphoinositide-3 kinase Catalytic domain
PK	Protein Kinase
POSTN	Periostin
PPAR $\gamma$	Peroxisome Proliferation Activated Receptor $\gamma$
PTC	Papillary thyroid Carcinoma
PTEN	Phosphatase and Tensin homolog
RET	Rearranged during Transfection
RHOC	Ras Homolog family member C
RTK	Receptor tyrosine Kinase
SCS	Saethre-Chotzen Syndrome
TNF $\alpha$	Tumor Necrosis Factor $\alpha$
WDTC	Well differentiated thyroid carcinoma
YB1	Y box-binding protein I

## ABSTRACT

Thyroid cancer is the most common malignancy of endocrine organs and accounts for about 1% of newly diagnosed cancer cases. Anaplastic thyroid carcinoma (ATC) is one of the most aggressive human tumors; it is characterized by local invasion, distant metastasis, chemoresistance and radioresistance. Effective systemic therapy capable of reversing the aggressive biology of this disease is currently not available. Therefore, there is an urgent need for a better understanding of the molecular mechanisms underlying anaplastic thyroid cancer pathogenesis. Through, a cDNA microarray analysis we have isolated Twist1 as a gene up-regulated in ATC. Twist1 is a basic helix-loop-helix transcription factor that has been shown to contribute to cancer development and progression but its mechanism of action is poorly defined. In this Dissertation we showed that approximately 50% of ATCs up-regulated Twist1 with respect to normal thyroids as well as to poorly and well-differentiated thyroid carcinomas. Silencing of Twist1 by RNA interference in ATC cells reduced cell migration and invasion and increased sensitivity to apoptosis. The ectopic expression of Twist1 in thyroid cancer cells induced resistance to apoptosis and increased cell migration and invasion. To uncover the molecular mechanisms underlying Twist1 biological effects, we have performed a gene expression profile of Twist1 ectopically expressing thyroid cancer TPC cells in comparison to vector control cells. We founded 158 genes up-regulated and 221 genes down-regulated by more than 1.5 fold in TPC-Twist1 cells. We used the Ingenuity Systems Pathway Analysis (IPA) software to classify these genes. Consistent with the biological function of Twist1 in ATC, the top three molecular and cellular functions enriched in TPC-Twist1 cells were: cellular movement, cellular growth and proliferation, cell death and survival. In this dissertation we focused on the up-regulated genes by more than 4 fold. Silencing of the 11 top up-regulated genes reduced cell viability of TPC-Twist1 cells. Silencing of *COL1A1*, *KRT7*, *PDZK1* induced also apoptosis. Silencing of *HS6ST2*, *THRB*, *ID4*, *RHOB*, and *PDZKIIP*, also impaired cell migration and invasion of TPC-Twist1 cells. Thus, our data demonstrate that Twist1 plays a key role in determining malignant features of anaplastic thyroid cancer cells. These effects are mediated by a set of genes whose expression is under Twist1 control. The identified target genes are potential novel molecular determinants of ATC.

## **1. BACKGROUND**

### **1.1 Thyroid tumors**

#### **1.1.1 Morphological and clinical characteristics of thyroid tumors**

Thyroid cancer is the most common malignancy of endocrine organs and has rapidly increased in global incidence in recent decades (Jemal et al. 2011). The increased incidence is limited to the papillary type of thyroid cancer and is mostly due to tumors of small size (<1 cm) (Nikiforov and Nikiforova 2011).

There are several histological types and subtypes of thyroid cancer with different cellular origins, characteristics and prognosis (Xing 2013). There are two types of thyroid cells: follicular thyroid cells and parafollicular C cells, from which thyroid cancers are derived. Follicular thyroid cell derived malignancies (~95% of cases), include papillary thyroid carcinoma (PTC), follicular thyroid carcinoma (FTC), poorly differentiated thyroid carcinoma (PDC) and anaplastic thyroid carcinoma (ATC). PTC and FTC are collectively classified as well differentiated thyroid carcinoma (WDTC). PTC and FTC account for ~80% and ~10% of cases, respectively, PDC accounts for ~5%, ATC accounts for ~2% of cases. These tumors differ noticeably in aggressiveness, ranging from well differentiated to ATC (**Figure 1**).

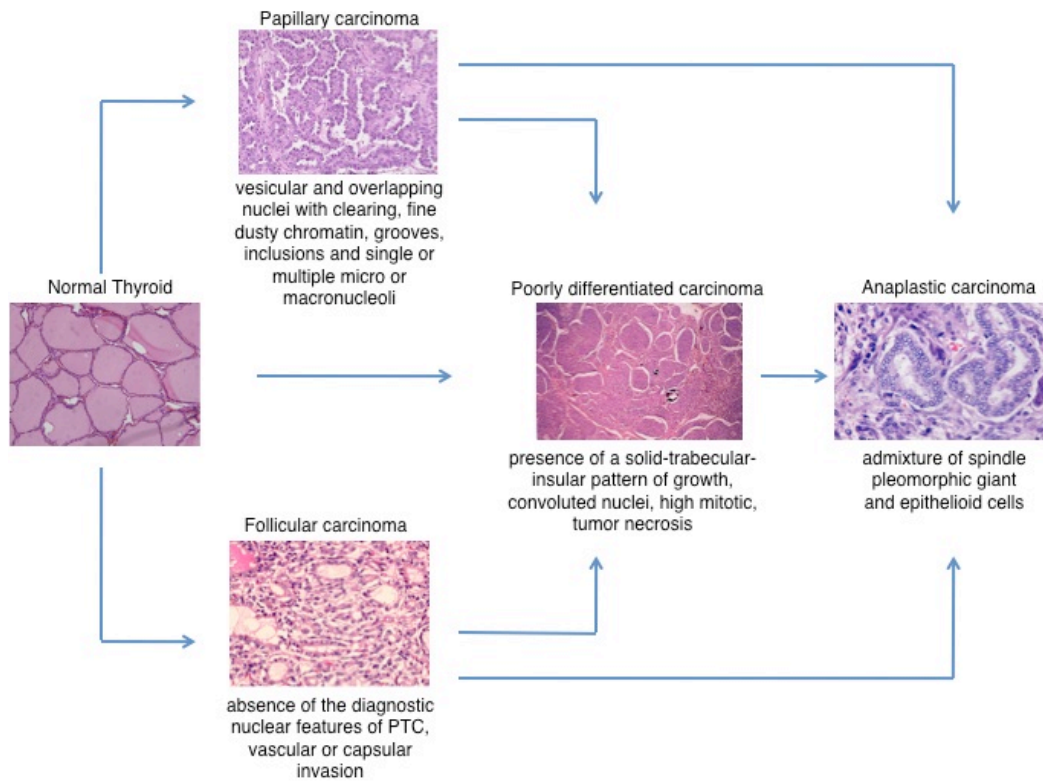


**Figure 1. Model of thyroid multi-step carcinogenesis.** Scheme of step-wise dedifferentiation of follicular cell-derived thyroid carcinoma with underlined main histological features.

PTC is characterized by typical features of the cell nuclei, including enlarged, vesicular and overlapping nuclei with clearing, fine dusty chromatin, grooves, inclusions and single or multiple micro or macronucleoli (De Lellis 2006) (**Figure 1**). PTC is closely linked to radiation exposure and its incidence sharply increased in children after the Chernobyl accident (Williams 2008). PTC is more frequent in women than men and affects patients of ~20-50 years old.

FTC is characterized by follicular cell differentiation in the absence of the diagnostic nuclear features of PTC, vascular or capsular invasion and propensity for metastasis via the blood stream (**Figure 1**). It mostly affects 40-60 years old patients (Kondo et al. 2006).

PDC are rare neoplasms characterized by a partial loss of differentiation and less favorable prognosis in comparison with WDTC. Diagnostic criteria for PDC include the presence of a solid-trabecular-insular pattern of growth, absence of the nuclear features typical of PTC and the presence of at least one of these

features: convoluted nuclei, high mitotic rate, and tumor necrosis (Volante et al. 2010) (**Figure 1**).

ATC is the most aggressive thyroid tumor, and it is described among the most lethal human malignancies, with a median survival from diagnosis of ~3-6 months (Perri et al. 2011). ATC is characterized by admixture of spindle pleomorphic giant and epithelioid cells (**Figure 1**). Clinically, these tumors usually present during the 6<sup>th</sup> to 7<sup>th</sup> decade of life as a rapidly enlarging neck mass that extends locally, compressing the adjacent structures and tends to disseminate both to regional nodes and to distant sites, including lung, pleura, bone and brain. Current treatment of ATC has often only palliative purposes, particularly relief of airway compression, having little impact on patient's survival (Smallridge and Copland 2010).

Parafollicular C cell-derived medullary thyroid carcinoma (MTC) accounts for a small proportion (~5% of cases) of thyroid malignancies (Xing 2013). MTC is sporadic in ~75% of cases, and in the others it is a component of the autosomal dominant cancer syndrome known as “multiple endocrine neoplasia type 2” (MEN2) that includes: MEN2A (~80% of cases), MEN2B and familial MTC (FMTC) (Waguespack et al. 2011). MEN2-associated hereditary MTC is typically bilateral and multicentric and it is usually preceded by multifocal C-cell hyperplasia (CCH). In MEN2A, MTC is associated with pheochromocytoma, parathyroid hyperplasia and, rarely, cutaneous lichen amyloidosis (CLA) and Hirschsprung's disease. In MEN2B, MTC is associated with pheochromocytoma, multiple ganglioneuromas of the lips and gastrointestinal tract and marfanoid body habitus. Total thyroidectomy is recommended. Clinical recurrence in the neck or in mediastinum is a common problem for MTC patients (Leboulleux et al. 2004, Cote and Gagel 2003).

### 1.1.2 Genetics alterations in follicular thyroid cell derived tumors

Similar to other cancer types, thyroid cancer initiation and progression occurs through a gradual accumulation of various genetic and epigenetic alterations, including activating and inactivating somatic mutation, alteration in gene expression patterns, microRNA (miRNA) dysregulation and aberrant gene methylation (Nikiforov and Nikiforova 2011). Thyroid cancer represents a type of neoplasia in which critical genes are frequently mutated via two distinct molecular mechanisms: point mutation or chromosomal rearrangement (**Table 1**).

**Table 1.** Genetic alterations in follicular thyroid cell derived tumors.

Tumor type	Molecular lesion and approximate prevalence (%)
PTC	<ul style="list-style-type: none"> <li>-RET/PTC rearrangements (10-20%)</li> <li>-NTRK1 rearrangements (&lt;5%)</li> <li>-BRAF point mutation (45%)</li> <li>-RAS point mutation (10-20%)</li> </ul>
FTC	<ul style="list-style-type: none"> <li>-PAX8/PPAR<math>\gamma</math> rearrangements (&gt; 60%)</li> <li>-RAS point mutation (30-45%)</li> <li>-PIK3CA mutation (&lt;10%)</li> <li>-PTEN mutation (&lt;10%)</li> </ul>
PDC	<ul style="list-style-type: none"> <li>-RAS point mutation (20-40%)</li> <li>-PI3KCA point mutation or amplification (5-10%)</li> <li>-TP53 point mutation (15-30%)</li> <li>-CTNNB1 point mutation (25%)</li> <li>-BRAF point mutation (10-20%)</li> <li>- AKT point mutation (5-10%)</li> </ul>
ATC	<ul style="list-style-type: none"> <li>-TP53 point mutation (70-80%)</li> <li>-BRAF point mutation (25%)</li> <li>-RAS point mutation (20-30%)</li> <li>-CTNNB1 point mutation (60-65%)</li> <li>-PI3KCA point mutation (15-25%)</li> <li>- AKT point mutation (15%)</li> <li>-PTEN mutation (10-20%)</li> <li>-ALK point mutation (10%)</li> </ul>

## Genetic alterations in PTC

Over 70% of PTC features genetic alterations causing activation of the MAPK pathway (Mitogen-Activated Protein Kinases) (Kondo et al. 2006). PTC is characterized by mutations of various MAPK components, including rearrangements of the *RET* (REarranged during Transfection) tyrosine kinase receptor, or more rarely *NTRK1* (neurotrophic receptor-tyrosine kinase), or activation of *BRAF* (B-type RAF family kinase) (**Table 1**).

In the thyroid gland, *RET* is normally expressed at high levels in parafollicular C-cells, but not in follicular cells. *RET* is a proto-oncogene encoding a cell membrane receptor tyrosine kinase (RTK) with four cadherin-related motifs in the extracellular domain, and it is located on chromosome 10q11.2 (Santoro et al. 2006). *RET-PTC* is a chromosomal rearrangement found in PTC, and occurs as a consequence of genetic recombination between the 3' tyrosine kinase portion of *RET* and the 5' portion of a partner genes (Santoro et al. 1994). The rearrangement results in ligand-independent dimerization and constitutive tyrosine kinase activity of *RET* which leads to chronic stimulation of MAPK signaling. There are more than 10 types of *RET* rearrangements, as determined by the types of partner genes. Two of the most common types of rearrangements are *RET/PTC1* and *RET/PTC3*, in which *RET* is fused to either *CCDC6* (Coiled-Coil Domain Containing 6) (also known as *H4*) or *NCOA4* (Nuclear Receptor Coactivator 4) (also known as *ELE1* or *RFG*), respectively (Rabes et al. 2000; Santoro et al. 2000; Klugbauer et al. 1998). Both of these rearrangements are paracentric intrachromosomal inversion, and fusion partners reside on the long arm of chromosome 10 (Pierotti et al. 1992; Minoletti et al. 1994). Spatial contiguity of *RET* and the partner gene in the nucleus is a structural basis for the formation of *RET-PTC* rearrangement (Nikiforova et al. 2000). *RET* rearrangements are found in 10-20% of PTC, but the prevalence is significantly higher in patients with a history of accidental or therapeutic radiation exposure. *RET/PTC1* is more frequently associated with classic PTCs and with the diffuse sclerosing variant; conversely, *RET/PTC3* is more common in the solid variant and in PTC associated to ionizing radiations (Thomas et al. 1999).

Chromosomal rearrangements involving another receptor tyrosine kinase gene *NTRK1* also occur in PTC. The *NTRK1* gene resides on chromosome 1q22 and can be fused to at least three different partner genes located on the same or different chromosomes (Radice et al. 1991; Greco et al. 1992; Miranda et al. 1994). Rearrangement of the *NTRK1* genes occurs in ~5% of PTC (Musholt et al. 2000).

*BRAF* is a serine-threonine kinase belonging to the RAF family (*ARAF*, *BRAF*, *CRAF*) that is translocated to the cell membrane after being bound and

activated by RAS, resulting in intracellular activation of the MAPK signaling pathway (Davies et al. 2002). Among the RAF family members, *BRAF* appears to have the highest basal kinase activity and is the most potent activator of the MAPK pathway. In thyroid cancer, *BRAF* can be activated by point mutations, small in-frame deletions or insertions or by chromosomal rearrangement. The most common oncogenic mutation in *BRAF* is the replacement of valine 600 with a glutamic acid (V600E) caused by a thymine to adenosine substitution at nucleotide position 1799. *BRAF* V600E kinase function is ~500 fold more active with respect to the wild type protein. *BRAF* mutation represents the most common genetic event in PTC, occurring in ~45% of all cases (Xing 2007; Ciampi and Nikiforov 2005), and in particular V600E constitutes ~98-99% of all *BRAF* mutations found in thyroid cancer. V600E mutation has been observed in melanoma (~80%), and in other tumors (~0-18%), including colorectal (~5%) and lung cancer (~1-3%) (Namba et al. 2003).

*BRAF* mutations correlate with aggressive tumor behavior, tumor recurrence, decreased radioiodine concentration ability, failure to treat recurrent disease. Other *BRAF* mutations are the K601E point mutation, small in-frame insertions or deletions around codon 600, and *AKAP9/BRAF* rearrangement. The rearrangement is a paracentric inversion of chromosome 7q that leads to the fusion between *BRAF* protein kinase domain and the *AKAP9* (A Kinase (PRKA) Anchor Protein (yotiao) 9) gene. This rearrangement occurs in ionizing-radiation-induced PTC in 1-2% of cases. (Ciampi et al. 2005). Finally, point mutation or gene amplification of *PI3KCA* (phosphatidylinositol-3 kinase catalytic domain) has been reported in a small fraction of PTC (Wu et al. 2005).

Overall, the genetic alterations of *RET*, *BRAF* and *NTRK1* rarely overlap in the same tumor and in particular *RET/PTC* and *BRAF* alterations are mutually exclusive in PTC, suggesting that mutations at more than one of these sites are unlikely to confer additional biological advantage, a fact that is consistent with the overlap of the signaling pathways of these oncoproteins (Kimura et al. 2003; Soares et al. 2003; Frattini et al. 2004).

## Genetic alterations in FTC

FTC may develop through at least two different pathways, involving either *RAS* or *PPAR*  $\gamma$  (peroxisome proliferation activated receptor  $\gamma$ ). The human *RAS* gene family includes *HRAS*, *KRAS* and *NRAS*. These genes encode intracellular G-proteins, thereby propagating signals from cell receptor tyrosine kinases and G-coupled receptors along the MAPK, PI3K/AKT (v-Akt murine Thymoma viral oncogene) and other signaling pathways (Bhajee and Nikiforov 2011). Activating point mutations in *RAS* genes are common in human tumors and typically affect

codons 12,13 and 61. In thyroid cancer, *NRAS* codon 61 and *HRAS* codon 61 mutations are the most common. *RAS* mutations are identified in ~30-45% of FTC (**Table 1**).

*PPAR*  $\gamma$  is a member of the steroid nuclear-hormone receptor superfamily that forms heterodimers with retinoid X receptor. *PAX8/PPAR* $\gamma$  rearrangement results from t(2:3)(q12-13;p24-25) translocation, which leads to the fusion of *PAX8* (paired box 8) and *PPAR* $\gamma$  occurring in up to 60% of FTC (Eberhardt et al. 2010). *PAX8/PPAR* $\gamma$  exerts a dominant-negative effect on the wild-type tumor suppressor *PPAR* $\gamma$  and also transactivates certain *PAX8* responsive genes (Placzkowski et al. 2008). *PAX8/PPAR* $\gamma$  rearrangement and *RAS* point mutations rarely overlap in the same tumor, which suggests that they represent distinct pathogenetic pathways in the development of follicular thyroid carcinomas (Nikiforova et al. 2003).

#### Genetic alterations in PDC

PDC have genetic features intermediate between WDTC and ATC consistent with the hypothesis of a multi-step model of thyroid carcinogenesis (Tallini 2011) (**Figure 1**). Similar to WDTC, *RAS* point mutations occur in ~20-40% of PDC (Garcia-Rostan et al. 2005; Volante et al. 2007). Similar to ATC, PDC features in some cases, mutations in exon 5-9 of *TP53* (15-30%) or in *PIK3CA* and its downstream effector *AKT* or point mutations in exon 3 of *CTNNB1* (Catenin-cadherin-associated protein Beta 1) (Ricarte-Filho et al. 2009). About 10-20% of PDC harbor *BRAF* mutation, particularly those samples with morphological evidence of pre-existing PTC (Begum et al. 2004). A small number of PDC expresses rearranged tyrosine kinase genes such as *RET/PTC* or *NTRK1*, however there is no association with unfavorable clinicopathological features or decreased survival (Santoro et al. 2002) (**Table 1**).

#### Genetic alterations in ATC

ATC may derive *de novo* or from pre-existing PTC or FTC (**Figure 1**). *BRAF* and *RAS* mutations are frequently found in WDTC, PDC and ATC, therefore, probably represent an early event in thyroid cancer progression (Nikiforova et al. 2003). By contrast, the *RET/PTC* rearrangements and the *PAX8/PPAR*  $\gamma$  fusion protein detected in WDTC, are not observed in ATCs (Nikiforov 2004). ATCs frequently have additional genetic alterations that are not found in WDTC and, therefore, represent a late event, which may be required to

initiate tumor dedifferentiation. The late events include mutations of *TP53*, *CTNNB1* and *PIK3CA* genes.

*TP53* is a tumor suppressor gene located on chromosome 17p. *TP53* is nuclear transcription factor that plays a key role in regulation of the cell cycle, DNA repair, and apoptosis (O'Neill et al. 2010). Point mutations that affect *TP53* are found in ~70-80% of cases of ATC (Xing 2013). The mutations lead to loss of function of this important tumor suppressor gene.

Another gene frequently mutated in ATC is *CTNNB1*, which encodes  $\beta$ -catenin.  $\beta$ -catenin is a multifunctional protein that binds and stabilize E-cadherins to form the adherence junction, and it is an activator of *WNT* signaling pathway. Point mutations in exon 3 of the gene are found in up to 60-65% of ATC (Garcia-Rostan et al. 2001).

Thyroid cancer dedifferentiations also involves progressive accumulation of other mutations, in particular in gene that encode effectors of the *PI3K-AKT* pathway. They, in turn, phosphorylate substrates involved in cell growth and survival. *PIK3CA* gene located on 3q26.3 and encoding a catalytic subunit of PI3K, was found mutated in ~15-25% of ATC (Xing 2013; Santarpia et al. 2008). *AKT1* is activated in ~15% of cases of ATC (Nikiforov and Nikiforova 2011) and *PTEN* (Phosphatase and Tensin homolog) that negatively regulates the *PI3K* pathway is mutated in ~10-20% of ATC cases (Xing 2013).

Recently point mutations of the *ALK* (anaplastic lymphoma kinase) gene were found in ~10% of ATCs (Murugan and Xing 2011). *ALK* is a member of the insulin receptor sub-family of receptor tyrosine kinases (RTK) with its encoding gene located on the short arm of chromosome 2 (Kelleher and McDermott 2010). The gain-of-function mutations of *ALK* cause dual activation of the *PI3K/AKT* and MAP kinase pathways in ATC (**Table 1**).

## 1.2 The transcription factor Twist1

### 1.2.1 Structures of the Twist1 gene and protein

Little is known about the molecular events that lead from the highly curable differentiated tumors to the very aggressive ATC. Through a cDNA microarray analysis on different thyroid tumors in comparison to normal thyroids, we have isolated Twist1 transcription factor as a gene up-regulated in ATC (Salvatore et al. 2007).

Twist1 was originally identified in *Drosophila* as one of the genes essential for mesoderm specification during embryo development (Simpson 1983). Two *Twist* genes exist in vertebrates, Twist1 (Twist) and Twist2 (formerly known as *Dermo-1*). The human Twist2 protein contains 160 amino-acid residues and it shares 68% homology with human Twist1, but Twist2 lacks a glycine-rich region that is present in Twist1 at N-terminus (Li et al. 1995).

Human Twist1 gene is mapped on chromosome 7q21.2 and contains two exons and one intron (Wang et al. 1997) (**Figure 2A**). The first exon contains an ATG site followed by an open reading frame encoding 202 amino-acid residues. The open reading frame is followed by a 45-bp untranslated portion in exon 1, a 536-bp intron and a second untranslated exon with two potential polyadenylation sites that are 65 and 415 bp from the 5' end of exon 2. The molecular mass calculated from the amino-acid sequence of human Twist1 is ~21 kDa, with a theoretical isoelectric point of ~9.6. The protein contains relatively polar amino-acid residues in the region close to the NH<sub>2</sub>-terminus and non-polar residues at the COOH-terminus where the bHLH (basic helix–loop–helix) domain is located (Qin et al. 2011) (**Figure 2B**).

Twist1 is a highly conserved transcription factor that belongs to the family of bHLH proteins (Thisse et al. 1987). In the classification of bHLH proteins, based on their tissue distribution, partner choice, DNA-binding properties and structural features, Twist1 falls into class B. Class B proteins are tissue-specific and usually form heterodimers with class A bHLH factors such as the product of E2 genes, which are broadly expressed (Castanon and Baylies 2002). bHLH proteins are structurally and functionally characterized by two amphipathic helices that are separated by a interhelical loop of varying length, which is important in maintaining the tertiary structure of the HLH moiety. A basic amino acid-rich region precedes the first helix and is required for DNA binding (Castanon and Baylies 2002). The functional importance of this domain has been emphasized by the isolation of mutations within this region. For example, humans carrying point mutations in the bHLH domain display Saethre-Chotzen syndrome (SCS), an

autosomal dominant inherited disease characterized by a broad spectrum of malformations including short stature, craniosynostoses, high forehead, ptosis, small ears with prominent crus, and maxillary hypoplasia with a narrow and high palate (El Ghouzzi et al. 1997). The  $\alpha$ -helices mediate dimerization with a second bHLH factor (**Figure 2C**), leading to the formation of a bipartite DNA-binding domain that specifically binds to hexanucleotide sequences (CANNTG), known as E-boxes. The E-boxes are found in the regulatory elements of many lineage-specific genes. Consistently, bHLH are transcription factors acting in various differentiation processes, and play key roles in different developmental events like neurogenesis and myogenesis (Puisieux et al. 2006).

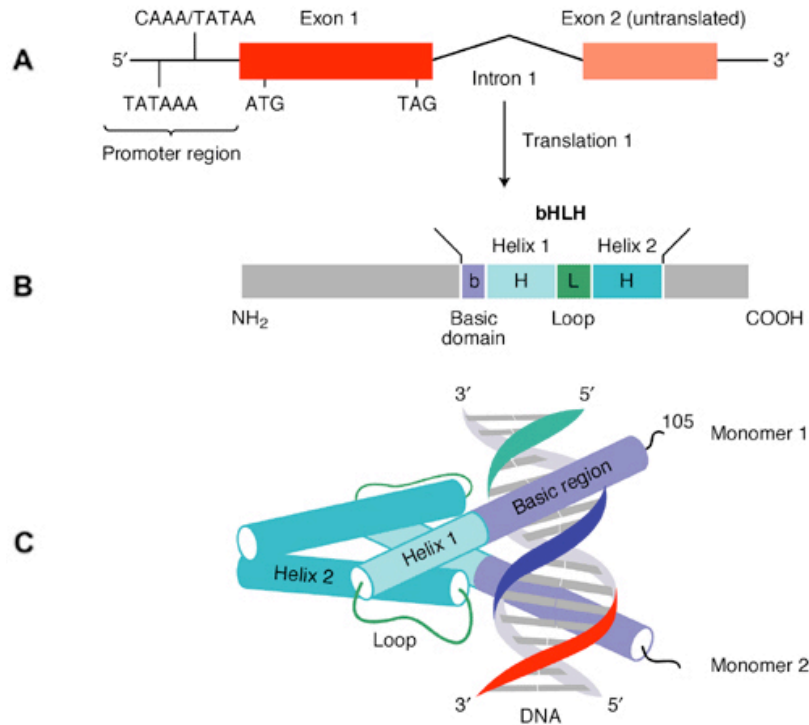


**Figure 2. Structure of human Twist1.** **A.** The human-*Twist1* gene comprises two exons separated by a unique intron. **B.** The human-*Twist1* protein is 202 amino acids long presenting a basic helix-loop-helix (bHLH) domain. **C.** Interaction of dimers of *Twist1* with DNA (modified from Bonaventure and El Ghouzzi 2003).

The *Twist1* protein displays a very high degree of conservation among a broad range of species, including human, mouse, frog, *Drosophila* and

*Caenorhabditis elegans*, a high degree of sequence similarity in their C-terminal half, including the bHLH domain and a Twist box protein interaction surface and are more divergent in their N-terminus.

The C-terminal part of the protein comprises the WR motif also called “*Twist box*” (Spring et al. 2000; Bialek et al. 2004). The WR motif is located between residues 20 and 55 C-terminal to the bHLH region. Recently it was demonstrated that through the Twist box, Twist1 establishes a direct interaction with p53 and this interaction is critical for Twist1 mediated inhibition of p53, suggesting that the binding via Twist box is leitmotif in the inhibition exerted by Twist1 on other transcription factors (Piccinin et al. 2012).

The Twist1 protein functions as a transcription factor in the cell nucleus and presents two nuclear localization signal (NLS) sequence <sup>37</sup>RKRR<sup>40</sup> and <sup>73</sup>KRGKK<sup>77</sup>. Regulation of transcriptional outcome mediated by Twist1 depends on different mechanisms. Binding of Twist1 to E-boxes in the promoter of the target genes could either activate (e.g. *N-cadherin*, *AKT2* or *Gli1*) or repress (e.g. *E-cadherin*) transcription (Alexander et al. 2006; Cheng et al. 2007). Twist1 can also influence gene expression via epigenetic mechanisms. The N-terminus of Twist1 can interact with p300, cAMP-response element binding protein (CREB), CREB-binding protein (*CBP*) and p300/CBP associated factor (PCAF), resulting in inhibition of the acetyl transferase activities of these histone remodeling enzymes (Hamamori et al. 1999). Since histone acetylation is usually coupled with transcriptional activation, the inhibition of p300, CBP and PCAF activities by Twist1 should repress gene expressions mediated by transcription factors that recruit these histone acetyltransferases.

The C-terminus of Twist1 interacts with the DNA-binding domain of Runx2 to repress Runx2 function necessary for osteoblast differentiation (Bialek et al. 2004). These findings suggests that Twist1 not only serves as a transcription factor to directly regulate its target genes, but also regulates other transcription factor/coregulator-mediated gene expression through interaction with other transcriptional regulators (**Figure 3**).

In addition, it was reported that Twist1 protein directly interacts with several other transcription factors, including MyoD, MEF2, RUNX1, PGC1- $\alpha$ , p53 and NF- $\kappa$ B (Nuclear Factor-KappaB) and inhibits their activities (Šošić et al. 2003; Bialek et al. 2004; Sharabi et al. 2008; Shiota et al. 2008; Pan et al. 2009) (**Figure 3**). Furthermore, a recent paper showed that Twist1 directly negatively regulates formation of miRNA *let-7i* which (Yang et al. 2012).

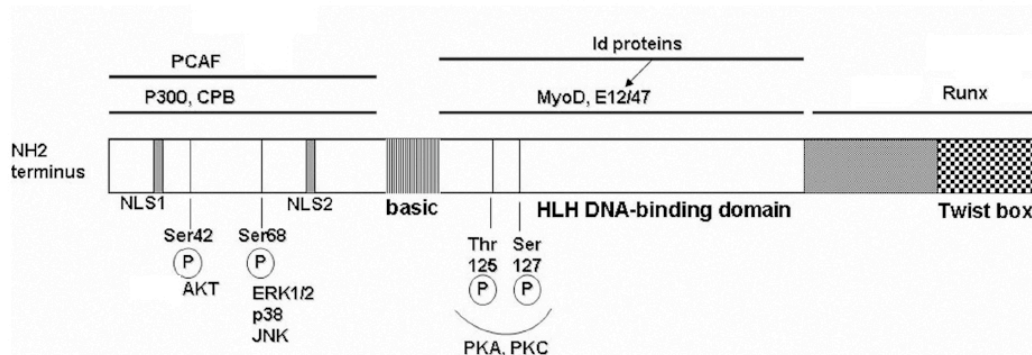


**Figure 3. Structure of the human Twist1 protein.** Twist1 has the typical modular structure of bHLH transcriptional factor family. At the N-terminus two nuclear localization signals (NLS) are located. In the C-terminal region, the functional Twist box can bind Runx. The protein-protein interactions are delineated with black bars on top. A number of functional Ser/Thr residues allow post-translational modifications of Twist1 are illustrated on the bottom. (CBP, cAMP-response element binding protein (CREB)-binding protein; PCAF, p300/ CBP-associated factor, Runx, Runt-related transcription factor; E12/47, a bHLH transcription factor that form dimer with Twist1; MyoD, a bHLH transcription factor that regulates muscle differentiation; Id family of proteins can sequester the E-box transcription factor and therefore prevent formation of the dimers with Twist1 (modified from Dobrian 2012).

### 1.2.2 Twist1 protein phosphorylation

Regulation of protein stability is an important way to control Twist1 function. Recently, it was reported that Twist1 protein stability is largely regulated by MAPK-mediated phosphorylation on serine68 (S68). The S68 in Twist1 can be phosphorylated by p38, JNK and ERK1/2 (Extracellular signal-Regulated Kinase) MAPKs, and this phosphorylation prevents Twist1 protein from ubiquitination-mediated degradation (Hong et al. 2011). Twist1 can heterodimerize with different transcription factors. Partner choice could also be regulated by the phosphorylation state of specific threonine (Thr 125) and serine (Ser 127) residues that are conserved in the first  $\alpha$ -helix of the HLH domain of Twist1 protein. The phosphorylation state is determined by protein kinase A (PKA) and C (PKC) (Friulli et al. 2003) (**Figure 3**). Recently, AKT has also been linked to the phosphorylation of Twist1 at serine 42 (Vichalkovski et al. 2010).

### 1.2.3 Physiological functions of Twist1 protein

Twist1, identified originally in *Drosophila* as a zygotic developmental gene, is considered crucial for the establishment of the ventral furrow, a prerequisite for the development of all mesoderm-derived internal organs (Thisse et al. 1987). The name “*Twist*” was given to this gene on the basis of observations that *Drosophila* embryos lacking the Twist1 gene failed to gastrulate normally, produced no mesoderm and died at the end of embryogenesis with a ‘twisted’ appearance (Simpson 1983).

In mouse, the KO of Twist1 was shown to be embryonic lethal and die at E10.5-11 displaying severe defects in closure of the cephalic neural tube, deficient cranial mesoderm, malformed branchial arches and facial primordium, and retarded limb bud development (El Ghouzzi et al. 1997). Twist1 KO mice also present a significant increase in apoptotic cells, especially in the developing sclerotome (Chen and Behringer 1995). The lethality of the Twist1 knockout mouse led to the development of a Cre-mediated conditional knockout mouse to studying the regulatory functions of Twist1 post-neural crest cell migration (Bildsoe et al. 2009). A Twist1-null heterozygous mouse has also been developed that presents a Saethre-Chatzen syndrome-like (SCS) phenotype (Bourgeois et al. 1998), thus providing an animal model for studying the SCS craniosynostosis phenotype. After birth, Twist1 is expressed in the adult stem cells of the mesenchyme (Figeac et al. 2007) and mRNA has also been detected in primary osteoblastic cells derived from newborn mouse (Murray et al. 1992) and in mouse brown and white adipocytes (Pan et al. 2009; Pettersson et al. 2010). The Twist1 protein is also likely to be important for maintaining the immature phenotype of chondrocytes (Dong et al. 2007).

The expression profile of Twist1 during human embryogenesis is unknown. Twist1 mRNA expression pattern was examined in various adult human tissues, as well as several cell lines originated from different normal human tissues (Wang et al. 1997). Among the human tissues analyzed, the strongest signals for Twist1 mRNA were observed in the placenta, a tissue containing a large fetal portion and a small maternal portion. In particular, strong Twist1 signals were seen in the fetal portion of the placenta developed from the chorionic sac, which is mostly derived from the mesoderm. Intermediate strength signals were seen in the adult heart and skeletal muscle, which are also mostly derived from the mesoderm. Weak signals were found in the kidney and pancreas, while no signals were observed in the ectoderm- derived cells in the brain and endoderm-derived cells in the lung and liver. Additionally, Twist1 expression is also observed in human white adipocytes (Pettersson et al. 2011). Twist1 expression was not observed in

human epithelial cells, although its mRNA was detected in both fetal and adult human skin fibroblasts (Wang et al. 1997).

#### **1.2.4 Role of Twist1 in human cancer**

Twist1 overexpression is associated with many types of aggressive tumors (**Table 2**) and in some cases correlates with poor prognosis and high or invasive grade/stage of the tumor

Cancer is a complex multistep process involving genetic and epigenetic changes that eventually result in the activation of oncogenic pathways and/or inactivation of tumor suppressor signals. During cancer progression, cancer cells acquire a number of hallmarks that promote tumor growth and invasion (Hanahan, and Weinberg 2011). A crucial mechanism by which tumor cells enhance their invasive capacity is the dissolution of intercellular adhesions and the acquisition of a motile mesenchymal phenotype as part of an epithelial- to-mesenchymal transition (EMT). EMT is a critical mechanism of migration and invasion during development and in the case of cancer cells is a mechanism of increased invasion, metastasis, and resistance to chemotherapy. A hallmark of EMT is the functional loss of the E-cadherin protein encoded by the CDH1 gene (De Craene and Berx 2013).

Twist1 has been identified as a master regulator of EMT (Yang et al. 2004). Twist1 down regulates epithelial markers such as E-cadherin, and up-regulates mesenchymal markers such as N-cadherin. Repression of CDH1 gene by Twist1 is either direct (Vesuna et al. 2008) or mediated by SNAI1 (Smit et al. 2009). Twist1 plays multiple roles in cancer initiation, progression and metastasis and.

**Table 2.** Overexpression of Twist1 in human cancer (modified by Ansieau et al. 2010).

<b>Human cancer type</b>	<b>Poor prognosis *</b>	<b>High or invasive grade/stage *</b>	<b>Reference</b>
Ameloblastoma		√	Feng et. al 2009
Bladder carcinoma		√	Zhang et al. 2007
Breast carcinoma	√	√	Mironchik et al. 2005
Cervical carcinoma	√		Shibata et al. 2008
Choroid plexus carcinoma			Hasselblatt et al. 2009
Colon carcinoma			Ansieau et al. 2008 a,b
Endometrial carcinoma	√	√	Kyo et al. 2006
Gastric carcinoma			Rosivatz et al. 2002
Glioma		√	Elias et al. 2005
Head and neck carcinoma	√	√	Ou et al. 2008
Hepatocarcinoma			Lee et al. 2006
Kidney carcinoma			Ansieau et al. 2008 a,b
Melanoma	√	√	Hoek et al. 2004
Nasopharyngeal carcinoma	√		Song et al. 2006
Neuroblastoma			Valsesia-Wittmann et al. 2004
Oesophageal squamous cell carcinoma			Yuen et al. 2007
Ovarian carcinoma	√	√	Hosono et al. 2007
Pancreas carcinoma			Ohuchida et al. 2007
Parathyroid carcinoma			Fendrich et al. 2009
Pheochromocytoma			Waldmann et al. 2009
Prostate carcinoma		√	Kwok et al. 2005
Sarcoma		√	Maestro et al. 1999
Thyroid carcinoma		√	Salerno et al. 2011 (attached manuscript II)

\* correlation with Twist1 overexpression

### 1.2.5 Mechanisms of overexpression of Twist1 in human cancer

The mechanisms leading to the aberrant overexpression of Twist1 appear to be various and complex. Interestingly, stress conditions seem to control both the physiological and aberrant expression of Twist1. Hypoxic conditions are defined as potent inducers of Twist1 expression in cancer cell. Up-regulation of Twist1 by

HIF1 $\alpha$  (Hypoxia Inducible Factor 1,  $\alpha$ ) during hypoxic conditions has significant implications in tumor invasion and angiogenesis (Yang et al. 2008).

It was reported that also YB1 (Y box-binding protein I) is able to modulate Twist1 expression. The DNA/RNA binding protein YB1 was found to enhance the cap-independent translation of EMT-inducing mRNA including Twist1, thereby promoting growth arrest and cell dissemination (Evdokimova et al. 2009).

In breast cancer Cheng and colleagues (2008) postulated that activated STAT3 transcriptionally induces Twist1 expression, which subsequently promotes the migration, invasion and anchorage-independent growth of breast cancer cells.

Epstein-Barr virus (EBV)-associated nasopharyngeal carcinoma is highly metastatic compared to other head and neck tumors. A study showed that the principal EBV oncoprotein, latent membrane protein 1 (LMP1), up-regulates Twist1 to induce EMT, suggesting the contribution of Twist1 to the highly metastatic nature of nasopharyngeal carcinoma (Horikawa et al. 2007). Furthermore, this study revealed that LMP1 regulates Twist1 through the NF- $\kappa$ B pathway.

Moreover, it was described that Twist1 forms a negative loop with inflammatory cytokines, as Twist1 is transcriptionally induced by NF- $\kappa$ B and in turn binds to the TNF $\alpha$  (Tumor Necrosis Factor  $\alpha$ ) and IL1 $\beta$  promoters blocking NF- $\kappa$ B transcriptional activity (Šošić et al. 2003).

In a recent paper it was also demonstrated that HMGA2 (high mobility group A2) protein in association with Smad complex directly associates with A:T-rich sequences and promotes transcription from the Twist1 promoter (Tan et al. 2012).

### **1.2.6 Twist1 target genes**

Twist1 regulates gene expression as a transcriptional activator through binding as a homodimer or heterodimer to the E-box DNA consensus sequence. All the genes that present an E-box consensus sequence in the promoter are potentially Twist1 target genes.

However in accordance with its important role in EMT, it was demonstrated that Twist1 down-regulates the epithelial marker E-cadherin and on the other hand up-regulates the mesenchymal marker N-cadherin (Vesuna et al. 2008). Moreover, Twist1 directly activates the cell adhesion protein periostin (POSTN), involved in cancer metastasis (Oshima et al. 2002). Twist1 induces also PDGFR $\alpha$  (Platelet-derived Growth Factor Receptor  $\alpha$ ) expression, which in turn activates Src, to promote invadopodia formation. Invadopodia are specialized membrane protrusions for extracellular matrix degradation (Eckert et al. 2011).

Twist1 can promote cancer cell invasion and metastasis also by repressing the expression of TIMP1 a key inhibitor of MMPs (metalloproteinase) (Okamura et al. 2009).

Direct regulation of genes involved in cancer progression has also been observed. AKT2 is a modulator of YB-1 function, and both are central to tumor proliferation (Shiota et al. 2008). Twist1 can up-regulate the proto-oncogene AKT2 by directly binding to its promoter (Cheng et al. 2007). Additionally, Twist1 directly regulated, in the presence of E12, the cyclin-dependent kinase inhibitor p21 (Funato et al. 2001; Murakami et al. 2008).

Twist1 directly up-regulates Bmi1, a polycomb-group protein that maintains stem cell self-renewal and is frequently overexpressed in human cancers. Twist1 targets Bmi1 expression and works with Bmi1 to promote tumor-initiating capability and EMT by repressing E-cadherin expression (Yang et al. 2010).

Twist1 can regulate gene expression indirectly by regulating microRNAs expression. Recent evidence has shown that Twist1 can directly activate miR-10b by binding to its promoter (Ma et al. 2007). Activation of miR-10b by Twist1 leads to inhibition of translation of the homeobox D10 mRNA resulting in increased expression of the pro-metastatic gene RHOC (Ras Homolog family member C) (Ma et al. 2007).

Recently it was reported that Twist1 cooperates with Bmi1 to suppress let-7i expression, which results in up-regulation of NEDD9 (Neural precursor cell Expressed, Developmentally Down-regulated 9) and DOCK3 (Dedicator of Cytokinesis 3), leading to RAC1 activation and enabling mesenchymal-mode movement in three-dimensional environments (Yang et al. 2012).

## **2. AIM OF THE STUDY**

The aim of this study (main body of dissertation and attached manuscript II) was to identify genes that mediate Twist1 effects in thyroid cancer cells.

The specific aims were as follows:

1. To study the functional consequences of silencing of top up-regulated genes on cell proliferation and survival.
2. To study the functional consequences of silencing of top up-regulated genes on cell migration.
3. To study the functional consequences of silencing of top up-regulated genes on cell invasion.

Besides Twist1 study, projects developed during my PhD program regarded:

- Identification of AGR2, as a novel marker of PTC, involved in thyroid cancer cells survival, migration and invasion and in protection from Endoplasmic Reticulum (ER) stress (attached manuscript III).
- A novel method to characterize *in vivo* the VEGFR-2 expression in the tumor vasculature of a mouse model of thyroid cancer (Tg-TRK-T1) (attached manuscript IV).

### **3. MATERIALS AND METHODS**

#### **3.1 Cell lines**

Human papillary thyroid cancer cell line TPC, was obtained from M. Nagao (Carcinogenesis Division, National Cancer Center Research Institute, Tokyo, Japan). The TPC cell line was authenticated based on the unique presence of the RET/PTC1 rearrangement. Human anaplastic thyroid cancer cell line, CAL62 was purchased from DSMZ (Deutsche Sammlung von Mikroorganismen und Zellkulturen GmbH, Braunschweig, Germany). CAL62 cells were DNA profiled by short tandem repeat analysis in 2009 and shown to be unique and identical to those reported in Schweppe et al. 2008. TPC and CAL62 were grown in DMEM (Dulbecco's Modified Eagle Medium), supplemented with 10% FBS (fetal bovine serum), L-glutamine and penicillin/streptomycin. HUVEC cells were purchased from Lonza and cultured in EBM-2 (Endothelial Cell Basal Medium) medium supplemented with SingleQuote growth supplements (Lonza, Switzerland) up to passage 7.

The generation of TPC-Twist1 and CAL62-shTwist1 cells is described in the attached manuscript II.

#### **3.2 Tissue samples**

Tumors and normal thyroid tissue samples for immunohistochemical analysis were retrieved from the files of the Pathology Department of the Hospital Central de Asturias (Oviedo University, Asturias, Spain) and of the Hospital Clinico Universitario de Santiago de Compostela (Santiago de Compostela University, Galicia, Spain). Tumors and normal thyroid tissue samples for RNA extraction and quantitative RT-PCR were retrieved from the files of the Department of Surgery, University of Pisa (Italy). Detailed histological analysis is described in the attached manuscript II.

#### **3.3 Immunohistochemistry**

The experimental procedure is discussed in detail in the attached manuscript II. Briefly, slides of tumor sections deparaffinized were incubated with a mouse monoclonal antibody against Twist1 (sc-81417, Santa Cruz Biotechnology, USA) and processed according to standard procedures. Cases were

scored as positive when unequivocal brown staining was observed in the nuclei of tumor cells. Immunoreactivity was expressed as the percentage of positively stained target cells in four intensity categories [-, no staining; +, low/weak; ++ moderate/distinct; +++, high/ intense staining].

### **3.4 Microarray analysis**

300 ng purified total RNA from TPC-Twist1 cells (Twist1 mp1, Twist1 mp2, Twist1 C12) and pcDNA control cells was transcribed into cDNA using Superscript RT (Invitrogen), in the presence of T7-oligo (dT) 24 primer, deoxyribonucleoside triphosphates (dNTPs), and T7 RNA polymerase promoter (Invitrogen). An *in vitro* transcription reaction was then performed to generate biotinylated cRNA which, after fragmentation, was used in a hybridization assay on Affymetrix U133 plus 2.0 GeneChip microarrays, according to manufacturer's protocol (GeneChip 3' ivt Express Kit, Affymetrix). The screening was conducted in collaboration with Aarhus Biotechnology (Aarhus, Denmark). Normalization was performed by global scaling and analysis of differential expression was performed by Microarray Suite software 5.0 (Affymetrix). The final results were imported into Microsoft Excel (Microsoft).

### **3.5 Network and gene ontology analysis**

For functional analysis, the set of input genes (158 up-regulated and 221 down-regulated genes) were uploaded into the Ingenuity Pathway Analysis (IPA) online tool (Ingenuity System Inc, [www.ingenuity.com](http://www.ingenuity.com)). IPA is a system that transforms large data sets into a group of relevant networks biological processes, and pathways, containing direct or indirect relationships between genes based on known interactions in the literature. IPA computes a score for each biological process according to the fit of the user's set of significant genes. The score indicates the likelihood of the genes in a biological process to cluster together due to random chance.

### 3.6 RNA extraction, cDNA synthesis, and quantitative real-time PCR

Total RNA was isolated with the RNeasy Kit (Qiagen, Crawley, West Sussex, UK). The quality and concentration of the RNA was verified by the NanoDrop 2005 (Thermo Scientific). One  $\mu\text{g}$  of total RNA from each sample was reverse-transcribed with the QuantiTect® Reverse Transcription (Qiagen) according to manufacturer's instructions. The expression level of each gene was measured by quantitative PCR assay, using the Universal ProbeLibrary Set, Human (Roche). PCR reactions were performed in triplicate and fold changes were calculated with the formula:  $2^{-(\text{sample 1 } \Delta\text{Ct} - \text{sample 2 } \Delta\text{Ct})}$ , where  $\Delta\text{Ct}$  is the difference between the amplification fluorescent thresholds of the mRNA of interest and the mRNA of RNA polymerase 2 used as an internal reference. The primers used were:

- HS6ST2 F: tgcatcttctccaagatttc, HS6ST2 R: cgatcacggcaaataaggaag;
- CD24 F: ggctttggatttgacattgc, CD24 R: tgcttggatctgggtagat;
- COL1A1 F: atgttcagctttgtggacctc, COL1A1 R: ctgtacgcaggtgattggtg;
- KRT7 F: caggctgagatcgacaacatc, KRT7 R: cttggcacgagcatcctt;
- VANGL2 F: gccagccgcttctacaac, VANGL2 R: tctccaggatccacactgc;
- PKP2 F: tgcagaggaaccattgcag, PKP2 R: gggtatgaagaatgcacacaaa;
- F2RL1 F: tgctagcagcctctctctcc, F2RL1 R: aggcttctccttagaggatctatt;
- LEPREL1 F: tgcagattgcttaattccttga, LEPREL1 R: ctcagggttagccacgaaaa;
- THRB F: gggcactggtaatttgcta, THRB R: cagaaggaaatcgagatcc;
- ZBED2 F: gagagaagtccagagccttgc, ZBED2 R: aagcagctcaccatactccac;
- ADAMTS5 F: taagccctgggtccaaatgc, ADAMTS5 R: aggtccagcaaacagttacca;
- ID4 F: tgcagtgcgatatgaacgac, ID4 R: gcaggatctccactttgctg;
- RHOB F: tatgtggccgacattgagg, RHOB R: gcggtcgtagctcctctg;
- PDZK1 F: ccggtctgctatctcgt, PDZK1 R: tcatgtacaccccttttacc
- PDZK1IP1 F: gcagtcaaccacttctggtg, PDZK1IP1 R: gacggtcaggatcatgtgtg;
- RNAPol F: gcgatgagaacaagatgcaa, RNAPol R: cgcaggaagacatcatc;
- Twist1 F: ggctcagctacgccttctc, Twist1 R: ccttctctggaaacaatgacattct.

### 3.7 RNA silencing

TPC-Twist1 cells were transfected with the specific siRNA (Qiagen) in 6-well plate in triplicate. For each transfection, 5  $\mu\text{l}$  of 100 micromolar siRNA (25 nM) were mixed with 20  $\mu\text{l}$  of HiPerFect Transfection reagent (Qiagen) and 300  $\mu\text{l}$  of OptiMem medium (Invitrogen). Following 10 minutes of incubation, the transfection mix was delivered to each well and incubated at 37°C for 72h. Specific siRNAs (Qiagen) used were: siRNA HS6ST2 (SI04269020), siRNA

CD24 (SI04180078), siRNA COL1A1 (SI04434773), siRNA KRT7 (SI04339776), siRNA F2RL1 (SI04435088), siRNA LEPREL1 (SI04265184), siRNA THRB (SI03027535), siRNA ID4 (SI00445389), siRNA RHOB (SI00058912), siRNA PDZK1 (SI04314723), siRNA PDZK1IP1 (SI04164587), and AllStars Negative Control siRNA (SI03650318).

### **3.8 Trypan-Blue assay**

Cells were collected by trypsinization after 48h and 72h of transfection, stained for 10 minutes with 0.4% trypan-blue (Sigma) according to manufacturer's instructions, and counted in triplicate with TC10™ Automated Cell Counter (Bio-Rad, Richmond, VA, USA).

### **3.9 Wound Closure Assay**

A wound was induced on the confluent monolayer cells by scraping a gap using a micropipette tip after 48h of transfection with specific siRNA. Photographs were taken at 10 X magnification using phase-contrast microscopy immediately after wound incision and 24h later. Pixel densities in the wound areas were measured using the Cell<sup>a</sup> software (Olympus Biosystem Gmb) and expressed as percentage of wound closure where 100 % is the value obtained at 24h for control cells.

### **3.10 Transwell migration and Matrigel assay**

The cells suspension ( $1 \times 10^5$  cells) was resuspended in serum free culture medium (100  $\mu$ l) and loaded onto the upper well of prehydrated polycarbonate membrane filter of 8  $\mu$ m pore size (Costar, Cambridge, MA) coated with (invasion assay) or without (migration assay) 35  $\mu$ g of reconstituted extracellular matrix (Matrigel, BD Biosciences, San Jose, CA). Medium (500  $\mu$ l) that contained 2.5% serum was added to the lower well and cells were allowed to migrate or invade for 24h at 37°C. Then cells were fixed with 10% glutaraldehyde solution (Sigma-Aldrich) for 30 minutes, stained with crystal violet in 20% methanol for 30 minutes, mounted on glass slides using mounting medium and stained with Hoechst (Sigma). Cell migration or invasion was quantified by counting the

number of stained nuclei in five individual fields in each transwell membrane, by fluorescence microscopy, in triplicate.

### **3.11 Collagen Migration and Invasion Assay**

The migration into collagen matrix was evaluated with CytoSelected™ 24-Well Cell Haptotaxis Assay (8 µm, Collagen 1-Coated, Colorimetric Format) (Cell Biolabs, San Diego, CA) where Collagen I was present at the bottom side of the insert. The invasion through collagen matrix was evaluated with CytoSelected™ 24-Well Cell Invasion assay (Collagen 1, Colorimetric Format) (Cell Biolabs) where Collagen I was present at the upper side of the insert. The cells suspension ( $1 \times 10^5$  cells) was resuspended in serum free culture medium (300 µl) seeded on the inside of each insert and allow to migrate or invade toward 2.5% FBS for 24h. Migratory or invaded cells were stained and quantified at OD 560 nm after color extraction.

### **3.12 Transendothelial Cell Migration Assay**

Millipore's QCM™ Tumor Cell Transendothelial Migration Assay was used to analyze the ability of tumor cells to invade the endothelium. HUVEC ( $1 \times 10^5$  cells) were grown to confluence for 48h on cell culture inserts coated with fibronectin and then treated with 20 ng/ml of TNF $\alpha$  for 18h. The cells suspension ( $1 \times 10^5$  cells) was resuspended in serum free culture medium (250 µl) added on the endothelial layer and left to migrate for 24h at 37°C. Media (500 µl) that contained 2.5% serum was added to the lower well. Migrated cells were stained and color intensity was measured by OD 560 nm according to the assay instruction.

### **3.13 Statistical analysis**

Data are presented as mean  $\pm$  standard deviation. Two-tailed paired Student's t test (normal distributions and equal variances) was used for statistical analysis. Differences were significant when  $p < 0.05$ . Statistical analyses were carried out using the GraphPad InStat software program (version 3.1a, San Diego, CA).

## 4. RESULTS

### 4.1 Up-regulation of Twist1 in ATC

We evaluated Twist1 expression levels by immunohistochemistry in 157 human tissues including: 15 normal thyroids (NT), 13 PTC, 88 PDC, and 41 ATC samples. The data are detailed in the attached manuscript II. Twist1 was virtually undetectable in NT, PTC, and PDC samples. In contrast, 49% of the ATC samples were positive for Twist1 expression (**Figure 4**).

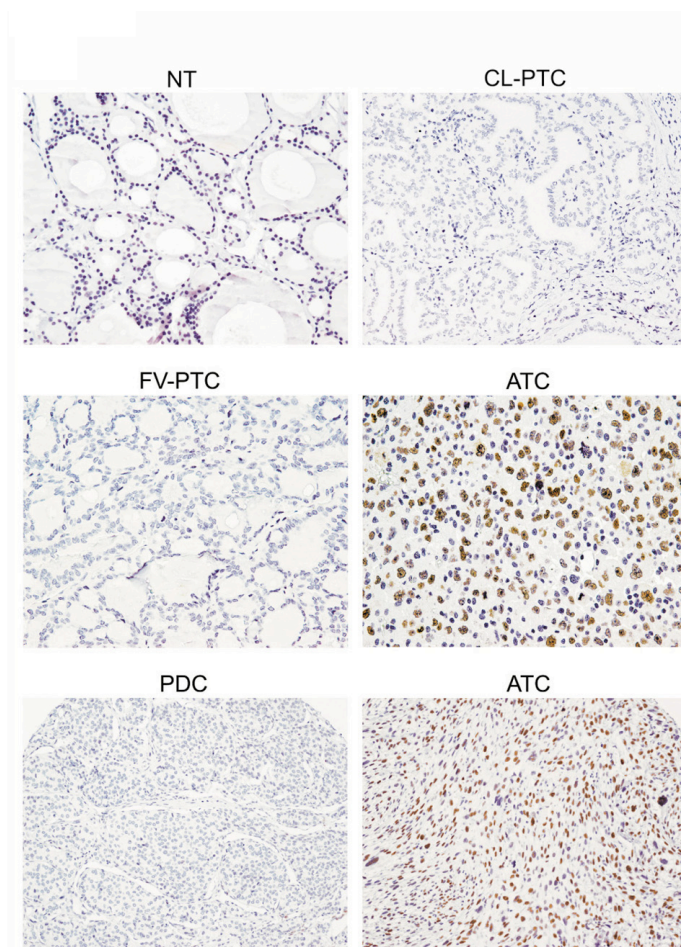


**Figure 4. Immunohistochemical analysis of Twist1 protein expression in normal and malignant thyroid tissues.** Representative histological sections from NT, classical PTC, follicular variant PTC, PDC and ATC stained with a mouse monoclonal anti-Twist1 antibody are shown.



the attached manuscript II). Thus, these data suggest that Twist1 plays a pleiotropic role in determining the anaplastic thyroid cancer phenotype.

#### **4.2 Identification of Twist1 target genes**

To determine the molecular mechanisms by which Twist1 regulates anaplastic thyroid cancer phenotype, we analyzed gene expression profiles in TPC-Twist1 cells in comparison to control cells. Total RNA extracted from three TPC-Twist1 stable transfectants (Twist1 mp1, Twist1 mp2 and Twist1 Cl2) was used to examine gene expression profile in comparison to vector control cells (pcDNA). The screening was conducted in collaboration with Aarhus Biotechnology (Aarhus, Denmark) using the human Genome U133 Plus 2.0 Array GeneChips (Affymetrix) containing > 47,000 gene transcripts. We analyzed only the genes that were changed in all the three Twist1 transfectants compared to vector control cells. Genes were analyzed only if the signal intensity was  $\geq 50$ . We found 158 genes up-regulated (attached Table 1) and 221 down-regulated (attached Table 2) by more than 1.5 fold in TPC-Twist1 cells compared to control cells.

We used the Ingenuity pathways Analysis (IPA) (Ingenuity Systems, [www.ingenuity.com](http://www.ingenuity.com)) to classify Twist1 target genes. Consistent with the biological function of Twist1 in ATC, the top three molecular and cellular bio functions enriched in TPC-Twist1 cells compared to vector control were: cellular movement, cellular growth and proliferation, cell death and survival (**Figure 6**). Other top bio functions enriched were: cancer, reproductive system disease, tissue development, tumor morphology (**Figure 6**).

Top Bio Functions		
<b>Diseases and Disorders</b>		
Name	p-value	# Genes
Cancer	7,23E-11 - 2,65E-03	200
Reproductive System Disease	9,36E-08 - 2,15E-03	115
Skeletal and Muscular Disorders	1,39E-05 - 2,65E-03	13
Inflammatory Response	3,09E-05 - 2,49E-03	60
Endocrine System Disorders	6,39E-05 - 1,46E-04	31
<b>Molecular and Cellular Functions</b>		
Name	p-value	# Genes
Cellular Movement	7,73E-09 - 2,49E-03	115
Cellular Growth and Proliferation	2,05E-08 - 2,65E-03	160
Cell Death and Survival	3,01E-08 - 2,65E-03	155
Cellular Assembly and Organization	4,00E-07 - 2,65E-03	88
Cellular Function and Maintenance	4,00E-07 - 2,65E-03	141
<b>Physiological System Development and Function</b>		
Name	p-value	# Genes
Tissue Development	4,00E-07 - 2,65E-03	94
Tumor Morphology	4,54E-07 - 2,65E-03	49
Cardiovascular System Development and Function	4,89E-06 - 2,65E-03	70
Lymphoid Tissue Structure and Development	8,26E-06 - 2,27E-03	40
Tissue Morphology	8,26E-06 - 2,65E-03	65

(c) 2000-2012 Ingenuity Systems, Inc. All rights reserved.

INGENUITY  
SYSTEMS

**Figure 6. Summary of IPA's analysis.** List of Top Bio Function is divided in three different categories: Disease and Disorders, Molecular and Cellular Function, Physiological System Development and Function. The number of genes and p values corresponding to each single function are indicated on the right side.

In detail 53.6% (203/379) of the genes that changed 1.5 fold, belonged to: Cellular Movement, Cellular Growth and Proliferation, Cell Death and Survival. 17.6% (67/379) belonged to other top functions (mainly to cancer) and 28.7% (109/379) of genes were not classified (**Figure 7**).

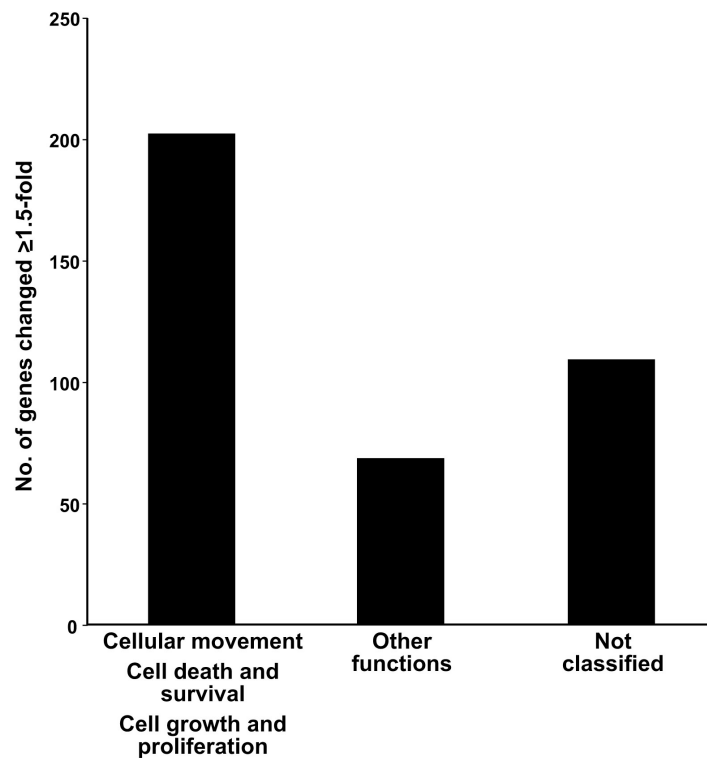


**Figure 7. Graphic representation of IPA's classification.** The number of the genes is reported on y axis.

There was no difference in the distribution in the different groups among up-regulated and down-regulated genes (data not shown).

Among the top three molecular and cellular function: ~33.5% of the genes were common to all three categories (Cellular Growth and Proliferation/ Cell Death and Survival/ Cellular Movement), ~28.6% were present in two different categories, and ~38% of the genes was present in a single category (**Figure 8**).

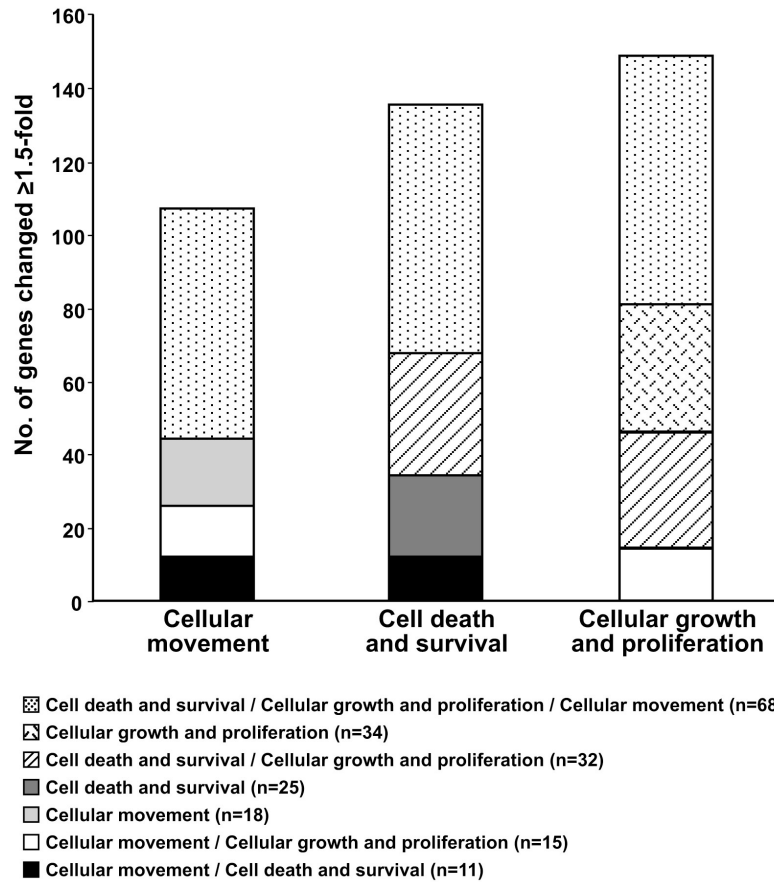


**Figure 8. Graphic representation of IPA's classification.** The number of the genes is reported on y axis.

This work has been focused on the up-regulated genes, because more is known about the role of Twist1 as transcriptional activator. We studied the up-regulated genes by  $\geq 4$  fold (**Table 3**). PDZK1IP1, up-regulated  $\sim 3$  fold, was also studied because it is the interacting protein of PDZK1, a gene up-regulated by 3.99 fold (Carnero 2012) (**Table 3**).

**Table 3.** List of top up-regulated genes  $\geq 4$  fold.

Gene	Fold Change	IPA Molecular and Cellular Bio Function
HS6ST2	10.28	Cellular Growth and Proliferation
CD24	8.66	Cellular Growth and Proliferation/ Cell Death and Survival/ Cellular Movement
COL1A1	7.22	Cellular growth and Proliferation/ Cell Death and Survival/ Cellular Movement
GFRA1	6.91	Cellular growth and Proliferation/ Cell Death and Survival/ Cellular Movement
KRT7	5.56	Cellular growth and Proliferation/ Cellular Movement
VANGL2	5.48	Cellular Assembly and Organization/ Cellular Function and Maintenance
MXRA8	5.41	Cancer
PKP2	5.33	Cellular Assembly and Organization
F2RL1	5.31	Cellular growth and Proliferation/ Cell Death and Survival/ Cellular Movement
LEPREL1	4.99	Cellular Growth and Proliferation
THRB	4.88	Cellular growth and Proliferation/ Cellular Movement
ZBED2	4.59	Not Classified
ADAMTS5	4.36	Cancer
ID4	4.33	Cellular growth and Proliferation/ Cell Death and Survival
RHOB	4.13	Cellular Growth and Proliferation/ Cell Death and Survival/ Cellular Movement
PDZK1	3.99	Cellular Growth and Proliferation/ Cell Death and Survival
PDZK1IP1	2.90	Cellular Growth and Proliferation

Initially, we confirmed the microarray data by performing quantitative RT-PCR of the top 17 up-regulated genes, in the cell lines used in the screening in comparison to vector control cells. As shown in **Figure 9**, the quantitative RT-PCR confirmed the microarray screening, albeit with some variability in the different Twist1 clones. The expression of MXRA8 and GFRA1 was undetectable by quantitative RT-PCR and thus these genes were not further studied.

### TPC-1

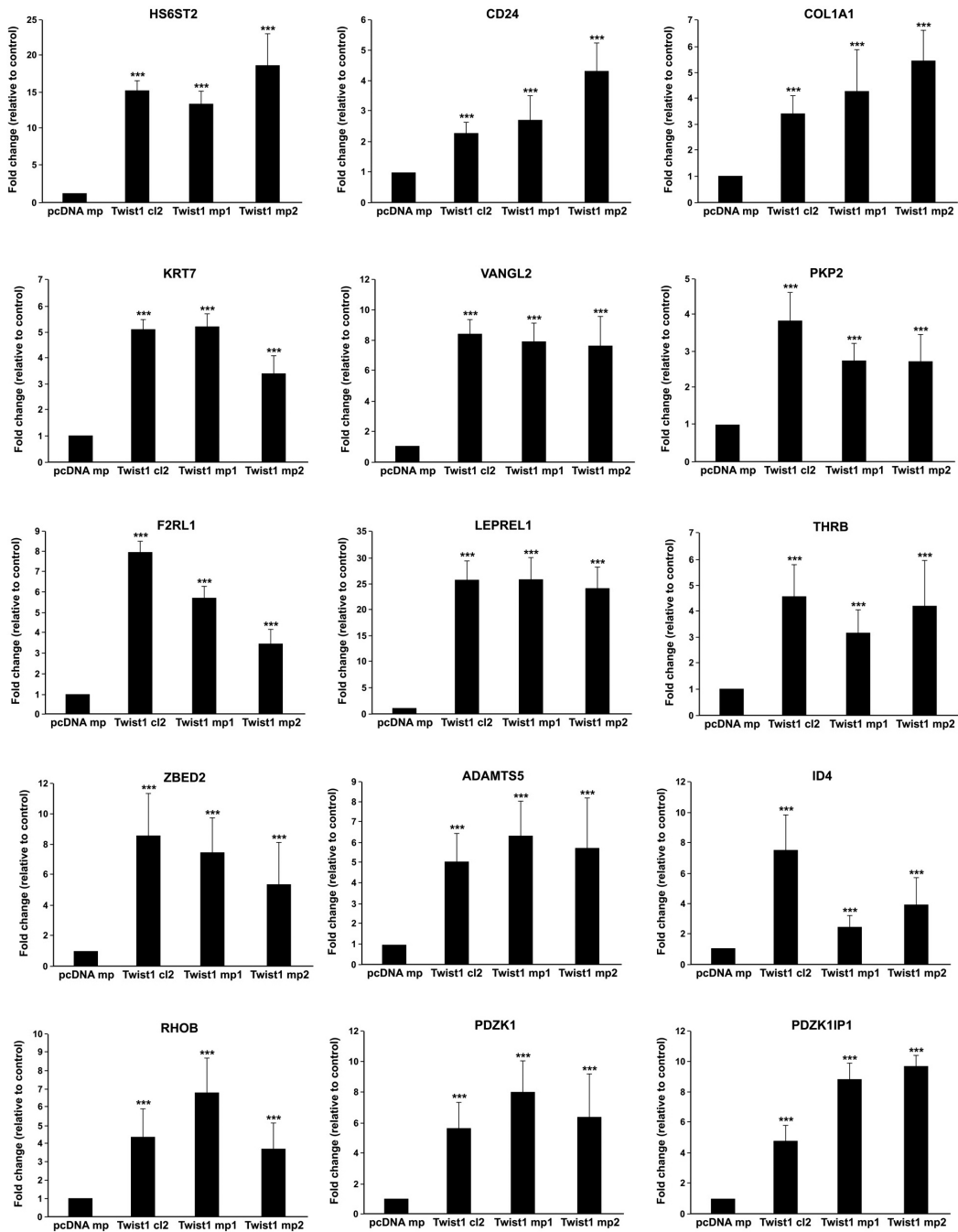


**Figure 9. Quantitative RT-PCR in TPC-Twist1 cells.** Quantitative RT-PCR of the indicated genes in TPC-Twist1 cells in comparison to vector control cells (pcDNA mp). Values represents the average of triplicate experiments  $\pm$  standard deviations. Asterisks indicate  $p < 0.001$  (\*\*\*)

### 4.3 Down-regulation of the Twist1 target genes in CAL62-shTwist1 cells

To further confirm that Twist1 transcriptionally regulates these genes, we studied whether silencing of Twist1 affected their expression levels. Thus, we performed quantitative RT-PCR of the top 15 up-regulated target genes in the ATC, CAL62 cell line stably transfected with an shTwist1 plasmid. CAL62 cell line presents high endogenous level of Twist1 (attached manuscript II). In CAL62-shTwist1 cells, Twist1 mRNA was down-regulated of ~ 2 fold (**Figure 10**) and Twist1 ablation affected several hallmarks of malignancy, including anchorage independent proliferation, survival, and invasion (attached manuscript II).

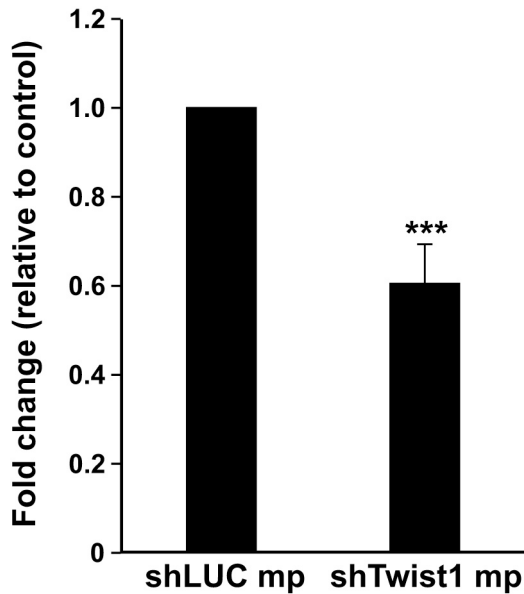


**Figure 10. Quantitative RT-PCR of Twist1 in CAL62 sh-Twist1 cells.** Quantitative RT-PCR of Twist1 in CAL62 sh-Twist1 cells in comparison to vector control cells (shLUC mp). Values represents the average of triplicate experiments  $\pm$  standard deviations. Asterisks indicate  $p < 0.001$  (\*\*\*).

As shown in **Figure 11**, transfection of CAL62 with a Twist1 shRNA promoted a blunted expression of mRNAs of up-regulated genes respect to the control cell ( $p < 0.001$ ).

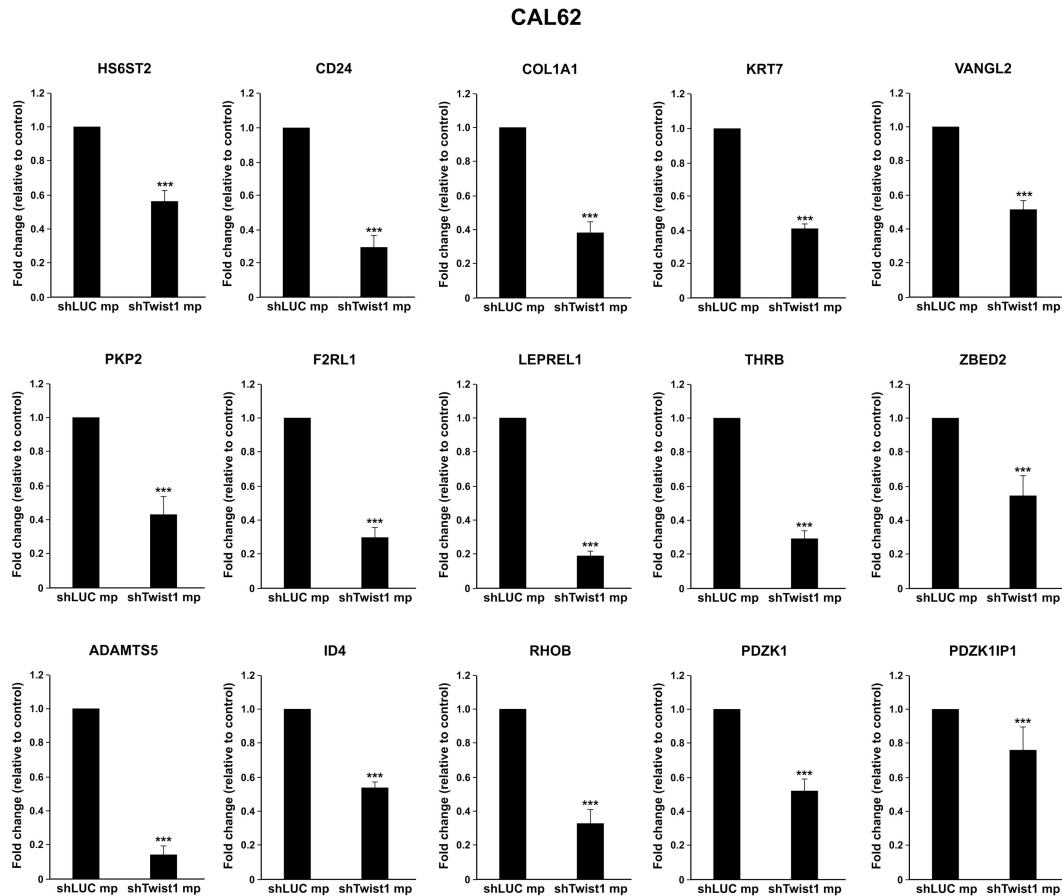


**Figure 11. Quantitative RT-PCR in CAL62-shTwist1 cells.** Quantitative RT-PCR of the indicated genes in CAL62-shTwist1 cells in comparison to control. Values represents the average of triplicate experiments  $\pm$  standard deviations. Asterisks indicate  $p < 0.001$  (\*\*\*)

#### 4.4 Silencing of Twist1 positive targets in TPC-Twist1 cells impairs cell viability

Of the top 15 up-regulated genes confirmed by RT-PCR, VANGL2, PKP2, ADAMTS5 that belong to other top functions or ZBED2 that was not classified by the IPA's software (**Table 3**), were not further studied.

Thus, we transiently transfected TPC-Twist1 cells with siRNA of *HS6ST2*, *CD24*, *COL1A1*, *KRT7*, *F2RL1*, *LEPREL1*, *THRB*, *ID4*, *RHOB*, *PDZK1*, *PDZK1IP1* or a scrambled siRNA and examined at 48 and 72 hours post-transfection cell viability using trypan blue assay. As shown in **Figure 12A**, transient silencing of these genes decreased cell number in TPC-Twist1 cells at

different time points. Silencing of *COL1A1*, *KRT7* and *PDZK1* increased also the cell death (in particular at 72 hours post-transfection).

Then, we verified by quantitative RT-PCR that the specific siRNA silenced the corresponding gene. Transfection of siRNA of *HS6ST2*, *CD24*, *COL1A1*, *KRT7*, *F2RL1*, *LEPREL1*, *THRB*, *ID4*, *RHOB*, *PDZK1* and *PDZK1IP1* in TPC-Twist1 cells efficiently down-regulated the specific gene, albeit with some variability ( $p < 0.001$ ) (**Figure 12B**).

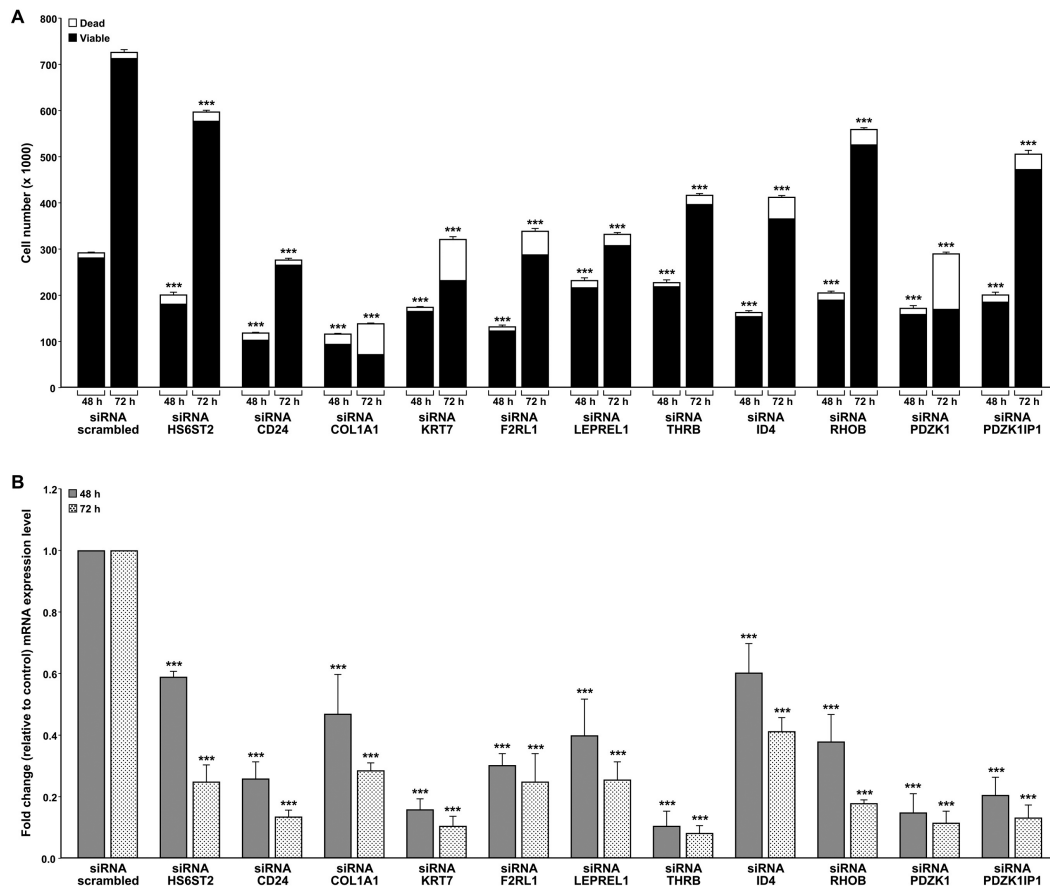


**Figure 12. Silencing of the top 11 genes impairs cell viability.** **A.** TPC-Twist1 cells were transfected with indicated siRNA or scrambled siRNA; after 48 and 72 hours, cells were collected by trypsinization, stained for 10 min with trypan-blue and counted. **B.** Cells were transiently transfected with the indicated siRNA. After 48 and 72 hours RNA was extracted and mRNA expression levels were measured by quantitative RT-PCR. Results are reported as fold change in comparison to the scrambled control. Values represents the average of triplicate experiments  $\pm$  standard deviations. Asterisks indicate  $p < 0.001$  (\*\*\*)

#### **4.5 Silencing of HS6ST2, THRB, ID4, RHOB and PDZK1IP1 in TPC-Twist1 cells impairs cell migration**

Another of the most enriched molecular and cellular functions in TPC-Twist1 cells was cellular movement. Thus, to study whether the silencing of top up-regulated genes impaired the cell migration ability, we performed a wound closure assay. We selected *HS6ST2*, *THRB*, *ID4*, *RHOB* and *PDZK1IP1* because silencing of these genes affected the cell viability less than the silencing of the other genes (**Figure 12**).

A scraped wound was introduced on the confluent monolayer of TPC-Twist1 cells transfected with specific siRNAs or scrambled siRNA, and the cell migration into the wound was monitored after 24 hours. Wound closure was measured by calculating pixel densities in the wound area using Cell<sup>a</sup> software (Olympus Biosystem Gmb) and expressed as percentage of wound closure of triplicate areas  $\pm$  standard deviations. TPC-Twist1 cells transfected with the scrambled control efficiently migrated into the wound; by contrast, cells transfected with *HS6ST2*, *THRB*, *ID4*, *RHOB* and *PDZK1IP1* siRNA had a reduced migrating ability ( $p < 0.001$ ) (**Figure 13A**). The result was particularly evident in TPC-Twist1 transfected with siRNA of *RHOB* or *PDZK1IP1* (**Figure 13A**). Quantitative analysis of wound closure assay is shown in **Figure 13B**.

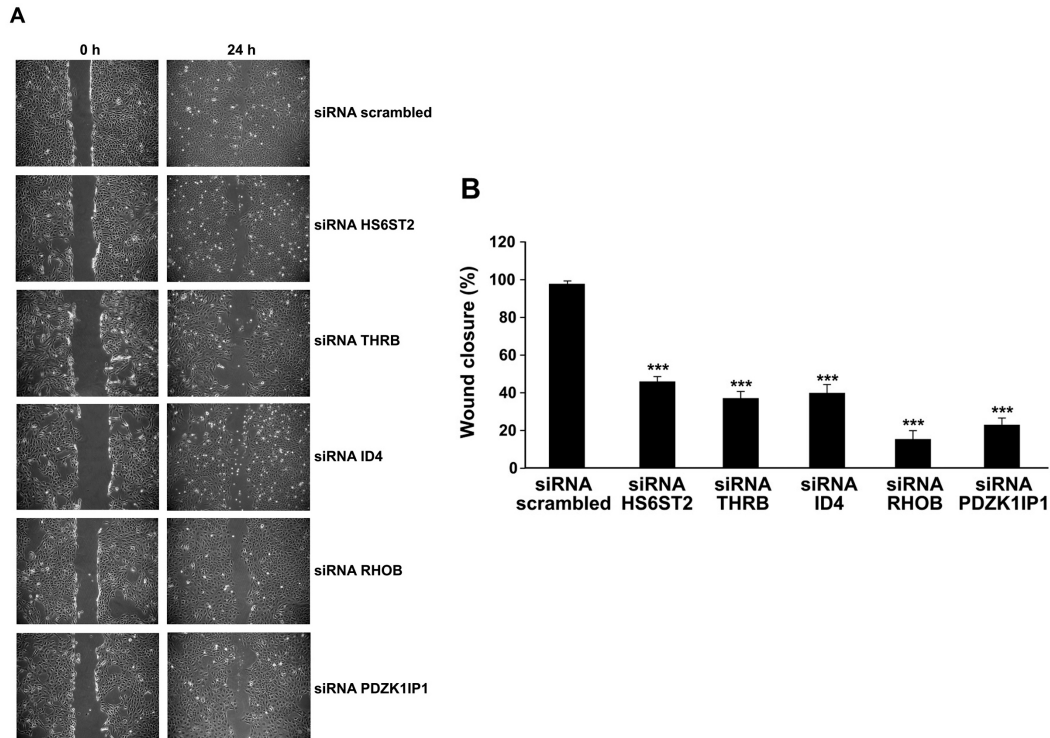


**Figure 13. Silencing of indicated genes reduces the migration ability through the wound of TPC-Twist1 cells.** **A.** Cells were transfected with specific siRNA, 48h post transfection scratch wounds were inflicted on confluent cell monolayer and after 24h cells were photographed. **B.** Wound closure was measured by calculating pixel densities in the wound area and expressed as percentage of wound closure of triplicate areas  $\pm$  standard deviations. Asterisks indicate  $p < 0.001$  (\*\*\*)

To further study the effect of the silencing of *HS6ST2*, *THR*, *ID4*, *RHOB* and *PDZK1IP1* on cell migration ability, we performed a transwell migration assay. TPC-Twist1 cells were transfected with specific siRNA or scrambled control, 48 hours post transfection cells were collected, counted and plated on top of transwell insert. The lower chambers were filled with media that contained 2.5% serum. Cells were allowed to migrate for 24h (**Figure 14A**) and quantified by counting the number of migrated cells in three different fields (**Figure 14B**). The transwell migration assay showed that silencing of *HS6ST2*, *THR*, *ID4*, *RHOB* and *PDZK1IP1* reduced the number of migrated cells, and in particular the silencing of *RHOB* decreased the ability to migrate in transwell of ~49%.

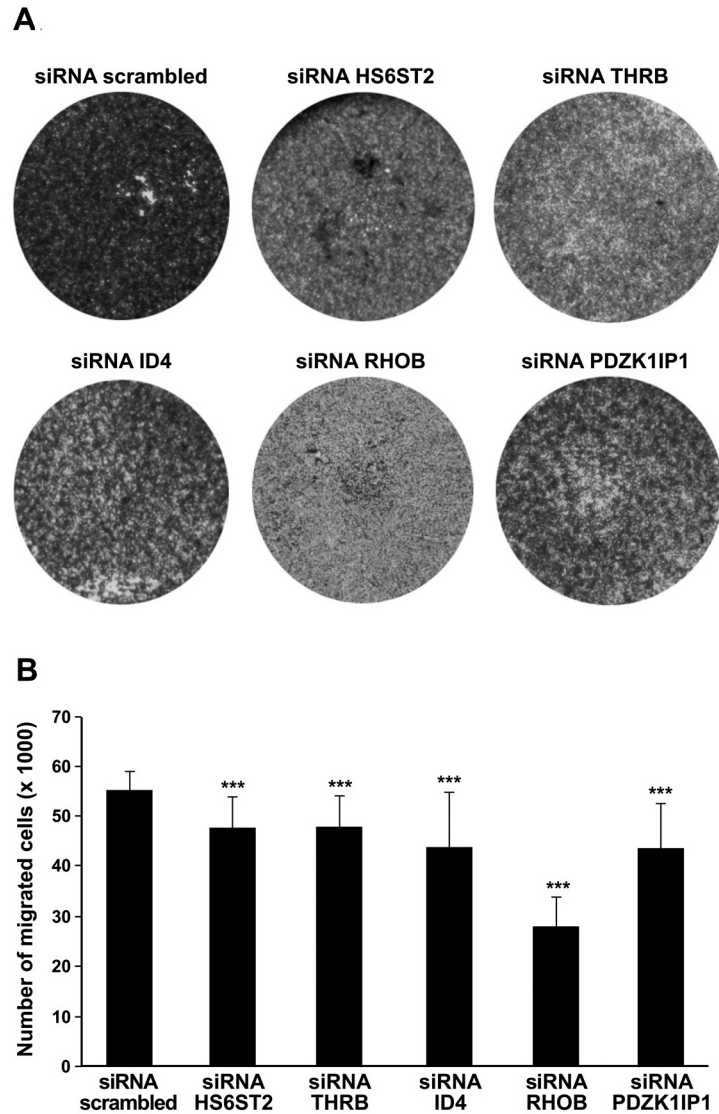


**Figure 14. Silencing of indicated genes reduces the migration ability through the transwell of the TPC-Twist1 cells.** **A.** 48h post-transfection cells were seeded in upper chamber of transwells and allowed to migrate for 24h. The upper surface of the filter was wiped clean, and cells on the lower surface were stained and counted in three different fields. **B.** Migration ability was expressed as number of migrated cells. Values represents the average of triplicate experiments  $\pm$  standard deviations. Asterisks indicate  $p < 0.001$  (\*\*\*)

## Silencing of *HS6ST2*, *THRB*, *ID4*, *RHOB* and *PDZK1IP1* in TPC-Twist1 cells impairs cell migration in Collagen I matrix

To further investigate the migration ability of these cells, we evaluated the migration rate through the Collagen I matrix.

We initially evaluated TPC-Twist1 cells ability to migrate within collagen I matrix. TPC-Twist1 and control cells (pcDNA), were plated onto the polycarbonate membrane inserts coated with Collagen I matrix at the bottom side. After 24 hours migrated cells on the bottom of the polycarbonate membrane were stained, photographed (**Figure 15A**) and quantified at OD 560 nm after color extraction (**Figure 15B**). As shown in **Figure 15**, Twist1 increased (~2 fold) the ability of TPC cells to migrate into Collagen I matrix.

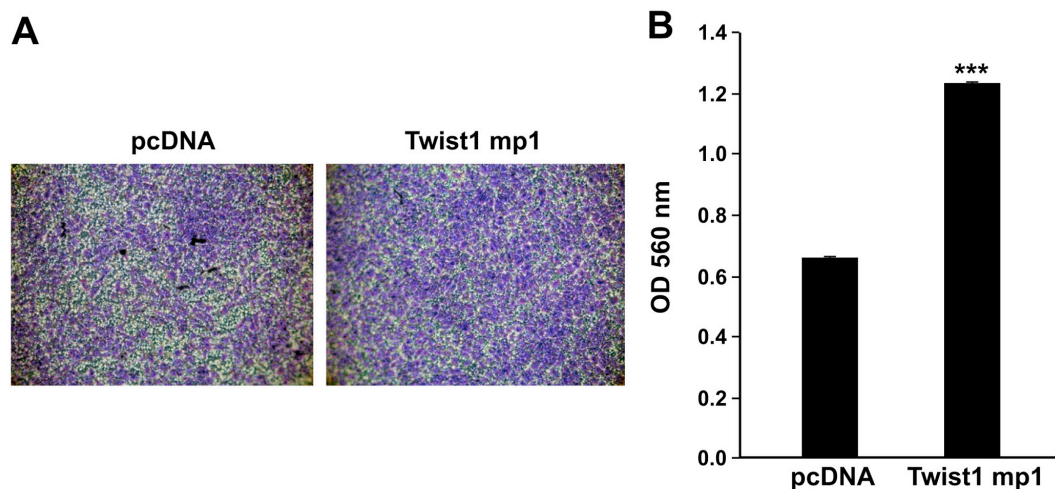


**Figure 15. Twist1 increases the ability of TPC cells to migrate in collagen I matrix.**

**A.** Cells were seeded onto the insert and incubated for 24h. After 24h cells were stained and photographed. **B.** Migration ability was expressed as absorbance at OD 560 nm. Values represent the average of triplicate experiments  $\pm$  standard deviations. Asterisks indicate  $p < 0.001$  (\*\*\*)

Then, we studied whether the silencing of *HS6ST2*, *THRB*, *ID4*, *RHOB* and *PDZK1IP1* affected the ability of TPC-Twist1 cells to migrate into Collagen I matrix. TPC-Twist1 cells were transfected with specific siRNA or scrambled control and after 48 hours, cells were collected, counted and plated on the insert. After 24 hours of incubation, cells were colored and photographed (**Figure 16A**) and quantified by measuring the absorbance at OD 560 nm (**Figure 16B**).

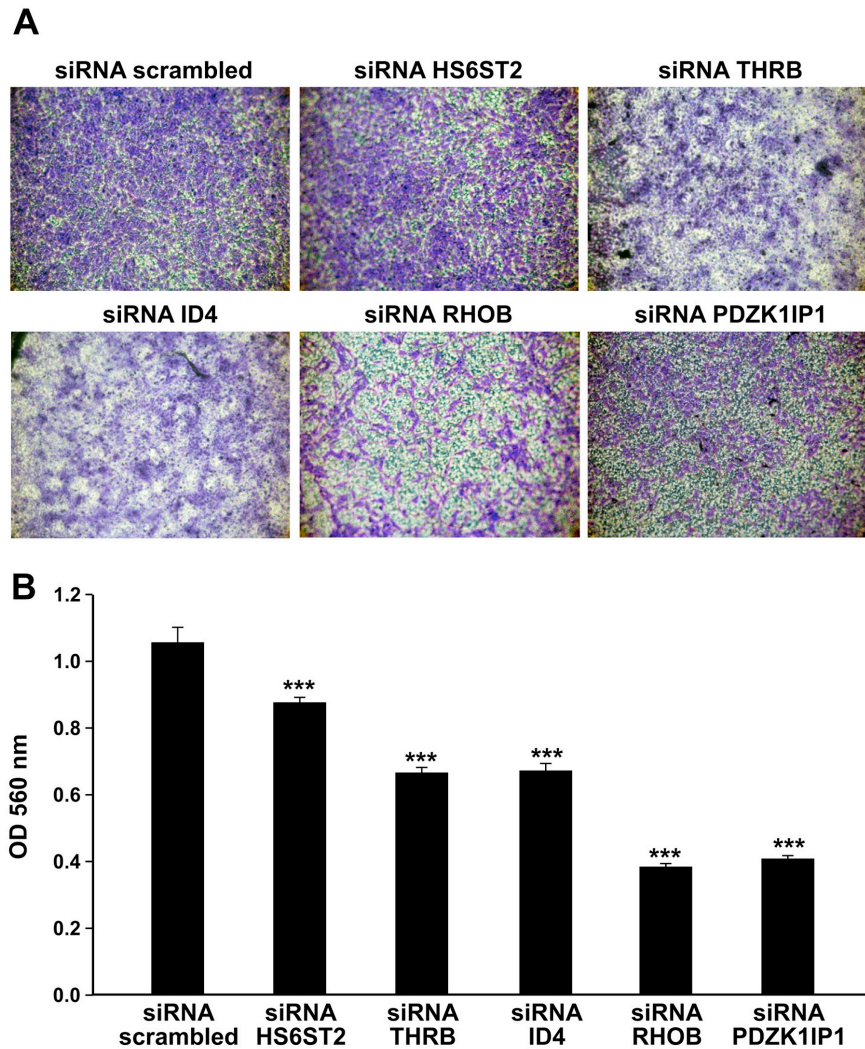


**Figure 16. Silencing of indicated genes reduces the migration ability through the Collagen I matrix of the TPC-Twist1 cells. A.** Forty-eight hours post-transfection cells were seeded on the insert coated with Collagen I matrix at the bottom side and allowed to migrate for 24h. Then, cells were stained and photographed. **B.** Migration ability was expressed as absorbance at OD 560 nm. Values represent the average of triplicate experiments  $\pm$  standard deviations. Asterisks indicate  $p < 0.001$  (\*\*\*)

TPC-Twist1 cells transfected with *HS6ST2*, *THR*, *ID4*, *RHOB* and *PDZK1IP1* siRNA presented a decreased ability to migrate in Collagen I matrix compared to siRNA scrambled transfected cells. In particular the silencing of *RHOB* and *PDZK1IP1* reduced the migration ability in Collagen I matrix of ~64% and ~62% respectively.

#### 4.6 Silencing of *HS6ST2*, *THRB*, *ID4*, *RHOB* and *PDZK1IP1* in TPC-Twist1 cells impairs cell invasion

We asked whether TPC-Twist1 cells were more or less able to invade the Collagen I matrix compare to TPC-pcDNA vector control cells.

Thus TPC-Twist1 and TPC-pcDNA cells were plated on the membrane insert coated at the upper surface with a uniform layer of dried Bovine Type I Collagen matrix, and allowed to invade for 24 hours. Hence cells were stained (**Figure 18 A**) and quantified (**Figure 18 B**). As shown in the figure below, Twist1 increased the ability of TPC cells to invade the Collagen I matrix of ~2 fold.

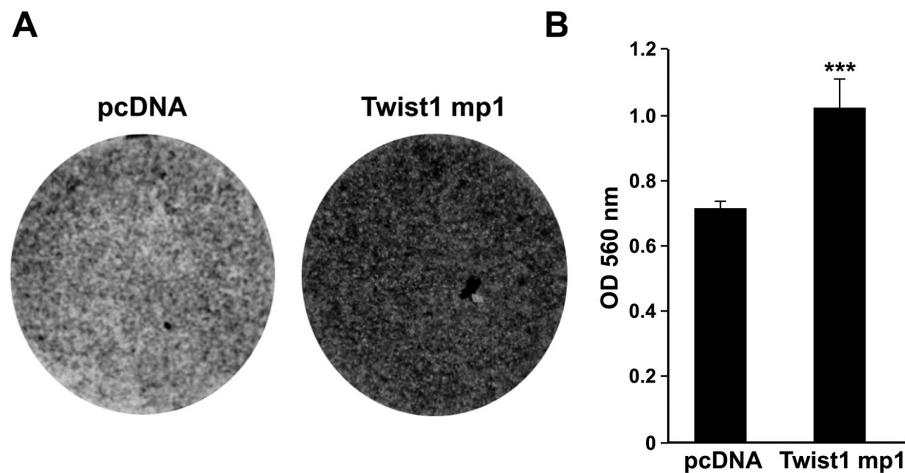


**Figure 18. Twist1 increases the ability of TPC cells to invade the Collagen I matrix.**

**A.** TPC-Twist1 and TPC-pcDNA cells were seeded on insert and allowed to invade for 24h. **B.** Invasive ability was expressed as absorbance at OD 560 nm. Values represents the average of triplicate experiments  $\pm$  standard deviations. Asterisks indicate  $p < 0.001$  (\*\*\*)

Then, TPC-Twist1 cells were transfected with *HS6ST2*, *THRB*, *ID4*, *RHOB* and *PDZK1IP1* siRNA or with siRNA scrambled for 48 hours and then were plated into the chamber coated with Collagen I matrix. After 24 hours of invasion, cells were stained, photographed (**Figure 19 A**) and quantified at OD 560 nm (**Figure 19 B**). The silencing of *HS6ST2*, *THRB*, *ID4*, *RHOB* and *PDZK1IP1* reduced the ability of TPC-Twist1 cells to invade the Collagen I matrix compared to cells transfected with scrambled siRNA. In particular silencing of *RHOB* reduced the ability to invade the Collagen I matrix of ~32%.

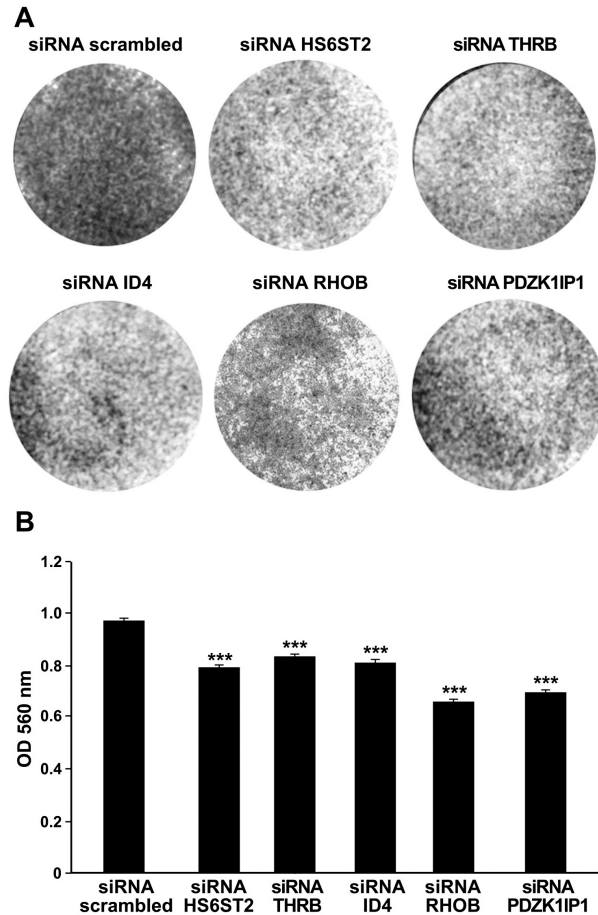


**Figure 19. Silencing of indicated genes reduces the invasion ability in Collagen I matrix of TPC-Twist1 cells.** **A.** TPC-Twist1 cells were seeded in the upper chamber of transwells coated with Collagen I matrix and incubated for 24 hours; the upper surface of the filter was wiped clean and cells on the lower surface were stained and counted. **B.** Invasive ability was expressed as absorbance at OD 560 nm. Values represents the average of triplicate experiments  $\pm$  standard deviations. Asterisks indicate  $p < 0.001$  (\*\*\*)

Silencing of HS6ST2, THR, ID4, RHOB and PDZK1IP1 in TPC-Twist1 cells impairs cell invasion in Matrigel

Twist1 increased the invasion ability of TPC cells of about 5 fold in Matrigel (attached manuscript II). Thus, we transfected TPC-Twist1 cells with *HS6ST2*, *THR*, *ID4*, *RHOB* and *PDZK1IP1* siRNA or with scrambled siRNA. At 48 hours post transfection cells were seeded into the top chamber of transwells coated with Matrigel. The cells were allowed to invade for 24 hours and

photographed (**Figure 17 A**). The quantification of the assay was performed by counting the number of invaded cells in three different fields (**Figure 17 B**).

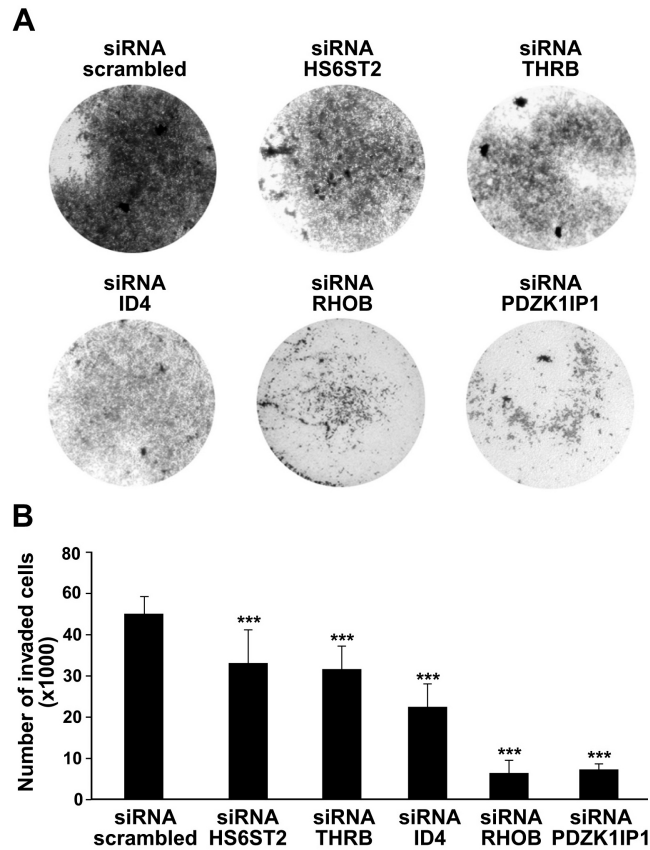


**Figure 17. Silencing of indicated genes reduces the invasion ability in Matrigel of the TPC-Twist1 cells.** **A.** TPC-Twist1 transfected cells were seeded in the upper chamber of transwells coated with Matrigel and incubated for 24 hours; the upper surface of the filter was wiped clean and cells on the lower surface were stained and counted. **B.** Invasive ability was expressed as number of invaded cells. Values represents the average of triplicate experiments  $\pm$  standard deviations. Asterisks indicate  $p < 0.001$  (\*\*\*)

The TPC-Twist1 cells transfected with *HS6ST2*, *THR B*, *ID4*, *RHOB* and *PDZK1IP1* specific siRNA presented a reduced ability to invade Matrigel compared to siRNA scrambled transfected cells. In particular the silencing of *RHOB* and *PDZK1IP1* induced a dramatic reduction of ~86% and ~84% respectively, of invasion ability.

#### 4.7 Silencing of *HS6ST2*, *THRB*, *ID4*, *RHOB* and *PDZK1IP1* in TPC-Twist1 cells impairs transendothelial cell migration

The cell ability to penetrate into the endothelium represents another important aspect of tumor progression. In order to investigate this phenomenon we performed a transendothelial cell migration assay.

To this aim, the endothelial cell line HUVEC, was plated and allowed to grow to confluence on 8  $\mu\text{m}$  pore size cell culture insert coated with fibronectin. HUVEC cells were then activated with  $\text{TNF}\alpha$  for 18 hours. TPC-Twist1 and control TPC-pcDNA cells were plated on confluent monolayer of activated HUVEC cells and allowed to migrate for 24 hours. After 24 hours, cells were stained (**Figure 20 A**) and quantified by measuring the absorbance at OD 560 nm (**Figure 20 B**). TPC-Twist1 cells presented an increased ability to migrate through endothelial cells compared to control cells. HUVEC cells did not migrate.

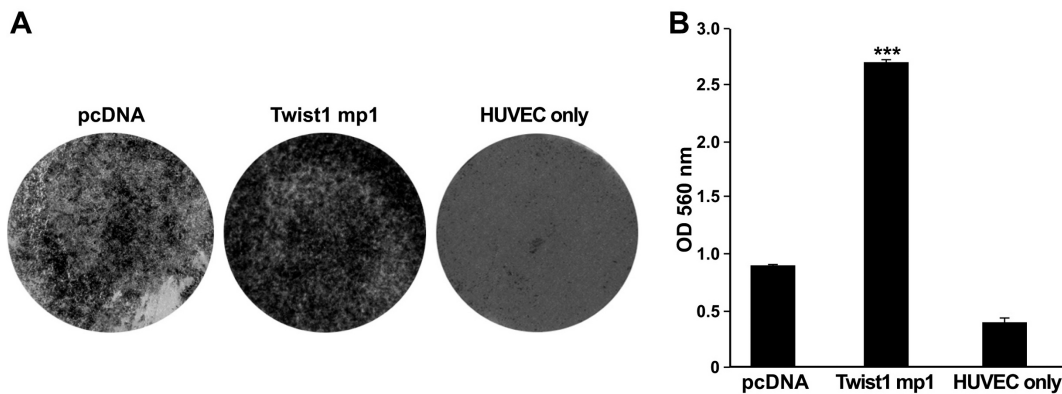


**Figure 20. Twist1 increased the ability of TPC cells to migrate through endothelium cells. A.** Cells were seeded on confluent monolayer of endothelial HUVEC cells and incubated for 24h. After 24h cells were stained and photographed. HUVEC only was used as negative control. **B.** Quantification of the assay, migration ability was expressed as absorbance at OD 560 nm. Values represents the average of triplicate experiments  $\pm$  standard deviations. Asterisks indicate  $p < 0.001$  (\*\*\*)).

Then we studied whether the silencing of *HS6ST2*, *THRB*, *ID4*, *RHOB* and *PDZK1IP1* affected the ability to migrate through endothelial cells.

TPC-Twist1 cells were transfected with specific siRNA for 48 hours and then plated on confluent monolayer of activated HUVEC cells and left to migrate for 24 hours. Migrated cells were stained, photographed (**Figure 21 A**) and quantified at OD 560 nm (**Figure 21 B**). As it is shown in figure 21, TPC-Twist1 cells transfected with *HS6ST2*, *THRB*, *ID4* and *PDZK1IP1* siRNA presented a

modest decrease in the transendothelial cell migration ability compared to cells transfected with scrambled siRNA. Noteworthy, silencing of *RHOB* decreased this ability of ~35%.

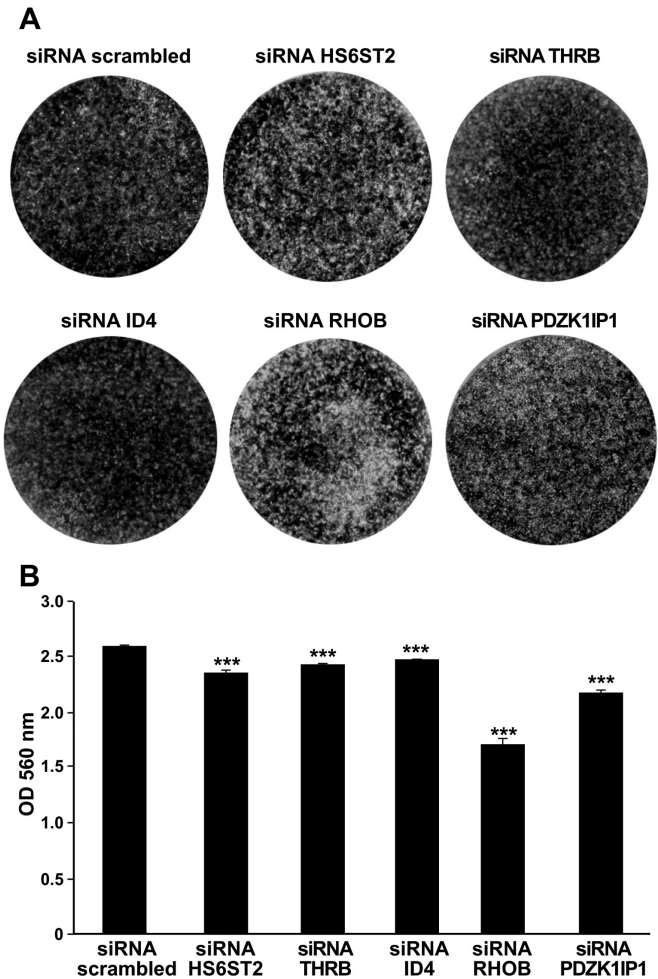


**Figure 21. Silencing of indicated genes reduces the migration ability through endothelial cells of the TPC-Twist1 cells. A.** Cells were seeded on confluent monolayer of endothelial HUVEC cells 48h post-transfection and left to migrate for 24h. Then, cells were stained and photographed. **B.** Migration ability was expressed as absorbance at OD 560 nm. Values represents the average of triplicate experiments  $\pm$  standard deviations. Asterisks indicate  $p < 0.001$  (\*\*\*)

## 5. DISCUSSION

Thyroid cancer includes tumor types as different as well differentiated carcinomas that have a very good prognosis and undifferentiated carcinomas or ATC that are among the most aggressive human cancers and present a dismal prognosis. The molecular players sustaining such aggressive behavior are largely unknown.

In this Dissertation, we have demonstrated that Twist1 is up-regulated in ATC and that silencing of Twist1 by RNA interference in ATC cells reduced cell migration and invasion and increased sensitivity to apoptosis. The ectopic expression of Twist1 in thyroid carcinoma cells induced resistance to apoptosis and increased cell migration and invasion (attached manuscript II).

Although some direct and indirect targets of Twist1 have been identified, the exact mechanisms through which Twist1 contributes to tumorigenesis are still largely unknown. This Dissertation focused on the identification of Twist1 target genes in thyroid carcinoma cells. To this aim, we have performed a gene expression profile of Twist1 overexpressing cells in comparison to control cells. Gene signature obtained was enriched for genes involved in cellular movement, cellular growth and proliferation, cell death and survival consistent with the role of Twist1 in anaplastic thyroid cancer cells.

We focused on the up-regulated genes because more is known about the role of Twist1 as transcriptional activator. The top up-regulated genes by more than 4 fold studied were: *HS6ST2*, *CD24*, *COL1A1*, *KRT7*, *F2RL1*, *LEPREL1*, *THRB*, *ID4*, *RHOB*, *PDZK1*, *PDZK1IP1*.

*HS6ST2* is a member of the heparan sulfate (HS) sulfotransferase gene family. Heparan sulfate proteoglycans are ubiquitous components of the cell surface, extracellular matrix, and basement membranes, and interact with various ligands to influence cell growth, differentiation, adhesion, and migration. *HS6ST2*, catalyze the transfer of sulfate to HS (Song et al. 2011).

*CD24* is a glycosylphosphatidylinositol-anchored membrane protein with a small protein core and a high level of glycosylation. It is overexpressed in many human carcinomas and is correlated with poor prognosis. *CD24* is a marker for pancreatic and ovarian cancer stem cells, whereas breast cancer stem cells are negative for *CD24*. *CD24* has been shown to recruit adhesion molecules to lipid rafts, thereby contributing to tumor cell migration, dissemination and metastasis (Bretz et al. 2012).

*COL1A1* encodes the pro-alpha1 chains of type I collagen whose triple helix comprises two alpha1 chains and one alpha2 chain (Speakman 1968).

*KRT7* is a member of the keratin gene family. The type II cytokeratins consist of basic or neutral proteins which are arranged in pairs of heterotypic

keratin chains coexpressed during differentiation of simple and stratified epithelial tissues (Harbaum et al. 2011).

*F2RL1*, also known as *PAR2*, is a member of the large family of 7-transmembrane-region receptors that couple to guanosine-nucleotide-binding proteins. *F2RL1* is also a member of the protease-activated receptor family (Zhang et al. 2012).

*LEPREL1* encodes a member of the prolyl 3-hydroxylase subfamily of 2-oxo-glutarate-dependent dioxygenases. These enzymes play a critical role in collagen chain assembly, stability and cross-linking by catalyzing post-translational 3-hydroxylation of proline residues (Fernandes et al. 2011).

*THRB* is a nuclear hormone receptor for triiodothyronine. It is one of the several receptors for thyroid hormone, and has been shown to mediate the biological activities of thyroid hormone (Kim and Cheng 2012).

*ID* proteins (*ID*-1 to 4) are dominant negative regulators of basic helix-loop-helix transcription factors. They play a key role during development, preventing cell differentiation while inducing cell proliferation. They are poorly expressed in adult life but can be reactivated in tumorigenesis. Several evidences indicate that *ID* proteins are associated with loss of differentiation, unrestricted proliferation and neoangiogenesis in diverse human cancers (Dell'Orso et al. 2010).

*RHOB* is a member of the Ras superfamily small GTPases. Overexpression of RHO GTPases in human tumors often correlates with a poor prognosis. Furthermore, coordinated RHO GTPase signaling is considered to be part of mechanism underlying tumor cell invasion (Street et al. 2011).

*PDZK1* is a member of the Na<sup>+</sup>/H<sup>+</sup> exchanger regulatory family (NHERF) and is a multi-PDZ domain containing protein, possessing four PDZ domains. These domains facilitate the interaction of *PDZK1* with a range of binding partners (Birrane et al. 2013).

*PDZK1IP1* (interacting protein *PDZK1*) is a small 17 kDa non-glycosylated membrane protein overexpressed in a great variety of human carcinomas. Immunohistochemical analysis of *PDZK1IP1* during cancer progression shows, at least in prostate and ovarian carcinomas, that overexpression of the protein strongly correlates with tumoral progression. Moreover, it was described that *PDZK1IP1* promoter is activated by different oncogenes (Guijarro et al. 2007).

The data presented in this dissertation showed that Twist1 effects on thyroid cancer cell survival are mediated by *COL1A1*, *KRT7* and *PDZK1* target genes, while Twist1 effects on thyroid cancer cell migration and invasion are mediated by *HS6ST2*, *THRB*, *ID4*, *RHOB* and *PDZK1IP1* genes with a prominent effect mediated by *RHOB*.

Further studies are on going in our laboratory to test the expression levels of the 11 identified Twist1 target genes in thyroid carcinoma samples in comparison to normal thyroids. We will correlate target genes expression with Twist1 levels. Based on the results obtained, we will further perform western blot and immunohistochemistry studies to clarify the role of these genes in thyroid carcinogenesis.

We are currently verifying whether Twist1 binds to the promoter of the identified genes. Possible binding sites for Twist1 are E-box (5'-CANNTG-3') sequence motif. In the promoter of all 11 up-regulated genes we have found several E-box sequences. We are performing chromatin immunoprecipitation to formally prove that these genes are direct Twist1 targets.

Identification of genes downstream transcription factors is important for clinical translation of basic research. Directly inhibiting the transcription factors is currently difficult, as targeting large binding interfaces is not amenable to small-molecule inhibition. Instead, downstream targets of these transcription factors could be more realistic for therapeutic intervention.

## 6. ACKNOWLEDGEMENTS

All my work has been conducted at the Dipartimento di Medicina Molecolare e Biotecnologie Mediche (DMMBM), Università degli studi di Napoli “ Federico II”.

I wish to present my sincere gratitude to all contributors in my PhD period. First of all, I'm deeply grateful to my supervisor Prof. Giuliana Salvatore for having encouraged my interest in research and whose passion and enthusiasm I had the privilege to appreciate since I started taking part of the group.

I express my sincere thanks to the Coordinator of the School of Doctorate in Molecular Oncology and Endocrinology, Prof. Massimo Santoro. His commitment towards work has been a constant source of inspiration for me.

A special thanks goes to Dr Paolo Salerno, Dr Francesca Maria Orlandella, Dr Tammara Claudio Bencivenga that actively contributed to all the phases of this project.

I would also to thank all my recent and former colleagues, Annamaria, Valentina, Mariolina, Mara, Roberto, Magesh, Nello, Donatella, Anna, Preziosa, Chiara, Alessia, for their kind co-operation, friendship and instructive scientific discussion, from them I learned most of “secrets” of this work.

A particular thank go to Prof. Giancarlo Vecchio that has devoted and continues to devote his life to the research, he is for me a great model to follow!!

A special thank go to Salvatore, Massimo and Antonella for animal care.

A very special thank you goes to my girlfriend *Anita* that during these years I have always been close and supported and encouraged me especially in difficult moments. I am very lucky to have her as a girlfriend I love her very much.

*Finally, I wish to express my gratitude to **my family** that has always been there for me, supporting me in all my decisions and for the values they have given me. This work is dedicated to them.*

## 7. REFERENCES

- Alexander NR, Tran NL, Rekapally H, Summers CE, Glackin C, Heimark RL. N-cadherin gene expression in prostate carcinoma is modulated by integrin-dependent nuclear translocation of Twist1. *Cancer Res* 2006; 66(7): 3365-9.
- Ansieau S, Bastid J, Doreau A, Morel AP, Bouchet BP, Thomas C, Fauvet F, Puisieux I, Doglioni C, Piccinin S, Maestro R, Voeltzel T, Selmi A, Valsesia-Wittmann S, Caron de Fromental C, Puisieux A. Induction of EMT by twist proteins as a collateral effect of tumor-promoting inactivation of premature senescence. *Cancer Cell* 2008 (a); 14: 79-89.
- Ansieau S, Hinkal G, Thomas C, Bastid J, Puisieux A. Early origin of cancer metastases: dissemination and evolution of premalignant cells. *Cell Cycle*. 2008 (b);7(23):3659-63.
- Ansieau S, Morel AP, Hinkal G, Bastid J, Puisieux A. TWISTing an embryonic transcription factor into an oncoprotein. *Oncogene* 2010 3; 29(22):3173-84.
- Begum S, Rosenbaum E, Henrique R, Cohen Y, Sidransky D, Westra WH. BRAF mutations in anaplastic thyroid carcinoma: implications for tumor origin, diagnosis and treatment. *Mod Pathol*. 2004; 17(11): 1359-63.
- Bhaijee F, Nikiforov YE. Molecular analysis of thyroid tumors. *Endocr Pathol*. 2011; 22(3):126-33.
- Bialek P, Kern B, Yang X, Schrock M, Sosic D, Hong N, Wu H, Yu K, Ornitz DM, Olson EN, Justice MJ, Karsenty G. A twist code determines the onset of osteoblast differentiation. *Dev Cell* 2004; 6: 423-35.
- Bildsoe H, Loebel DA, Jones VJ, Chen YT, Behringer RR, Tam PP. Requirement for Twist1 in frontonasal and skull vault development in the mouse embryo. *Dev Biol*. 2009 15; 331 (2):176-88.
- Birrane G, Mulvaney EP, Pal R, Kinsella BT, Kocher O. Molecular Analysis of the Prostacyclin Receptor's Interaction with the PDZ1 Domain of Its Adaptor Protein PDZK1. *PLoS One*. 2013;8 (2): e53819.
- Bonaventure J, El Ghouzzi V. Molecular and cellular bases of syndromic craniosynostoses. *Expert Rev Mol Med*. 2003;5(4):1-17.
- Bourgeois P, Bolcato-Bellemin AL, Danse JM, Bloch-Zupan A, Yoshida K, Stoetzel C, Perrin-Schmitt F. The variable expressivity and incomplete penetrance of the twist-null heterozygous mouse phenotype resemble those of human Saethre-Chotzen syndrome. *Hum Mol Genet*. 1998 (6): 945-57.

- Bretz NP, Salnikov AV, Perne C, Keller S, Wang X, Mierke CT, Fogel M, Erbe-Hofmann N, Schlange T, Moldenhauer G, Altevogt P. CD24 controls Src/STAT3 activity in human tumors. *Cell Mol Life Sci.* 2012; 69(22):3863-79.
- Carnero A. MAP17 and the double-edged sword of ROS. *Biochim Biophys Acta.* 2012; 1826(1):44-52.
- Castanon I, Baylies MK. A Twist in fate: evolutionary comparison of Twist structure and function. *Gene.* 2002; 287(1-2):11-22.
- Chen ZF, Behringer RR. Twist is required in head mesenchyme for cranial neural tube morphogenesis. *Genes Dev* 1995; 9: 686-99.
- Cheng GZ, Chan J, Wang Q, Zhang W, Sun CD, Wang LH. Twist transcriptionally up-regulates AKT2 in breast cancer cells leading to increased migration, invasion, and resistance to paclitaxel. *Cancer Res.* 2007; 67(5):1979-87.
- Cheng GZ, Zhang WZ, Sun M, Wang Q, Coppola D, Mansour M, Xu LM, Costanzo C, Cheng JQ, Wang LH. Twist is transcriptionally induced by activation of STAT3 and mediates STAT3 oncogenic function. *J Biol Chem.* 2008 May 23;283(21):14665-73.
- Ciampi R, Knauf JA, Kerler R, Gandhi M, Zhu Z, Nikiforova MN, Rabes HM, Fagin JA, Nikiforov YE. Oncogenic AKAP9-BRAF fusion is a novel mechanism of MAPK pathway activation in thyroid cancer. *J Clin Invest.* 2005; 115(1): 94-101.
- Ciampi R, Nikiforov YE. Alterations of the BRAF gene in thyroid tumors. *Endocr Pathol* 2005; 16: 163-72.
- Cote GJ, Gagel RF. Lessons learned from the management of a rare genetic cancer. *N Engl J Med.* 2003; 349(16): 1566-8.
- Davies H, Bignell GR, Cox C, Stephens P, Edkins S, Clegg S, Teague J, Woffendin H, Garnett MJ, Bottomley W, Davis N, Dicks E, Ewing R, Floyd Y, Gray K, Hall S, Hawes R, Hughes J, Kosmidou V, Menzies A, Mould C, Parker A, Stevens C, Watt S, Hooper S, Wilson R, Jayatilake H, Gusterson BA, Cooper C, Shipley J, Hargrave D, Pritchard-Jones K, Maitland N, Chenevix-Trench G, Riggins GJ, Bigner DD, Palmieri G, Cossu A, Flanagan A, Nicholson A, Ho JW, Leung SY, Yuen ST, Weber BL, Seigler HF, Darrow TL, Paterson H, Marais R, Marshall CJ, Wooster R, Stratton MR, Futreal PA. Mutations of the BRAF gene in human cancer. *Nature* 2002; 417:949-54.
- De Craene B, Berx G. Regulatory networks defining EMT during cancer initiation and progression. *Nat Rev Cancer.* 2013;13(2):97-110.
- DeLellis RA. Pathology and genetics of thyroid carcinoma. *J Surg Oncol* 2006; 94: 662-9.

- Dell'Orso S, Ganci F, Strano S, Blandino G, Fontemaggi G. ID4: a new player in the cancer arena. *Oncotarget* 2010; 1:48-58.
- Dobrian AD. A tale with a Twist: a developmental gene with potential relevance for metabolic dysfunction and inflammation in adipose tissue. *Front Endocrinol (Lausanne)*. 2012; 3:108.
- Dong YF, Soung do Y, Chang Y, Enomoto-Iwamoto M, Paris M, O'Keefe RJ, Schwarz EM, Drissi H. Transforming growth factor-beta and Wnt signals regulate chondrocyte differentiation through Twist1 in a stage-specific manner. *Mol Endocrinol*. 2007; 21(11):2805-20.
- Eberhardt NL, Grebe SK, McIver B, Reddi HV. The role of the PAX8/PPARgamma fusion oncogene in the pathogenesis of follicular thyroid cancer. *Mol Cell Endocrinol*. 2010; 321(1):50-6.
- Eckert MA, Lwin TM, Chang AT, Kim J, Danis E, Ohno-Machado L, Yang J. Twist1-induced invadopodia formation promotes tumor metastasis. *Cancer Cell*. 2011; 19(3): 372-86.
- El Ghouzzi V, Le Merrier M, Perrin-Schmitt F, Lajeunie E, Benit P, Renier D et al. Mutations of the TWIST gene in the Saethre- Chotzen syndrome. *Nat Genet* 1997; 15: 42-46.
- Elias MC, Tozer KR, Silber JR, Mikheeva S, Deng M, Morrison RS, Manning TC, Silbergeld DL, Glackin CA, Reh TA, Rostomily RC. TWIST is expressed in human gliomas and promotes invasion. *Neoplasia*. 2005; 7(9):824-37.
- Evdokimova V, Tognon C, Ng T, Ruzanov P, Melnyk N, Fink D, Sorokin A, Ovchinnikov LP, Davicioni E, Triche TJ, Sorensen PH. Translational activation of snail1 and other developmentally regulated transcription factors by YB-1 promotes an epithelial-mesenchymal transition. *Cancer Cell*. 2009;15(5):402-15.
- Fendrich V, Waldmann J, Feldmann G, Schlosser K, König A, Ramaswamy A, Bartsch DK, Karakas E. Unique expression pattern of the EMT markers Snail, Twist and E-cadherin in benign and malignant parathyroid neoplasia. *Eur J Endocrinol*. 2009; 160 (4):695-703.
- Feng Y, Zhou YM, Hua CG, Tang XF, He DQ. Expression of Twist in different subtype of ameloblastomas. *Oral Surg Oral Med Oral Pathol Oral Radiol Endod*. 2009; 108(4):565-70.
- Fernandes RJ, Farnand AW, Traeger GR, Weis MA, Eyre DR. A role for prolyl 3-hydroxylase 2 in post-translational modification of fibril-forming collagens. *J Biol Chem*. 2011; 286(35):30662-9
- Figeac N, Daczewska M, Marcelle C, Jagla K. Muscle stem cells and model systems for their investigation. *Dev Dyn* 2007; 236: 3332-42.
- Firulli BA, Howard MJ, McDaid JR, McIlreavey L, Dionne KM, Centonze VE, Cserjesi P, Virshup DM, Firulli AB. PKA, PKC, and the protein

phosphatase 2A influence HAND factor function: a mechanism for tissue-specific transcriptional regulation. *Mol Cell*; 12(5): 1225-37.

- Frattini M, Ferrario C, Bressan P, Balestra D, De Cecco L, Mondellini P, Bongarzone I, Collini P, Gariboldi M, Pilotti S, Pierotti MA, Greco A. Alternative mutations of BRAF, RET and NTRK1 are associated with similar but distinct gene expression patterns in papillary thyroid cancer. *Oncogene* 2004; 23: 7436-40.
- Funato N, Ohtani K, Ohyama K, Kuroda T, Nakamura M. Common regulation of growth arrest and differentiation of osteoblasts by helix-loop-helix factors. *Mol Cell Biol*. 2001; 21(21): 7416-28.
- Garcia-Rostan G, Camp RL, Herrero A, Carcangiu ML, Rimm DL, Tallini G. Beta-catenin dysregulation in thyroid neoplasms: down-regulation, aberrant nuclear expression, and CTNNB1 exon 3 mutations are markers for aggressive tumor phenotypes and poor prognosis. *Am J Pathol* 2001; 158: 987-96.
- Garcia-Rostan G, Costa AM, Pereira-Castro I, Salvatore G, Hernandez R, Hermsem MJ, Herrero A, Fusco A, Cameselle-Teijeiro J, Santoro M. Mutation of the PIK3CA gene in anaplastic thyroid cancer. *Cancer Res* 2005; 65: 10199-207.
- Greco A, Pierotti MA, Bongarzone I, Pagliardini S, Lanzi C, Della Porta G. TRK-T1 is a novel oncogene formed by the fusion of TPR and TRK genes in human papillary thyroid carcinomas. *Oncogene*. 1992; 7(2): 237-42.
- Guijarro MV, Leal JF, Fominaya J, Blanco-Aparicio C, Alonso S, Leonart M, Castellvi J, Ruiz L, Ramon Y Cajal S, Carnero A. MAP17 overexpression is a common characteristic of carcinomas. *Carcinogenesis* 2007; 28: 1646-52.
- Hamamori Y, Sartorelli V, Ogryzko V, Puri PL, Wu HY, Wang JY, Nakatani Y, Keddes L. Regulation of histone acetyltransferases p300 and PCAF by the bHLH protein twist and adenoviral oncoprotein E1A. *Cell* 1999; 96: 405-13.
- Hanahan D, Weinberg RA. Hallmarks of cancer: the next generation. *Cell*. 2011 Mar 4;144(5):646-74.
- Harbaum L, Pollheimer MJ, Kornprat P, Lindtner RA, Schlemmer A, Rehak P, Langner C. Keratin 7 expression in colorectal cancer-- freak of nature or significant finding? *Histopathology*. 2011; 59(2):225-34.
- Hasselblatt M, Mertsch S, Koos B, Riesmeier B, Stegemann H, Jeibmann A, Tamm M, Schmitz N, Wrede B, Wolff JE, Zheng W, Paulus W. TWIST-1 is overexpressed in neoplastic choroid plexus epithelial cells and promotes proliferation and invasion. *Cancer Res*. 2009; 69(6):2219-23.
- Hoek K, Rimm DL, Williams KR, Zhao H, Ariyan S, Lin A, Kluger HM, Berger AJ, Cheng E, Trombetta ES, Wu T, Niinobe M, Yoshikawa K,

Hannigan GE, Halaban R. Expression profiling reveals novel pathways in the transformation of melanocytes to melanomas. *Cancer Res.* 2004; 64(15):5270-82.

- Hong J, Zhou J, Fu J, He T, Qin J, Wang L, Liao L, Xu J. Phosphorylation of serine 68 of Twist1 by MAPKs stabilizes Twist1 protein and promotes breast cancer cell invasiveness. *Cancer Res.* 2011; 71(11): 3980-90.
- Horikawa T, Yang J, Kondo S, Yoshizaki T, Joab I, Furukawa M, Pagano JS. Twist and epithelial-mesenchymal transition are induced by the EBV oncoprotein latent membrane protein 1 and are associated with metastatic nasopharyngeal carcinoma. *Cancer Res.* 2007 67(5): 1970-8.
- Hosono S, Kajiyama H, Terauchi M, Shibata K, Ino K, Nawa A, Kikkawa F. Expression of Twist increases the risk for recurrence and for poor survival in epithelial ovarian carcinoma patients. *Br J Cancer.* 2007 Jan 29;96(2):314-20.
- Jemal A, Bray F, Center MM, Ferlay J, Ward E, Forman D. Global cancer statistics. *CA Cancer J Clin.* 2011 Mar-Apr;61(2):69-90.
- Kelleher FC, McDermott R. The emerging pathogenic and therapeutic importance of the anaplastic lymphoma kinase gene. *Eur J Cancer.* 2010;46(13):2357-68.
- Kim WG, Cheng SY. Thyroid hormone receptors and cancer. *Biochim Biophys Acta.* 2012
- Kimura ET, Nikiforova MN, Zhu Z, KnaufJA, Nikiforov YE, Fagin JA. High prevalence of BRAF mutations in thyroid cancer: genetic evidence for constitutive activation of the RET/PTC-RAS-BRAF signaling pathway in papillary thyroid carcinoma. *Cancer Res* 2003; 63: 1454-7.
- Klugbauer S, Demidchik EP, Lengfelder E, Rabes HM. Molecular analysis of new subtypes of ELE/RET rearrangements, their reciprocal transcripts and breakpoints in papillary thyroid carcinomas of children after Chernobyl. *Oncogene.* 1998 Feb 5;16(5):671-5.
- Kondo T, Ezzat S, Asa SL. Pathogenetic mechanisms in thyroid follicular-cell neoplasia. *Nat Rev Cancer* 2006; 6:292–306.
- Kwok WK, Ling MT, Lee TW, Lau TC, Zhou C, Zhang X, Chua CW, Chan KW, Chan FL, Glackin C, Wong YC, Wang X. Up-regulation of TWIST in prostate cancer and its implication as a therapeutic target. *Cancer Res.* 2005 Jun 15;65(12):5153-62.
- Kyo S, Sakaguchi J, Ohno S, Mizumoto Y, Maida Y, Hashimoto M, Nakamura M, Takakura M, Nakajima M, Masutomi K, Inoue M. High Twist expression is involved in infiltrative endometrial cancer and affects patient survival. *Hum Pathol.* 2006 Apr;37(4):431-8.
- Leboulleux S, Baudin E, Travagli JP, Schlumberger M. Medullary thyroid carcinoma. *Clin Endocrinol (Oxf).* 2004; 61(3):299-310.

- Lee TK, Poon RT, Yuen AP, Ling MT, Kwok WK, Wang XH, Wong YC, Guan XY, Man K, Chau KL, Fan ST. Twist overexpression correlates with hepatocellular carcinoma metastasis through induction of epithelial-mesenchymal transition. *Clin Cancer Res.* 2006;12(18):5369-76.
- Li L, Cserjesi P, Olson EN. Dermo-1: a novel twist-related bHLH protein expressed in the developing dermis. *Dev Biol* 1995; 172: 280-92.
- Ma L, Teruya-Feldstein J, Weinberg RA. Tumour invasion and metastasis initiated by microRNA-10b in breast cancer. *Nature.* 2007 Oct 11;449(7163):682-8.
- Maestro R, Dei Tos AP, Hamamori Y, Krasnokutsky S, Sartorelli V, Kedes L, Doglioni C, Beach DH, Hannon GJ. Twist is a potential oncogene that inhibits apoptosis. *Genes Dev.* 1999 Sep 1;13(17):2207-17.
- Minoletti F, Butti MG, Coronelli S, Miozzo M, Sozzi G, Pilotti S, Tunnacliffe A, Pierotti MA, Bongarzone I. The two genes generating RET/PTC3 are localized in chromosomal band 10q11.2. *Genes Chromosomes Cancer.* 1994 Sep;11(1):51-7.
- Miranda C, Minoletti F, Greco A, Sozzi G, Pierotti MA. Refined localization of the human TPR gene to chromosome 1q25 by in situ hybridization. *Genomics.* 1994; 23(3):714-5.
- Mironchik Y, Winnard PT Jr, Vesuna F, Kato Y, Wildes F, Pathak AP, Kominsky S, Artemov D, Bhujwala Z, Van Diest P, Burger H, Glackin C, Raman V. Twist overexpression induces in vivo angiogenesis and correlates with chromosomal instability in breast cancer. *Cancer Res.* 2005 Dec 1;65(23):10801-9.
- Murakami M, Ohkuma M, Nakamura M. Molecular mechanism of transforming growth factor-beta-mediated inhibition of growth arrest and differentiation in a myoblast cell line. *Dev Growth Differ.* 2008 Feb;50(2):121-30.
- Murray SS, Glackin CA, Winters KA, Gazit D, Kahn AJ, Murray EJ. Expression of helix-loop-helix regulatory genes during differentiation of mouse osteoblastic cells. *J Bone Miner Res* 1992; 7: 1131-8.
- Murugan AK, Xing M. Anaplastic thyroid cancers harbor novel oncogenic mutations of the ALK gene. *Cancer Res.* 2011 Jul 1;71(13):4403-11.
- Musholt TJ, Musholt PB, Khaladj N, Schulz D, Scheumann GF, Klempnauer J. Prognostic significance of RET and NTRK1 rearrangements in sporadic papillary thyroid carcinoma. *Surgery.* 2000 Dec;128(6):984-93.
- Namba H, Nakashima M, Hayashi T, Hayashida N, Maeda S, Rogounovitch TI, Ohtsuru A, Saenko VA, Kanematsu T, Yamashita S. Clinical implication of hot spot BRAF mutation, V599E, in papillary thyroid cancers. *J Clin Endocrinol Metab* 2003; 88: 4393-7.

- Nikiforov YE, Nikiforova MN. Molecular genetics and diagnosis of thyroid cancer. *Nature Review of Endocrinology* 2011;7(10):569–580.
- Nikiforov YE. Genetic alterations involved in the transition from well-differentiated to poorly differentiated and anaplastic thyroid carcinomas. *Endocr Pathol.* 2004; 15(4): 319-27.
- Nikiforova MN, Kimura ET, Gandhi M, Biddinger PW, Knauf JA, Basolo F, Zhu Z, Giannini R, Salvatore G, Fusco A, Santoro M, Fagin JA, Nikiforov YE. BRAF mutations in thyroid tumors are restricted to papillary carcinomas and anaplastic or poorly differentiated carcinomas arising from papillary carcinomas. *Journal of Clinical Endocrinology & Metabolism* 2003;88:5399–5404.
- Nikiforova MN, Stringer JR, Blough R, Medvedovic M, Fagin JA, Nikiforov YE. Proximity of chromosomal loci that participate in radiation-induced rearrangements in human cells. *Science.* 2000 Oct 6;290(5489):138-41.
- O'Neill JP, Power D, Condron C, Bouchier-Hayes D, Walsh M. Anaplastic thyroid cancer, tumorigenesis and therapy. *Ir J Med Sci.* 2010 Mar;179(1):9-15.
- O'Rourke MP, Tam PP. Twist functions in mouse development. *Int J Dev Biol.* 2002;46(4):401-13.
- Ohuchida K, Mizumoto K, Ohhashi S, Yamaguchi H, Konomi H, Nagai E, Yamaguchi K, Tsuneyoshi M, Tanaka M. Twist, a novel oncogene, is upregulated in pancreatic cancer: clinical implication of Twist expression in pancreatic juice. *Int J Cancer.* 2007 Apr 15;120(8):1634-40.
- Okamura H, Yoshida K, Haneji T. Negative regulation of TIMP1 is mediated by transcription factor TWIST1. *Int J Oncol.* 2009 Jul;35(1):181-6.
- Oshima A, Tanabe H, Yan T, Lowe GN, Glackin CA, Kudo A. A novel mechanism for the regulation of osteoblast differentiation: transcription of periostin, a member of the fasciclin I family, is regulated by the bHLH transcription factor, twist. *J Cell Biochem.* 2002;86(4):792-804.
- Ou DL, Chien HF, Chen CL, Lin TC, Lin LI. Role of Twist in head and neck carcinoma with lymph node metastasis. *Anticancer Res.* 2008 Mar-Apr;28(2B):1355-9.
- Pan D, Fujimoto M, Lopes A, Wang YX. Twist-1 is a PPARdelta-inducible, negative-feedback regulator of PGC-1alpha in brown fat metabolism. *Cell* 2009; 137: 73-86.
- Perri F, Lorenzo GD, Scarpati GD, Buonerba. Anaplastic thyroid carcinoma: A comprehensive review of current and future therapeutic options. *World J Clin Oncol.* 2011; 2(3):150-7.

- Pettersson AT, Laurencikiene J, Mejhert N, Näslund E, Bouloumié A, Dahlman I, Arner P, Rydén M. A possible inflammatory role of twist1 in human white adipocytes. *Diabetes*. 2010 Mar;59(3):564-71.
- Pettersson AT, Mejhert N, Jernås M, Carlsson LM, Dahlman I, Laurencikiene J, Arner P, Rydén M. Twist 1 in human white adipose tissue and obesity. *J Clin Endocrinol Metab*. 2011; 96(1): 133-41.
- Piccinin S, Tonin E, Sessa S, Demontis S, Rossi S, Pecciarini L, Zanatta L, Pivetta F, Grizzo A, Sonogo M, Rosano C, Dei Tos AP, Doglioni C, Maestro R. A "twist box" code of p53 inactivation: twist box: p53 interaction promotes p53 degradation. *Cancer Cell*. 2012 Sep 11;22(3):404-15.
- Pierotti MA, Santoro M, Jenkins RB, Sozzi G, Bongarzone I, Grieco M, Monzini N, Miozzo M, Herrmann MA, Fusco A, Hay ID, Della Porta G, Vecchio G. Characterization of an inversion on the long arm of chromosome 10 juxtaposing D10S170 and RET and creating the oncogenic sequence RET/PTC. *Proc Natl Acad Sci U S A*. 1992 Mar 1;89(5):1616-20.
- Placzkowski KA, Reddi HV, Grebe SK, Eberhardt NL, McIver B. The Role of the PAX8/PPARgamma Fusion Oncogene in Thyroid Cancer. *PPAR Res*. 2008;2008:672829.
- Puisieux A, Valsesia-Wittmann S, Ansieau S. A twist for survival and cancer progression. *Br J Cancer* 2006; 94: 13-17.
- Qin Q, Xu Y, He T, Qin C, Xu J. Normal and disease-related biological functions of Twist1 and underlying molecular mechanisms. *Cell Res*. 2012 Jan;22(1):90-106.
- Rabes HM, Demidchik EP, Sidorow JD, Lengfelder E, Beimfohr C, Hoelzel D, Klugbauer S. Pattern of radiation-induced RET and NTRK1 rearrangements in 191 post-chernobyl papillary thyroid carcinomas: biological, phenotypic, and clinical implications. *Clin Cancer Res*. 2000 Mar;6(3):1093-103
- Radice P, Sozzi G, Miozzo M, De Benedetti V, Cariani T, Bongarzone I, Spurr NK, Pierotti MA, Della Porta G. The human tropomyosin gene involved in the generation of the TRK oncogene maps to chromosome 1q31. *Oncogene*. 1991; 6 (11):2145-8.
- Ricarte-Filho JC, Ryder M, Chitale DA, Rivera M, Heguy A, Ladanyi M, Janakiraman M, Solit D, Knauf JA, Tuttle RM, Ghossein RA, Fagin JA. Mutational profile of advanced primary and metastatic radioactive iodine-refractory thyroid cancers reveals distinct pathogenetic roles for BRAF, PIK3CA, and AKT1. *Cancer Research* 2009;69(11):4885-4893.
- Rosivatz E, Becker I, Specht K, Fricke E, Lubert B, Busch R, Höfler H, Becker KF. Differential expression of the epithelial-mesenchymal

transition regulators snail, SIP1, and twist in gastric cancer. *Am J Pathol.* 2002 Nov;161(5):1881-91.

- Salvatore G, Nappi TC, Salerno P, Jiang Y, Garbi C, Ugolini C, Miccoli P, Basolo F, Castellone MD, Cirafici AM, Melillo RM, Fusco A, Bittner ML, Santoro M. A cell proliferation and chromosomal instability signature in anaplastic thyroid carcinoma. *Cancer Res* 2007; 67(21):10148-58.
- Santaripa L, El-Naggar AK, Cote GJ, Myers JN, Sherman SI. Phosphatidylinositol 3-kinase/akt and ras/ raf-mitogen-activated protein kinase pathway mutations in anaplastic thyroid cancer. *Journal of Clinical Endocrinology and Metabolism* 2008; 93: 278-84.
- Santoro M, Dathan NA, Berlingieri MT, Borganzone I, Paulin C, Grieco M, Pierotti MA, Vecchio G, Fusco A. Molecular characterization of RET/PTC3; a novel rearranged version of the RET proto-oncogene in human thyroid papillary carcinoma. *Oncogene* 1994; 9: 509-16.
- Santoro M, Melillo RM, Fusco A. RET/PTC activation in papillary thyroid carcinoma: European Journal of Endocrinology Prize Lecture. *Eur J Endocrinol.* 2006; 155(5):645-53.
- Santoro M, Papotti M, Chiappetta G, Garcia-Rostan G, Volante M, Johnson C, Camp RL, Pentimalli F, Monaco C, Herrero A, Carcangiu ML, Fusco A, Tallini G. RET activation and clinicopathologic features in poorly differentiated thyroid tumors. *J Clin Endocrinol Metab.* 2002;87(1):370-9.
- Santoro M, Thomas GA, Vecchio G, Williams GH, Fusco A, Chiappetta G, Pozcharkaya V, Bogdanova TI, Demidchik EP, Cherstvoy ED, Voscoboinik L, Tronko ND, Carss A, Bunnell H, Tonnachera M, Parma J, Dumont JE, Keller G, Höfler H, Williams ED. Gene rearrangement and Chernobyl related thyroid cancers. *Br J Cancer.* 2000; 82(2):315-22.
- Schweppe RE, Klopper JP, Korch C, Pugazhenti U, Benezra M, Knauf JA, Fagin JA, Marlow LA, Copland JA, Smallridge RC, Haugen BR. Deoxyribonucleic acid profiling analysis of 40 human thyroid cancer cell lines reveals cross-contamination resulting in cell line redundancy and misidentification. *J Clin Endocrinol Metab.* 2008; 93(11):4331-41.
- Sharabi AB, Aldrich M, Sosic D, Olson EN, Friedman AD, Lee SH et al. Twist-2 controls myeloid lineage development and function. *PLoS Biol* 2008; 6: e316.
- Shibata K, Kajiyama H, Ino K, Terauchi M, Yamamoto E, Nawa A, Nomura S, Kikkawa F. Twist expression in patients with cervical cancer is associated with poor disease outcome. *Ann Oncol.* 2008; 19(1):81-5.
- Shiota M, Izumi H, Onitsuka T, Miyamoto N, Kashiwagi E, Kidani A, Hirano G, Takahashi M, Naito S, Kohno K. Twist and p53 reciprocally regulate target genes via direct interaction. *Oncogene* 2008. 27: 5543-53.

- Shiota M, Izumi H, Onitsuka T, Miyamoto N, Kashiwagi E, Kidani A, Yokomizo A, Naito S, Kohno K. Twist promotes tumor cell growth through YB-1 expression. *Cancer Res.* 2008;68(1):98-105.
- Simpson P. Maternal-Zygotic Gene Interactions during Formation of the Dorsoventral Pattern in *Drosophila* Embryos. *Genetics.* 1983 Nov;105(3):615-32.
- Smallridge RC, Copland JA. Anaplastic thyroid carcinoma: pathogenesis and emerging therapies. *Clinical Oncology (R Coll Radiol)* 2010;22(6):486–497.
- Smit MA, Geiger TR, Song JY, Gitelman I, Peeper DS. A Twist-Snail axis critical for TrkB-induced epithelial-mesenchymal transition-like transformation, anoikis resistance, and metastasis. *Mol Cell Biol.* 2009 Jul;29(13):3722-37.
- Soares P, Trovisco V, Rocha AS, Lima J, Castro P, Preto A, Maximo V, Botelho T, Seruca R, Sobrinho-Simoes M. BRAF mutations and RET/PTC rearrangements are alternative events in the etiopathogenesis of papillary thyroid carcinoma. *Oncogene* 2003; 22: 4578-80.
- Song K, Li Q, Peng YB, Li J, Ding K, Chen LJ, Shao CH, Zhang LJ, Li P. Silencing of hHS6ST2 inhibits progression of pancreatic cancer through inhibition of Notch signalling. *Biochem J* 2011; 436:271-82.
- Song LB, Liao WT, Mai HQ, Zhang HZ, Zhang L, Li MZ, Hou JH, Fu LW, Huang WL, Zeng YX, Zeng MS. The clinical significance of twist expression in nasopharyngeal carcinoma. *Cancer Lett.* 2006; 242(2):258-65.
- Šošić D, Richardson JA, Yu K, Ornitz DM, Olson EN. Twist regulates cytokine gene expression through a negative feedback loop that represses NF-kappaB activity. *Cell.* 2003 Jan 24;112(2):169-80.
- Speakman PT. Collagen-forming polyribosomes: size of the collagen precursor. *Nature.* 1968; 219(5155):724-5.
- Spring J, Yanze N, Middel AM, Stierwald M, Groger H, Schmid V. The mesoderm specification factor twist in the life cycle of jellyfish. *Dev Biol* 2000; 228: 363-75.
- Street CA, Bryan BA. Rho kinase proteins--pleiotropic modulators of cell survival and apoptosis. *Anticancer Res* 2011; 31(11) :3645-57.
- Tallini G. Poorly differentiated thyroid carcinoma. Are we there yet? *Endocr Pathol.* 2011 Dec;22(4):190-4.
- Tan EJ, Thuault S, Caja L, Carletti T, Heldin CH, Moustakas A. Regulation of transcription factor Twist expression by the DNA architectural protein high mobility group A2 during epithelial-to-mesenchymal transition. *J Biol Chem.* 2012 Mar 2;287(10):7134-45.

- Thisse B, el MM, Perrin-Schmitt F. The twist gene: isolation of a *Drosophila* zygotic gene necessary for the establishment of dorsoventral pattern. *Nucleic Acids Res* 1987; 15: 3439-53.
- Thomas GA, Bunnell H, Cook HA, Williams ED, Nerovnya A, Cherstvoy ED, Tronko ND, Bogdanova TI, Chiappetta G, Viglietto G, Pentimalli F, Salvatore G, Fusco A, Santoro M, Vecchio G. High prevalence of RET/PTC rearrangements in Ukrainian and Belarussian post-Chernobyl thyroid papillary carcinomas: a strong correlation between RET/PTC3 and the solid-follicular variant. *J Clin Endocrinol Metab* 1999; 84: 4232-8.
- Valsesia-Wittmann S, Magdeleine M, Dupasquier S, Garin E, Jallas AC, Combaret V, Krause A, Leissner P, Puisieux A. Oncogenic cooperation between H-Twist and N-Myc overrides failsafe programs in cancer cells. *Cancer Cell*. 2004 Dec;6(6):625-30.
- Vesuna F, van Diest P, Chen JH, Raman V. Twist is a transcriptional repressor of E-cadherin gene expression in breast cancer. *Biochem Biophys Res Commun*. 2008 Mar 7;367(2):235-41.
- Vichalkovski A, Gresko E, Hess D, Restuccia DF, Hemmings BA. PKB/AKT phosphorylation of the transcription factor Twist-1 at Ser42 inhibits p53 activity in response to DNA damage. *Oncogene*. 2010 Jun 17;29(24):3554-65.
- Volante M, Collini P, Nikiforov YE, Sakamoto A, Kakudo K, Katoh R, Lloyd RV, LiVolsi VA, Papotti M, Sobrinho-Simoes M, Bussolati G, Rosai J. Poorly differentiated thyroid carcinoma: the Turin proposal for the use of uniform diagnostic criteria and an algorithmic diagnostic approach. *Am J Surg Pathol*. 2007; 31(8): 1256-64.
- Volante M, Papotti M. Poorly differentiated thyroid carcinoma: 5 years after the 2004 WHO classification of endocrine tumours. *Endocrine Pathology* 2010;21(1):1–6.
- Waguespack SG, Rich TA, Perrier ND, Jimenez C, Cote GJ. Management of medullary thyroid carcinoma and MEN2 syndromes in childhood. *Nature Review of Endocrinology* 2011;7(10):596–607.
- Waldmann J, Slater EP, Langer P, Buchholz M, Ramaswamy A, Walz MK, Schmid KW, Feldmann G, Bartsch DK, Fendrich V. Expression of the transcription factor snail and its target gene twist are associated with malignancy in pheochromocytomas. *Ann Surg Oncol*. 2009 Jul;16(7):1997-2005.
- Wang SM, Coljee VW, Pignolo RJ, Rotenberg MO, Cristofalo VJ, Sierra F. Cloning of the human twist gene: its expression is retained in adult mesodermally-derived tissues. *Gene* 1997; 187: 83-92.

- Wang SM, Coljee VW, Pignolo RJ, Rotenberg MO, Cristofalo VJ, Sierra F. Cloning of the human twist gene: its expression is retained in adult mesodermally-derived tissues. *Gene*. 1997 Mar 10;187(1):83-92.
- Wheeler AP, Ridley AJ. Why three Rho proteins? RhoA, RhoB, RhoC, and cell motility. *Exp Cell Res*. 2004 Nov 15;301(1):43-9.
- Williams D. Radiation carcinogenesis: lessons from Chernobyl. *Oncogene* 2008;27 Suppl 2:S9–S18.
- Wu G, Mambo E, Guo Z, Hu S, Huang X, Gollin SM, Trink B, Ladenson PW, Sidransky D, Xing M. Uncommon mutation, but common amplifications, of the PIK3CA gene in thyroid tumors. *J Clin Endocrinol Metab* 2005; 90: 4688-93.
- Xing M. BRAF mutation in papillary thyroid cancer: pathogenic role, molecular bases, and clinical implications. *Endocrine Reviews* 2007;28:742–762.
- Xing M. Molecular pathogenesis and mechanisms of thyroid cancer *Nat Rev Cancer*. 2013 Mar;13(3):184-99.
- Yang J, Mani SA, Donaher JL, Ramaswamy S, Itzykson RA, Come C, Savagner P, Gitelman I, Richardson A, Weinberg RA. Twist, a master regulator of morphogenesis, plays an essential role in tumor metastasis. *Cell*. 2004; 117(7):927-39.
- Yang MH, Hsu DS, Wang HW, Wang HJ, Lan HY, Yang WH, Huang CH, Kao SY, Tzeng CH, Tai SK, Chang SY, Lee OK, Wu KJ. Bmi1 is essential in Twist1-induced epithelial-mesenchymal transition. *Nat Cell Biol*. 2010 Oct;12(10):982-92.
- Yang MH, Wu MZ, Chiou SH, Chen PM, Chang SY, Liu CJ, Teng SC, Wu KJ. Direct regulation of TWIST by HIF-1alpha promotes metastasis. *Nat Cell Biol*. 2008;10(3):295-305.
- Yang WH, Lan HY, Huang CH, Tai SK, Tzeng CH, Kao SY, Wu KJ, Hung MC, Yang MH. RAC1 activation mediates Twist1-induced cancer cell migration. *Nat Cell Biol*. 2012. 11;14(4):366-74.
- Yuen HF, Chan YP, Wong ML, Kwok WK, Chan KK, Lee PY, Srivastava G, Law SY, Wong YC, Wang X, Chan KW. Upregulation of Twist in oesophageal squamous cell carcinoma is associated with neoplastic transformation and distant metastasis. *J Clin Pathol*. 2007;60(5):510-4.
- Zhang Z, Xie D, Li X, Wong YC, Xin D, Guan XY, Chua CW, Leung SC, Na Y, Wang X. Significance of TWIST expression and its association with E-cadherin in bladder cancer. *Hum Pathol* 2007. 38(4):598-606.
- Zhang C, Gao GR, Lv CG, Zhang BL, Zhang ZL, Zhang XF. Protease-activated receptor-2 induces expression of vascular endothelial growth factor and cyclooxygenase-2 via the mitogen-activated protein kinase pathway in gastric cancer cells. *Oncol Rep*. 2012, 28(5):1917-23.

**Supplemental Table 1: Genes upregulated by Twist1 by  $\geq 1.5$  fold**

Gene Title	Gene Symbol	Fold Change	SD	Chromosomal Location	Cellular Growth and Proliferation	Cell Death and Survival	Cellular Movement	Other functions	Not Classified
heparan sulfate 6-O-sulfotransferase 2	HS6ST2	10,28173122	0,351188458	chrXq26.2	X				
CD24 molecule	CD24	8,662800421	1,817507451	chr6q21	X	X	X		
collagen, type I, alpha 1	COL1A1	7,222289403	1,410673598	chr17q21.33	X	X	X		
GDNF family receptor alpha 1	GFRA1	6,919557528	0,608276253	chr10q26	X	X	X		
keratin 7	KRT7	5,567294029	0,8326664	chr12q12-q13	X		X		
vang-like 2 (van gogh, Drosophila)	VANGL2	5,480655757	0,305505046	chr1q22-q23				X	
matrix-remodelling associated 8	MXRA8	5,415015976	0,577350269	chr1p36.33				X	
plakophilin 2	PKP2	5,339337988	0,873689495	chr12p11				X	
coagulation factor II (thrombin) receptor-like 1	F2RL1	5,312989839	0,953939201	chr5q13	X	X	X		
leprecan-like 1	LEPREL1	4,994543441	0,472581563	chr3q28	X				
thyroid hormone receptor, beta (erythroblastic leukemia viral (v-erb-a) oncogene homolog 2, avian)	THRB	4,883874803	0,871779789	chr3p24.2	X		X		
zinc finger, BED-type containing 2	ZBED2	4,597610544	0,655743852	chr3q13.13					X
ADAM metallopeptidase with thrombospondin type 1 motif, 5 (aggrecanase-2)	ADAMTS5	4,369317144	0,850490055	chr21q21.3				X	
inhibitor of DNA binding 4, dominant negative helix-loop-helix protein	ID4	4,336721203	0,264575131	chr6p22-p21	X	X			
ras homolog gene family, member B	RHOB	4,135412309	0,611010093	chr2p24	X	X	X		
PDZ domain containing 1	PDZK1	3,993886633	0,550757055	chr1q21	X	X			
netrin 4	NTN4	3,979515052	0,75055535	chr12q22-q23	X	X	X		
papilin, proteoglycan-like sulfated glycoprotein	PAPLN	3,94748841	0,702376917	chr14q24.2					X

cytochrome P450, family 24, subfamily A, polypeptide 1	CYP24A1	3,895790353	0,971253486	chr20q13	X				
filaggrin	FLG	3,72986228	0,692820323	chr1q21.3				X	
NUAK family, SNF1-like kinase, 2	NUAK2	3,644961964	0,519615242	chr1q32.1		X	X		
coiled-coil domain containing 80	CCDC80	3,585786458	0,86216781	chr3q13.2		X			
transforming growth factor, beta-induced, 68kDa	TGFBI	3,504545129	0,2	chr5q31	X	X	X		
Suppression of tumorigenicity 7 like	ST7L	3,453420992	0,871779789	chr1p13.2	X				
prostaglandin I2 (prostacyclin) synthase	PTGIS	3,43195669	0,776745347	chr20q13.13		X			
transgelin	TAGLN	3,405866218	1,006644591	chr11q23.2			X		
mal, T-cell differentiation protein 2	MAL2	3,381182308	0,519615242	chr8q23					X
EGF-like repeats and discoidin I-like domains 3	EDIL3	3,288688661	0,635085296	chr5q14		X	X		
tumor-associated calcium signal transducer 1	TACSTD1	3,241226113	0,953939201	chr2p21	X		X		
death-associated protein kinase 1	DAPK1	3,211787362	0,6244998	chr9q34.1		X			
LIM and cysteine-rich domains 1	LMCD1	3,202603619	0,461880215	chr3p26-p24				X	
WAS protein family, member 3	WASF3	3,116089412	0,585946528	chr13q12			X		
microphthalmia-associated transcription factor	MITF	2,945811369	0,854400375	chr3p14.2-p14.1	X	X	X		
phospholipase C, beta 4	PLCB4	2,936408568	0,793725393	chr20p12				X	
ADAM metallopeptidase with thrombospondin type 1 motif, 1	ADAMTS1	2,930214545	0,781024968	chr21q21.2	X	X	X		
chromosome 10 open reading frame 65	HOGA1	2,924178087	0,611010093	chr10q24.1					X
PDZK1 interacting protein 1	PDZK1IP1	2,901835211	0,577350269	chr1p33	X				
inositol(myo)-1(or 4)-monophosphatase 2	IMPA2	2,835027268	0,550757055	chr18p11.2					X

doublecortin domain containing 2	DCDC2	2,765568919	0,642910051	chr6p22.1			X		
Cbp/p300-interacting transactivator, with Glu/Asp-rich carboxy-terminal domain, 2	CITED2	2,717517969	0,86216781	chr6q23.3	X	X	X		
homolog of rat pragma of Rnd2	PRAGMIN	2,645044724	0,56862407	chr8p23.1					X
myosin, light chain kinase	MYLK	2,580367042	0,642910051	chr3q21	X	X	X		
thrombospondin 1	THBS1	2,470516694	0,4163332	chr15q15	X	X	X		
Kv channel interacting protein 1	KCNIP1	2,446433025	0,608276253	chr5q35.1		X			
argininosuccinate synthetase 1	ASS1	2,429964151	0,702376917	chr9q34.1				X	
O-6-methylguanine-DNA methyltransferase	MGMT	2,419540831	0,4163332	chr10q26	X	X			
endothelial PAS domain protein 1	EPAS1	2,36398258	0,435889894	chr2p21-p16	X	X	X		
syncoilin, intermediate filament 1	SYNC1	2,361554172	0,585946528	chr1p34.3-p33					X
alpha-kinase 2	ALPK2	2,336479509	0,513160144	chr18q21.31		X			
ring finger 144B	RNF144B	2,28151547	0,503322296	chr6p22.3		X			
apolipoprotein L domain containing 1	APOLD1	2,267236721	0,702376917	chr12p13.1				X	
ribokinase	RBKS	2,2545217	0,404145188	chr2p23.3					X
cystatin E/M	CST6	2,2545217	0,404145188	chr11q13	X		X		
SRY (sex determining region Y)-box 4	SOX4	2,247681135	0,556776436	chr6p22.3	X	X			
GLIS family zinc finger 3	GLIS3	2,246526787	0,529150262	chr9p24.2				X	
ATPase, class II, type 9A	ATP9A	2,246526787	0,529150262	chr20q13.2					X
melanoma cell adhesion molecule	MCAM	2,24373728	0,519615242	chr11q23.3	X	X	X		
RAB40B, member RAS oncogene family	RAB40B	2,237691725	0,351188458	chr17q25.3					X
growth arrest-specific 6	GAS6	2,216209577	0,251661148	chr13q34	X	X	X		
shroom family member 3	SHROOM3	2,205673738	0,435889894	chr4q21.1				X	

transducin-like enhancer of split 4 (E(sp1) homolog, Drosophila)	TLE4	2,204871835	0,550757055	chr9q21.31	X				
secreted phosphoprotein 1 (osteopontin, bone sialoprotein I, early T-lymphocyte activation 1)	SPP1	2,173953455	0,642910051	chr4q21-q25	X				
immediate early response 5-like	IER5L	2,168360602	0,264575131	chr9q34.11					X
tubulin, alpha 1a	TUBA1A	2,148548898	0,550757055	chr12q12-q14.3		X	X		
uncoupling protein 2 (mitochondrial, proton carrier)	UCP2	2,103543126	0,404145188	chr11q13	X	X	X		
collagen, type IV, alpha 1	COL4A1	2,09569795	0,057735027	chr13q34	X	X	X		
small nuclear RNA activating complex, polypeptide 1, 43kDa	SNAPC1	2,093480906	0,519615242	chr14q22					X
odz, odd Oz/ten-m homolog 2 (Drosophila)	ODZ2	2,057218164	0,550757055	chr5q34-q35.1	X	X			
UDP-glucose ceramide glucosyltransferase	UGCG	2,057218164	0,550757055	chr9q31					X
prickle homolog 1 (Drosophila)	PRICKLE1	2,051577463	0,4	chr12q12	X				
suppressor of cytokine signaling 2	SOCS2	2,004667006	0,550757055	chr12q	X	X	X		
interleukin 11	IL11	2,003204303	0,1	chr19q13.3-q13.4	X	X	X		
tuftelin 1	TUFT1	1,962675136	0,404145188	chr1q21					X
mixed lineage kinase 4	KIAA1804	1,95883413	0,404145188	chr1q42				X	
enabled homolog (Drosophila)	ENAH	1,95855963	0,115470054	chr1q42.12			X		
PRKC, apoptosis, WT1, regulator	PAWR	1,95571516	0,529150262	chr12q21	X	X			
PHD finger protein 17	PHF17	1,951719066	0,37859389	chr4q26-q27		X			
family with sequence similarity 83, member H	FAM83H	1,942631582	0,321455025	chr8q24.3					X
arrestin domain containing 3	ARRDC3	1,941529905	0,5	chr5q14.3	X		X		
Bardet-Biedl syndrome 10	BBS10	1,931443504	0,458257569	chr12q21.2				X	

keratin 80	KRT80	1,914189457	0,4	chr12q13.13					X
transmembrane, prostate androgen induced RNA	TMEPAI	1,90636884	0,360555128	chr20q13.31-q13.33	X	X			
progesterone receptor membrane component 2	PGRMC2	1,903870091	0,360555128	chr4q26					X
myosin, light chain 9, regulatory	MYL9	1,900435804	0,346410162	chr20q11.23	X				
phospholipase C, epsilon 1	PLCE1	1,887667543	0,264575131	chr10q23	X	X			
transducin-like enhancer of split 1 (E(sp1) homolog, Drosophila)	TLE1	1,872534505	0,404145188	chr9q21.32					X
fibroblast growth factor 2 (basic)	FGF2	1,867503395	0,37859389	chr4q26-q27	X	X	X		
RNA binding motif, single stranded interacting protein	RBMS3	1,861009508	0,513160144	chr3p24-p23					X
glutaminase	GLS	1,859225418	0,351188458	chr2q32-q34					X
Zinc finger protein 84	ZNF84	1,851404801	0,305505046	chr12q24.33					X
zinc finger protein 91	ZNF91	1,841776492	0,251661148	chr19p13.1-p12				X	
Rho guanine nucleotide exchange factor (GEF) 5	ARHGEF5	1,836384281	0,2081666	chr7q33-q35				X	
Regulating synaptic membrane exocytosis 2	RIMS2	1,833669061	0,4163332	chr8q22.3				X	
heterogeneous nuclear ribonucleoprotein A3	HNRPA3	1,831240653	0,404145188	chr2q31.2					X
GLI-Kruppel family member GLI2	GLI2	1,827656868	0,404145188	chr2q14	X	X	X		
LIM domain and actin binding 1	LIMA1	1,817570466	0,351188458	chr12q13	X				
transmembrane emp24 domain trafficking protein 2	TMED2	1,812539356	0,321455025	chr12q24.31				X	
FOS-like antigen 2	FOSL2	1,80210051	0,458257569	chr2p23.3	X	X	X		
hepatitis A virus cellular receptor 1	HAVCR1	1,800121539	0,251661148	chr5q33.2	X				
KIAA0802	KIAA0802	1,798202369	0,458257569	chr18p11.22					X
par-3 partitioning defective 3 homolog (C. elegans)	PARD3	1,797518837	0,230940108	chr10p11.22-p11.21			X		
SMAD family member 7	SMAD7	1,778705022	0,360555128	chr18q21.1	X	X	X		

kalirin, RhoGEF kinase	KALRN	1,778705022	0,360555128	chr3q21.1-q21.2				X	
eukaryotic translation elongation factor 1 alpha 1	EEF1A1	1,776276614	0,346410162	chr6q14.1	X	X			
Cysteine rich transmembrane BMP regulator 1 (chordin-like)	CRIM1	1,776276614	0,346410162	chr2p21	X	X			
protease, serine, 23	PRSS23	1,776276614	0,346410162	chr11q14.1				X	
unc-51-like kinase 2 (C. elegans)	ULK2	1,765837768	0,472581563	chr17p11.2				X	
angiomin like 2	AMOTL2	1,763571984	0,461880215	chr3q21-q22					X
collagen, type XVIII, alpha 1	COL18A1	1,743890634	0,1	chr21q22.3	X	X	X		
placenta-specific 8	PLAC8	1,743714804	0,404145188	chr4q21.22	X	X			
heat shock 22kDa protein 8	HSPB8	1,724993353	0,288675135	chr12q24.23	X	X			
guanine nucleotide binding protein (G protein), gamma 4	GNG4	1,71843823	0,251661148	chr1q42.3	X				
UDP-N-acetyl-alpha-D-galactosamine:polypeptide N-acetylgalactosaminyltransferase 4 (GalNAc-T4)	GALNT4	1,708607945	0,404145188	chr12q21.3-q22				X	
WW and C2 domain containing 1	WWC1	1,707627892	0,152752523	chr5q35.1				X	
heterogeneous nuclear ribonucleoprotein R	HNRNPR	1,702235682	0,057735027	chr1p36.12	X				
F11 receptor	F11R	1,699070132	0,37859389	chr1q21.2-q21.3	X		X		
galectin-related protein	HSPC159	1,69585321	0,351188458	chr2p14					X
Fucosyltransferase 1 (galactoside 2-alpha-L-fucosyltransferase, H blood group)	FUT1	1,69585321	0,351188458	chr19q13.3					X
thioredoxin reductase 2	TXNRD2	1,68141923	0,458257569	chr22q11.21	X	X	X		
KIT ligand	KITLG	1,68141923	0,458257569	chr12q22		X			
dual specificity phosphatase 16	DUSP16	1,677144378	0,230940108	chr12p13			X		
RAB11 family interacting protein 1 (class I)	RAB11FIP1	1,677144378	0,230940108	chr8p11.22				X	

inhibitor of DNA binding 1, dominant negative helix-loop-helix protein	ID1	1,677039394	0,435889894	chr20q11	X	X	X		
family with sequence similarity 115, member A	FAM115A	1,677039394	0,435889894	chr7q35	X	X	X		
cylindromatosis (turban tumor syndrome)	CYLD	1,673793557	0,2081666	chr16q12.1	X	X	X		
B-cell CLL/lymphoma 2	BCL2	1,673793557	0,2081666	chr18q21.33 18q21.3	X	X	X		
cleavage and polyadenylation specific factor 6, 68kDa	CPSF6	1,673793557	0,2081666	chr12q15					X
tumor necrosis factor, alpha-induced protein 2	TNFAIP2	1,66639871	0,4	chr14q32				X	
prenylcysteine oxidase 1	PCYOX1	1,657324683	0,346410162	chr2p13.3	X				
NUAK family, SNF1-like kinase, 1	NUAK1	1,648004234	0,3	chr12q23.3		X	X		
armadillo repeat containing, X-linked 3	ARMCX3	1,648004234	0,3	chrXq21.33-q22.2		X	X		
pleiomorphic adenoma gene-like 1	PLAGL1	1,645470844	0,461880215	chr6q24-q25	X	X			
zinc finger protein 395	ZNF395	1,643310043	0,264575131	chr8p21.1		X			
vesicle-associated membrane protein 3 (cellubrevin)	VAMP3	1,643310043	0,264575131	chr1p36.23					X
mitochondrial ribosomal protein L30	MRPL30	1,632499705	0,173205081	chr2q11.2					X
zinc finger protein 260	ZNF260	1,630135968	0,404145188	chr19q13.12					X
myristoylated alanine-rich protein kinase C substrate	MARCKS	1,627107495	0,1	chr6q22.2			X		
Ribosomal protein L37	RPL37	1,624504793	1,05367E-08	chr5p13		X			
phosphoribosyl pyrophosphate synthetase 1	PRPS1	1,611741492	0,305505046	chrXq21.32-q24				X	
nephroblastoma overexpressed gene	NOV	1,600570055	0,230940108	chr8q24.1	X	X	X		
ROD1 regulator of differentiation 1 (S. pombe)	ROD1	1,598665371	0,2081666	chr9q32	X				
programmed cell death 6 interacting protein	PDCD6IP	1,598665371	0,2081666	chr3p22.3		X			

CDC14 cell division cycle 14 homolog B ( <i>S. cerevisiae</i> )	CDC14B	1,598665371	0,2081666	chr9q22.33					X
nucleosome assembly protein 1-like 1	NAP1L1	1,596301634	0,4163332	chr12q21.2	X				
zinc finger protein 558	ZNF558	1,593273161	0,152752523	chr19p13.2					X
lysophosphatidylcholine acyltransferase 2	LPCAT2	1,582286993	0,351188458	chr16q12.2				X	
glucosamine (N-acetyl)-6-sulfatase (Sanfilippo disease IIID)	GNS	1,56709682	0,251661148	chr12q14				X	
arginine vasopressin-induced 1	AVPI1	1,56170461	0,2081666	chr10q24.2					X
KIAA1600	KIAA1600	1,557010418	0,152752523	chr10q25.3					X
deleted in liver cancer 1	DLC1	1,554407716	0,115470054	chr8p22	X	X	X		
mex-3 homolog D ( <i>C. elegans</i> )	MEX3D	1,548452659	0,360555128	chr19p13.3				X	
dopey family member 2	DOPEY2	1,533262485	0,264575131	chr21q22.2				X	
ubiquitin-conjugating enzyme E2H (UBC8 homolog, yeast)	UBE2H	1,532250111	0,264575131	chr7q32					X
cysteine-rich, angiogenic inducer, 61	CYR61	1,525441868	0,2	chr1p31-p22	X	X	X		
collagen, type IV, alpha 2	COL4A2	1,525441868	0,2	chr13q34	X	X	X		
protein-L-isoaspartate (D-aspartate) O-methyltransferase domain containing 1	PCMTD1	1,518144974	0,1	chr8q11.23					X
keratin 81	KRT81	1,518144974	0,1	chr12q13					X
actin binding LIM protein 1	ABLIM1	1,501693935	0,288675135	chr10q25					X

**Supplemental Table 2: Genes downregulated by Twist1 by  $\geq 1.5$  fold**

Gene Title	Gene Symbol	Fold Change	SD	Chromosomal Location	Cellular Growth and Proliferation	Cell Death and Survival	Cellular Movement	Other functions	Not Classified
peroxisomal biogenesis factor 5-like	PEX5L	-32,00208893	3,247049943	chr3q26.33				X	
NADPH oxidase, EF-hand calcium binding domain 5	NOX5	-25,62317608	2,821937868	chr15q23	X				
hydroxysteroid (11-beta) dehydrogenase 1	HSD11B1	-24,5629411	2,214347157	chr1q32-q41	X				
protocadherin 7	PCDH7	-23,26581277	2,571640203	chr4p15					X
interleukin 13 receptor, alpha 2	IL13RA2	-23,05602193	2,653927907	chrXq13.1-q28	X		X		
granzyme A (granzyme 1, cytotoxic T-lymphocyte-associated serine esterase 3)	GZMA	-19,474627	1,365039682	chr5q11-q12		X			
Rho GTPase activating protein 9	ARHGAP9	-15,03306137	1,855622088	chr12q14					X
interleukin 1, beta	IL1B	-13,13285389	2,107921567	chr2q14	X	X	X		
hematopoietic cell-specific Lyn substrate 1	HCLS1	-12,83846002	2,025668614	chr3q13	X	X	X		
G protein-coupled receptor 65	GPR65	-11,24875416	1,44222051	chr14q31-q32.1		X			
FAT tumor suppressor homolog 3 (Drosophila)	FAT3	-9,696293796	2,023198787	chr11q14.3					X
solute carrier family 22 (organic cation transporter), member 18 antisense	SLC22A18AS	-9,626602845	1,644181661	chr11p15.5					X
BCL2-related protein A1	BCL2A1	-9,266625608	1,662327685	chr15q24.3	X	X			
linker for activation of T cells family, member 2	LAT2	-8,215015976	1,40118997	chr7q11.23	X				
serpin peptidase inhibitor, clade D (heparin cofactor), member 1	SERPIND1	-8,148234742	1,607275127	chr22q11.2 22q11.21	X				
heat shock 70kDa protein 1A	HSPA1A	-7,849436164	1,473091986	chr6p21.3	X	X	X		

myeloma overexpressed gene (in a subset of t(11;14) positive multiple myelomas)	MYEOV	-7,781161268	0,680685929	chr11q13				X	
gap junction protein, beta 2, 26kDa	GJB2	-7,678658707	1,703917056	chr13q11-q12	X	X	X		
protease, serine, 3 (mesotrypsin)	PRSS3	-7,638278029	1,258305739	chr9p11.2			X		
growth hormone receptor	GHR	-7,38077076	1,006644591	chr5p13-p12	X	X			
interleukin 1, alpha	IL1A	-7,078349034	1,106044002	chr2q14	X	X	X		
synaptotagmin-like 3	SYTL3	-6,859924827	1,473091986	chr6q25.3					X
vanin 1	VNN1	-6,593199654	0,916515139	chr6q23-q24		X			
SLAIN motif family, member 1	SLAIN1	-6,301788353	1,053565375	chr13q22.3					X
keratin 15	KRT15	-6,145492176	1,135781669	chr17q21.2				X	
baculoviral IAP repeat- containing 3	BIRC3	-6,133066583	1,27410099	chr11q22	X	X			
podoplanin	PDPN	-6,117213292	1,30511813	chr1p36.21	X		X		
tissue factor pathway inhibitor 2	TFPI2	-6,022029743	1,386842938	chr7q22	X	X	X		
chemokine (C-X-C motif) ligand 3	CXCL3	-5,685529409	0,680685929	chr4q21	X	X	X		
interleukin 7	IL7	-5,619632538	0,971253486	chr8q12-q13	X	X	X		
phosphatidylinositol 3,4,5- trisphosphate-dependent RAC exchanger 1	PREX1	-5,467587256	1,115048579	chr20q13.13			X		
epithelial membrane protein 1	EMP1	-5,466602544	1,703917056	chr12p12.3	X	X			
sorbin and SH3 domain containing 1	SORBS1	-5,363523592	1,27410099	chr10q23.3- q24.1				X	
neurotrimin	HNT	-5,311194879	1,011599394	chr11q25					X
absent in melanoma 1	AIM1	-5,183017519	1,078579312	chr6q21				X	
signal-regulatory protein beta 1	SIRPB1	-5,17400814	1,2489996	chr20p13					X
thrombomodulin	THBD	-5,131473598	0,37859389	chr20p11.2	X		X		
Rho GDP dissociation inhibitor (GDI) beta	ARHGDI3	-4,985514301	1,153256259	chr12p12.3	X		X		
G0/G1switch 2	GOS2	-4,876670142	1,18462371	chr1q32.2-q41				X	

solute carrier family 7 (cationic amino acid transporter, y+ system), member 7	SLC7A7	-4,806772314	0,850490055	chr14q11.2	X				
carbohydrate (keratan sulfate Gal-6) sulfotransferase 1	CHST1	-4,765182973	1,289702808	chr11p11.2-p11.1			X		
metastasis suppressor 1	MTSS1	-4,707740182	0,602771377	chr8p22			X		
olfactomedin-like 2B	OLFML2B	-4,608607945	0,404145188	chr1q23.3					X
lysosomal associated multispinning membrane protein 5	LAPTM5	-4,546080177	1,18462371	chr1p34	X				
ChaC, cation transport regulator homolog 1 (E. coli)	CHAC1	-4,48800712	0,953939201	chr15q15.1					X
WD repeat domain 16	WDR16	-4,464309867	0,529150262	chr17p13.1					X
N-deacetylase/N-sulfotransferase (heparan glucosaminyl) 2	NDST2	-4,44771527	1,115048579	chr10q22				X	
potassium channel tetramerisation domain containing 12	KCTD12	-4,345765045	0,929157324	chr13q22.3					X
WD repeat domain 66	WDR66	-4,310515196	1,113552873	chr12q24.31					X
frizzled homolog 8 (Drosophila)	FZD8	-4,264582737	0,945163125	chr10p11.21				X	
Friend leukemia virus integration 1	FLI1	-4,181212521	0,953939201	chr11q24.1-q24.3	X	X			
stanniocalcin 1	STC1	-4,119437063	1,00166528	chr8p21-p11.2	X	X	X		
neuromedin U	NMU	-4,040514615	0,493288286	chr4q12			X		
sine oculis binding protein homolog (Drosophila)	SOBP	-4,039766071	0,793725393	chr6q21					X
secretory leukocyte peptidase inhibitor	SLPI	-4,039766071	0,793725393	chr20q12	X	X	X		
FOS-like antigen 1	FOSL1	-4,025425219	0,665832812	chr11q13	X	X	X		
HOP homeobox	HOPX	-4,000069042	0,754983444	chr4q11-q12	X				
roundabout homolog 4, magic roundabout (Drosophila)	ROBO4	-3,99855086	0,602771377	chr11q24.2			X		
interleukin 27 receptor, alpha	IL27RA	-3,976064992	0,7	chr19p13.11	X	X	X		

protein tyrosine phosphatase, receptor type, N polypeptide 2	PTPRN2	-3,940633834	0,655743852	chr7q36		X			
interleukin 7 receptor	IL7R	-3,931569838	0,850490055	chr5p13	X	X			
coronin, actin binding protein, 2B	CORO2B	-3,902653924	1,069267662	chr15q23					X
sprouty homolog 4 (Drosophila)	SPRY4	-3,88679978	0,838649708	chr5q31.3	X				
pentraxin-related gene, rapidly induced by IL-1 beta	PTX3	-3,847033709	0,642910051	chr3q25	X		X		
sema domain, immunoglobulin domain (Ig), transmembrane domain (TM) and short cytoplasmic domain, (semaphorin) 4B	SEMA4B	-3,834270139	0,776745347	chr15q25					X
glycine dehydrogenase (decarboxylating)	GLDC	-3,818011156	0,602771377	chr9p22					X
cystin 1	CYS1	-3,805593339	0,56862407	chr2p25.1				X	
cortactin	CTTN	-3,765607731	1,040833	chr11q13		X	X		
leucine rich repeat neuronal 3	LRRN3	-3,624993353	0,321455025	chr7q31.1				X	
spen homolog, transcriptional regulator (Drosophila)	SPEN	-3,612935374	0,964365076	chr1p36.33-p36.11				X	
v-maf musculoaponeurotic fibrosarcoma oncogene homolog F (avian)	MAFF	-3,608241183	0,953939201	chr22q13.1	X				
methylenetetrahydrofolate dehydrogenase (NADP+ dependent) 2-like	MTHFD2L	-3,591563779	0,850490055	chr4q13.3					X
Solute carrier family 20 (phosphate transporter), member 1	SLC20A1	-3,446013344	0,305505046	chr2q11-q14	X	X			
coiled-coil domain containing 4	CCDC4	-3,436091026	0,550757055	chr4p13					X
laminin, gamma 2	LAMC2	-3,420203012	0,8326664	chr1q25-q31			X		
six transmembrane epithelial antigen of the prostate 1	STEAP1	-3,368923358	0,6	chr7q21	X				
G protein-coupled receptor 92	GPR92	-3,3138468	0,458257569	chr12p13.31					X

nuclear receptor interacting protein 3	NRIP3	-3,29952912	0,665832812	chr11p15.3					X
ATP synthase mitochondrial F1 complex assembly factor 2	ATPAF2	-3,209763044	0,611010093	chr17p11.2					X
Rho GTPase activating protein 22	ARHGAP22	-3,181882232	0,550757055	chr10q11.22	X		X		
transmembrane protein 163	TMEM163	-3,180937097	0,721110255	chr2q21.3					X
calmin (calponin-like, transmembrane)	CLMN	-3,165679684	0,493288286	chr14q32.13					X
phytoceramidase, alkaline	PHCA	-3,155785481	0,814452782	chr11q13.5					X
high mobility group AT-hook 1	HMGA1	-3,14486116	0,655743852	chr6p21	X	X	X		
tumor necrosis factor (TNF superfamily, member 2)	TNF	-3,139665967	0,4163332	chr6p21.3	X	X	X		
cation channel, sperm associated 1	CATSPER1	-3,129743648	0,608276253	chr11q12.1			X		
leupaxin	LPXN	-3,103904226	0,556776436	chr11q12.1				X	
ras-related C3 botulinum toxin substrate 2 (rho family, small GTP binding protein Rac2)	RAC2	-3,070069891	0,458257569	chr22q13.1	X	X	X		
cystatin F (leukocystatin)	CST7	-3,064677681	0,435889894	chr20p11.21				X	
C-type lectin domain family 11, member A	CLEC11A	-3,040406025	0,346410162	chr19q13.3	X	X	X		
CD44 molecule (Indian blood group)	CD44	-2,954288755	0,577350269	chr11p13	X	X	X		
dedicator of cytokinesis 4	DOCK4	-2,925812237	0,692820323	chr7q31.1	X		X		
cytochrome P450, family 2, subfamily J, polypeptide 2	CYP2J2	-2,922882828	0,493288286	chr1p31.3-p31.2	X	X	X		
glycerophosphodiester phosphodiesterase domain containing 5	GDPD5	-2,892167463	0,404145188	chr11q13.4-q13.5	X				
fumarylacetoacetate hydrolase (fumarylacetoacetase)	FAH	-2,891815279	0,6244998	chr15q23-q25	X	X			
cyclin D1	CCND1	-2,887121087	0,608276253	chr11q13	X	X	X		
eukaryotic translation initiation factor 3, subunit M	EIF3M	-2,881357125	0,351188458	chr11p13					X

coiled-coil and C2 domain containing 2A	CC2D2A	-2,862655829	0,251661148	chr4p15.33					X
kynureninase (L-kynurenine hydrolase)	KYNU	-2,860910353	0,723417814	chr2q22.2				X	
interleukin-1 receptor-associated kinase 2	IRAK2	-2,831443504	0,458257569	chr3p25.3				X	
arrestin, beta 1	ARRB1	-2,831443504	0,458257569	chr11q13	X	X	X		
EH-domain containing 1	EHD1	-2,831443504	0,458257569	chr11q13		X	X		
SPC24, NDC80 kinetochore complex component, homolog (S. cerevisiae)	SPC24	-2,829027446	0,665832812	chr19p13.2				X	
axin 2 (conductin, axil)	AXIN2	-2,814189457	0,4	chr17q23-q24	X	X			
UDP-N-acetyl-alpha-D-galactosamine:polypeptide N-acetylgalactosaminyltransferase 12 (GalNAc-T12)	GALNT12	-2,804474836	0,776745347	chr9q22.33					X
Protocadherin alpha cluster	PCDHA	-2,803870091	0,360555128	chr5q31					X
serine/threonine kinase 17b	STK17B	-2,803870091	0,360555128	chr2q32.3	X	X			
microtubule associated serine/threonine kinase family member 4	MAST4	-2,79812252	0,757187779	chr5q12.3					X
Tetraspanin 18	TSPAN18	-2,793059753	0,3	chr11p11.2					X
tumor necrosis factor (ligand) superfamily, member 9	TNFSF9	-2,76654162	0,503322296	chr19p13.3	X	X	X		
FERM domain containing 4A	FRMD4A	-2,759244726	0,472581563	chr10p13					X
EGF, latrophilin and seven transmembrane domain containing 1	ELTD1	-2,755051535	0,665832812	chr1p33-p32					X
sorting nexin 8	SNX8	-2,739201172	0,404145188	chr7p22.2					X
tribbles homolog 3 (Drosophila)	TRIB3	-2,733220637	0,781024968	chr20p13-p12.2		X			
antigen p97 (melanoma associated) identified by monoclonal antibodies 133.2 and 96.5	MF12	-2,721217201	0,585946528	chr3q28-q29			X		
glucuronidase, beta pseudogene 1	GUSBP1	-2,694067418	0,115470054	chr5q13.2					X
unc-5 homolog B (C. elegans)	UNC5B	-2,68964865	0,493288286	chr10q22.1	X	X	X		

cytochrome P450, family 2, subfamily R, polypeptide 1	CYP2R1	-2,667002394	0,4163332	chr11p15.2				X	
AHNAK nucleoprotein	AHNAK	-2,64587269	0,321455025	chr11q12.2	X				
progesterone and adiponectin receptor family member VIII	PAQR8	-2,62186864	0,152752523	chr6p12.1					X
adaptor-related protein complex 1, sigma 2 subunit	AP1S2	-2,60210051	0,458257569	chrXp22.2					X
oligonucleotide/oligosaccharide-binding fold containing 1	OBFC1	-2,597406319	0,435889894	chr10q24.33				X	
UDP-GlcNAc:betaGal beta-1,3-N-acetylglucosaminyltransferase-like 1	B3GNTL1	-2,576373606	0,360555128	chr17q25.3					X
zinc finger CCCH-type containing 12C	ZC3H12C	-2,576276614	0,346410162	chr11q22.3				X	
SH3-domain binding protein 5 (BTK-associated)	SH3BP5	-2,557579098	0,550757055	chr3p24.3		X			
abhydrolase domain containing 2	ABHD2	-2,557579098	0,550757055	chr15q26.1			X		
adenylate kinase 5	AK5	-2,549669862	0,173205081	chr1p31		X			
glycine-N-acyltransferase-like 1	GLYATL1	-2,543890634	0,1	chr11q12.1					X
Rho GTPase activating protein 18	ARHGAP18	-2,513585774	0,404145188	chr6q22.33		X			
OTU domain, ubiquitin aldehyde binding 2	OTUB2	-2,509108946	0,4163332	chr14q32.13					X
RAB38, member RAS oncogene family	RAB38	-2,444207062	0,37859389	chr11q14				X	
ventricular zone expressed PH domain homolog 1 (zebrafish)	VEPH1	-2,420203012	0,305505046	chr3q24-q25					X
dysbindin (dystrobrevin binding protein 1) domain containing 2 /// SYS1-DBNDD2	DBNDD2 /// SYS1-DBNDD2	-2,407126891	0,2081666	chr20q13.12					X
carbonyl reductase 4	CBR4	-2,377039394	0,435889894	chr4q32.3					X
pleckstrin homology-like domain, family A, member 1	PHLDA1	-2,377039394	0,435889894	chr12q15	X	X			
dihydropyrimidinase-like 3	DPYSL3	-2,377039394	0,435889894	chr5q32		X	X		

popeye domain containing 3	POPDC3	-2,36639871	0,4	chr6q21					X
oxysterol binding protein-like 6	OSBPL6	-2,359590467	0,360555128	chr2q31-q32.1					X
UV radiation resistance associated gene	UVRAG	-2,348004234	0,3	chr11q13.5				X	
serpin peptidase inhibitor, clade A (alpha-1 antiproteinase, antitrypsin), member 1	SERPINA1	-2,342225007	0,264575131	chr14q32.1	X	X	X		
osteoclast associated, immunoglobulin-like receptor	OSCAR	-2,334928113	0,2	chr19q13.42		X			
reelin	RELN	-2,327107495	0,1	chr7q22				X	
rho/rac guanine nucleotide exchange factor (GEF) 2	ARHGEF2	-2,314251562	0,472581563	chr1q21-q22	X				
CDC42 effector protein (Rho GTPase binding) 4	CDC42EP4	-2,292422799	0,37859389	chr17q24-q25				X	
ERO1-like beta ( <i>S. cerevisiae</i> )	ERO1LB	-2,278408159	0,305505046	chr1q42.2-q43					X
differentially expressed in FDCP 6 homolog (mouse)	DEF6	-2,265332037	0,2081666	chr6p21.33-p21.1	X	X			
proteasome (prosome, macropain) subunit, beta type, 9 (large multifunctional peptidase 2)	PSMB9	-2,259939827	0,152752523	chr6p21.3				X	
CD82 molecule	CD82	-2,249349678	0,493288286	chr11p11.2	X	X	X		
protein kinase (cAMP-dependent, catalytic) inhibitor alpha	PKIA	-2,229634967	0,4163332	chr8q21.12				X	
family with sequence similarity 131, member A	FAM131A	-2,229634967	0,4163332	chr3q27.1					X
centaurin, delta 2	CENTD2	-2,215620327	0,351188458	chr11q13.4					X
citron (rho-interacting, serine/threonine kinase 21)	CIT	-2,211240491	0,321455025	chr12q24	X	X	X		
jun dimerization protein 2	JDP2	-2,207238396	0,305505046	chr14q24.3	X	X			
HIV-1 Tat interactive protein 2, 30kDa	HTATIP2	-2,204448889	0,288675135	chr11p15.1		X	X		
integrin-linked kinase	ILK	-2,200430153	0,251661148	chr11p15.5-p15.4	X	X	X		

nuclear factor of kappa light polypeptide gene enhancer in B-cells inhibitor, alpha	NFKBIA	-2,200430153	0,251661148	chr14q13	X	X	X		
endothelin converting enzyme 1	ECE1	-2,200430153	0,251661148	chr1p36.1		X			
t-complex 11 (mouse)-like 1	TCP11L1	-2,195037943	0,2081666	chr11p13					X
transforming growth factor beta regulator 1	TBRG1	-2,195037943	0,2081666	chr11q24.2	X				
zinc finger protein 91 homolog (mouse)	ZFP91	-2,148452659	0,360555128	chr11q12					X
fibrillin 2 (congenital contractural arachnodactyly)	FBN2	-2,148452659	0,360555128	chr5q23-q31	X	X			
extra spindle pole bodies homolog 1 (S. cerevisiae)	ESPL1	-2,137642321	0,3	chr12q	X	X			
tumor necrosis factor receptor superfamily, member 11a, NFKB activator	TNFRSF11A	-2,137642321	0,3	chr18q22.1	X	X			
family with sequence similarity 149, member A	FAM149A	-2,133262485	0,264575131	chr4q35.2					X
fatty acid desaturase 1	FADS1	-2,132250111	0,264575131	chr11q12.2-q13.1	X				
amyloid beta (A4) precursor-like protein 2	APLP2	-2,132250111	0,264575131	chr11q23-q25 11q24			X		
hydroxymethylbilane synthase	HMBS	-2,125441868	0,2	chr11q23.3					X
CD40 molecule, TNF receptor superfamily member 5	CD40	-2,122839165	0,173205081	chr20q12-q13.2	X	X	X		
moesin	MSN	-2,076826968	0,173205081	chrXq11.2-q12		X	X		
deformed epidermal autoregulatory factor 1 (Drosophila)	DEAF1	-2,070474653	0,305505046	chr11p15.5					X
LysM, putative peptidoglycan-binding, domain containing 2	LYSMD2	-2,070474653	0,305505046	chr15q21.2					X
cysteinyl-tRNA synthetase	CARS	-2,022735422	0,4163332	chr11p15.5		X			
solute carrier family 39 (zinc transporter), member 8	SLC39A8	-2,020762942	0,404145188	chr4q22-q24				X	
6-pyruvoyltetrahydropterin synthase	PTS	-2,001838683	0,305505046	chr11q22.3-q23.3					X

CHK1 checkpoint homolog (S. pombe)	CHEK1	-1,99923598	0,288675135	chr11q24-q24	X	X			
transmembrane protein 41B	TMEM41B	-1,995486367	0,251661148	chr11p15.4					X
Cas-Br-M (murine) ecotropic retroviral transforming sequence	CBL	-1,995486367	0,251661148	chr11q23.3	X	X	X		
ring finger and FYVE-like domain containing 1	RFFL	-1,995486367	0,251661148	chr17q12	X				
ring finger protein 26	RNF26	-1,993372316	0,230940108	chr11q23					X
transmembrane protein 179B	TMEM179B	-1,993372316	0,230940108	chr11q12.3					X
TRAF-interacting protein with a forkhead-associated domain	TIFA	-1,993372316	0,230940108	chr4q25	X				
interferon induced transmembrane protein 2 (1-8D)	IFITM2	-1,990455258	0,2081666	chr11p15.5				X	
HIRA interacting protein 3	HIRIP3	-1,990455258	0,2081666	chr16p11.2					X
proteasome (prosome, macropain) 26S subunit, non-ATPase, 13	PSMD13	-1,990455258	0,2081666	chr11p15.5					X
apolipoprotein B mRNA editing enzyme, catalytic polypeptide-like 3B	APOBEC3B	-1,986075422	0,152752523	chr22q13.1-q13.2				X	
ribosomal protein S6 kinase, 90kDa, polypeptide 5	RPS6KA5	-1,986075422	0,152752523	chr14q31-q32.1	X	X	X		
centaurin, delta 3	CENTD3	-1,986075422	0,152752523	chr5q31.3		X	X		
myosin phosphatase-Rho interacting protein	M-RIP	-1,986075422	0,152752523	chr17p11.2		X			
paired-like homeodomain 1	PITX1	-1,98138123	0,057735027	chr5q31				X	
multiple C2 domains, transmembrane 2	MCTP2	-1,98138123	0,057735027	chr15q26.2					X
mitogen-activated protein kinase kinase kinase 4	MAP4K4	-1,930584484	0,264575131	chr2q11.2-q12	X		X		
Rho GTPase activating protein 5	ARHGAP5	-1,930584484	0,264575131	chr14q12	X		X		
transmembrane emp24-like trafficking protein 10 (yeast)	TMED10	-1,930584484	0,264575131	chr14q24.3		X			
TMEM9 domain family, member B	TMEM9B	-1,923287589	0,2	chr11p15.3					X

fibroblast growth factor (acidic) intracellular binding protein	FIBP	-1,921173538	0,173205081	chr11q13.1					X
WD repeat domain 33	WDR33	-1,921173538	0,173205081	chr2q14.3					X
mediator complex subunit 19	MED19	-1,920859182	0,173205081	chr11q12.1				X	
DIX domain containing 1	DIXDC1	-1,916479347	0,1	---				X	
coiled-coil domain containing 15	CCDC15	-1,916479347	0,1	chr11q24.2					X
dehydrogenase/reductase (SDR family) member 1	DHRS1	-1,916479347	0,1	chr14q12					X
ATP binding domain 4	ATPBD4	-1,914213562	0	chr15q14					X
cannabinoid receptor interacting protein 1	CNRIP1	-1,862472237	0,251661148	chr2p14				X	
CD59 molecule, complement regulatory protein	CD59	-1,862472237	0,251661148	chr11p13	X	X	X		
ribonucleotide reductase M1 polypeptide	RRM1	-1,862472237	0,251661148	chr11p15.5	X	X			
CDK2-associated protein 2	CDK2AP2	-1,853691514	0,152752523	chr11q13				X	
twinfilin, actin-binding protein, homolog 2 (Drosophila)	TWF2	-1,851577463	0,115470054	chr3p21.1				X	
ataxia telangiectasia mutated	ATM	-1,849311679	0,057735027	chr11q22-q23	X	X	X		
Sin3A-associated protein, 30kDa	SAP30	-1,792876161	0,2081666	chr4q34.1					X
poly(A) polymerase alpha	PAPOLA	-1,78878963	0,152752523	chr14q32.31				X	
calcium/calmodulin-dependent protein kinase IV	CAMK4	-1,78878963	0,152752523	chr5q21.3	X	X	X		
peroxiredoxin 5	PRDX5	-1,78878963	0,152752523	chr11q13		X			
glucosidase, alpha; neutral AB	GANAB	-1,786523846	0,115470054	chr11q12.3					X
trafficking protein particle complex 4	TRAPPC4	-1,725708493	0,173205081	chr11q23.3				X	
protein phosphatase 2 (formerly 2A), regulatory subunit B'', gamma	PPP2R3C	-1,721621962	0,1	chr14q13.2					X
growth arrest-specific 2 like 1	GAS2L1	-1,721621962	0,1	chr22q12.2	X				
cofilin 1 (non-muscle)	CFL1	-1,665186445	0,2081666	chr11q13	X	X	X		
microsomal glutathione S-transferase 2	MGST2	-1,65883413	0,115470054	chr4q28.3				X	

metastasis associated lung adenocarcinoma transcript 1 (non-protein coding)	MALAT1	-1,656720078	0,057735027	chr11q13.1				X	
cyclic AMP phosphoprotein, 19 kD	ARPP-19	-1,533116893	0,1	chr15q21.2					X
calmodulin 1 (phosphorylase kinase, delta)	CALM1	-1,533116893	0,1	chr14q24-q31	X	X			
epithelial membrane protein 3	EMP3	-1,533116893	0,1	chr19q13.3	X	X			

## **Attached Manuscript # II**

Paolo Salerno, Ginesa Garcia-Rostan, Sara Piccinin, Tammaro Claudio Bencivenga, **Gennaro Di Maro**, Claudio Doglioni, Fulvio Basolo, Roberta Maestro, Alfredo Fusco, Massimo Santoro, Giuliana Salvatore

TWIST1 plays a pleiotropic role in determining the anaplastic thyroid cancer phenotype. *J Clin Endocrinol Metab.* 2011 May;96(5): E772-81.

## TWIST1 Plays a Pleiotropic Role in Determining the Anaplastic Thyroid Cancer Phenotype

Paolo Salerno, Ginesa Garcia-Rostan, Sara Piccinin, Tammaro Claudio Bencivenga, Gennaro Di Maro, Claudio Doglioni, Fulvio Basolo, Roberta Maestro, Alfredo Fusco, Massimo Santoro, and Giuliana Salvatore

Dipartimento di Biologia e Patologia Cellulare e Molecolare c/o Istituto di Endocrinologia ed Oncologia Sperimentale del Consiglio Nazionale delle Ricerche (P.S., T.C.B., G.D.M., A.F., M.S.), Università di Napoli "Federico II," 80131 Naples, Italy; Institute of Molecular Pathology and Immunology (G.G.-R.), University of Porto, 4200-465 Porto, Portugal; Instituto de Biología y Genética Molecular (G.G.-R.), Universidad Valladolid–Consejo Superior de Investigaciones Científicas, 47003 Valladolid, Spain; Experimental Oncology 1 (S.P., R.M.), Centro di Riferimento Oncologico, Istituto di Ricovero e Cura a Carattere Scientifico, Aviano National Cancer Institute, 33081 Aviano (Pordenone), Italy; Università Vita-Salute San Raffaele (C.D.), Istituto Scientifico San Raffaele, 20132 Milan, Italy; Division of Pathology (F.B.), Department of Surgery, University of Pisa, 56126 Pisa, Italy; and Dipartimento di Studi delle Istituzioni e dei Sistemi Territoriali (G.S.), Università "Parthenope," 80133 Naples, Italy

**Context:** Anaplastic thyroid carcinoma (ATC) is one of the most aggressive human tumors; it is characterized by chemoresistance, local invasion, and distant metastases. ATC is invariably fatal.

**Objective:** The aim was to study the role of TWIST1, a basic helix-loop-helix transcription factor, in ATC.

**Design:** Expression of TWIST1 was studied by immunohistochemistry and real-time PCR in normal thyroids and well-differentiated, poorly differentiated, and ATC. The function of TWIST1 was studied by RNA interference in ATC cells and by ectopic expression in well-differentiated thyroid carcinoma cells.

**Results:** ATCs up-regulate TWIST1 with respect to normal thyroids as well as to poorly and well-differentiated thyroid carcinomas. Knockdown of TWIST1 by RNA interference in ATC cells reduced cell migration and invasion and increased sensitivity to apoptosis. The ectopic expression of TWIST1 in thyroid cells induced resistance to apoptosis and increased cell migration and invasion.

**Conclusions:** TWIST1 plays a key role in determining malignant features of the anaplastic phenotype *in vitro*. (*J Clin Endocrinol Metab* 96: 0000–0000, 2011)

Thyroid neoplasms include a broad spectrum of histotypes, ranging from benign adenomas to differentiated papillary and follicular, poorly differentiated, and rapidly growing anaplastic carcinomas (1, 2). Papillary thyroid carcinoma (PTC) far outnumbers the other morphological subtypes and is characterized, in general, by an indolent phenotype with a 10-yr survival rate of up to 90% (1, 2). Poorly differentiated carcinomas (PDC) include a heterogeneous group of neoplasms with morphological

features and clinical characteristics intermediate between those of well-differentiated and anaplastic carcinomas (1, 2). Anaplastic thyroid carcinomas (ATC) represent less than 2% of all thyroid cancers but are responsible for more than 50% of thyroid cancer mortality, with a mean survival time from diagnosis of 4–12 months (3). ATC is highly invasive, and the majority of ATC patients die from suffocation due to locoregional disease extension or because of overwhelming distant metastatic disease. Surgical

ISSN Print 0021-972X ISSN Online 1945-7197

Printed in U.S.A.

Copyright © 2011 by The Endocrine Society

doi: 10.1210/jc.2010-1182 Received May 24, 2010. Accepted February 9, 2011.

Abbreviations: ATC, Anaplastic thyroid carcinoma; mp, mass population; NF- $\kappa$ B, nuclear factor  $\kappa$ B; NT, normal thyroid; PC, Fischer rat-derived thyroid follicular cell line PC Cl 3; PDC, poorly differentiated carcinoma; PTC, papillary thyroid carcinoma; SA- $\beta$ -gal, senescence-associated  $\beta$ -galactosidase; shRNA, short hairpin RNA.

treatment, radiotherapy, and chemotherapy, based primarily on doxorubicin and cisplatin, show little efficacy in ATC patients (3, 4). ATC cells feature a highly mitogenic and motile phenotype and epithelial-mesenchymal transition and are refractory to apoptotic cell death (3, 4). ATC features genetic lesions that are typical of a well-differentiated carcinoma, namely BRAF or RAS point mutations. Only a few genetic lesions have been identified exclusively in ATC, *i.e.* p53, PI3KCA, or  $\beta$ -catenin mutations (5–8). Therefore, the molecular mechanisms driving the establishment of the highly aggressive anaplastic phenotype are still largely unknown (2–5).

We have recently identified, through a cDNA microarray analysis, a gene expression signature that is associated with the highly proliferative and aneuploid ATC phenotype (9). Among the genes highly up-regulated in ATC *vs.* normal tissue and PTC, we have isolated TWIST1. TWIST1 is a highly conserved basic helix-loop-helix transcription factor that plays a key role in mesodermal, myoblast, and osteoblast differentiation (10, 11). Mutational inactivation of TWIST1 is responsible for the Saethre-Chotzen syndrome, an autosomal dominant disorder characterized by premature fusion of the cranial sutures, skull deformations, limb abnormalities, and facial dysmorphism (12). TWIST1 plays an important role in the development and progression of human cancer. TWIST1 overexpression is reported in many human tumors, including rhabdomyosarcoma, glioma, melanoma, breast, gastric, and prostate carcinomas (13, 14). Elevated TWIST1 protein levels are associated with advanced tumor stage and poor prognosis in several cancer types (14, 15). TWIST1 promotes epithelial-mesenchymal transition (16, 17). TWIST1 gene amplification is associated with resistance to chemotherapeutic agents (18, 19). Finally, TWIST1 inhibits premature senescence in cancer cells (20).

Here we report that TWIST1 plays a key role in the ATC phenotype *in vitro* and suggest that it may mediate chemoresistance of ATC cells.

## Materials and Methods

### Reagents

Staurosporine and cisplatin were obtained from Sigma-Aldrich (St. Louis, MO).

### Cell cultures

Human cell lines (S11N, P5 4N, 8505C, CAL62, SW1736, OCUT-2, ACT-1, TPC-1, BCPAP) (21–23), rat cell lines (PC RET/PTC1, PC RET/PTC3, PC *v*-HRAS, PC-BRAF-V600E, PC-TRK-T1, PC *v*-RAF, PC *v*-MOS, PC E1A, and PC E1A-*v*-RAF) (24, 25), and culture conditions are detailed in the Supplemental Data (published on The Endocrine Society's Journals Online web site at <http://jcem.endojournals.org>).

## Tissue samples

Tumors and normal thyroid (NT) tissue samples for immunohistochemical analysis were retrieved from the files of the Pathology Department of the Hospital Central de Asturias (Oviedo University, Asturias, Spain) and of the Hospital Clinico Universitario de Santiago de Compostela (Santiago de Compostela University, Galicia, Spain). Tumors and NT tissue samples for RNA extraction and quantitative RT-PCR were retrieved from the files of the Department of Surgery, University of Pisa (Pisa, Italy). Case selection was based on the histological findings and on the availability of adequate material for RNA extraction. All histological diagnoses were reviewed by two blinded pathologists (G.G.-R. and C.D.) according to the latest recommendations about diagnostic features of PTC, PDC, and ATC (26–28). PDC were defined as malignant tumors of follicular cells displaying predominant solid/trabecular/insular growth patterns, high-grade features such as mitoses (more than three to five mitoses  $\times$  10 high power field) and/or necrosis and convoluted nuclei, with or without concurrent differentiated components of the follicular or papillary type. ATC were defined as tumors displaying admixtures of spindle, pleomorphic giant, and epithelioid cells; high mitotic activity; extensive coagulative necrosis with irregular borders; and infiltration of vascular walls often accompanied by obliteration of the vascular lumina. After microscopic examination of exhaustively sampled specimens, 32 tumors were classified as PTC, 93 as PDC, and 56 as ATC. Processing of samples and of patient information proceeded in agreement with review board-approved protocols.

## Immunohistochemistry

Formalin-fixed and paraffin-embedded 3- to 5- $\mu$ m-thick tumor sections were deparaffinized, placed in a solution of absolute methanol and 0.3% hydrogen peroxide for 30 min, and treated with blocking serum for 20 min. The slides were incubated with mouse monoclonal antibodies against TWIST1 (sc-81417; Santa Cruz Biotechnology, Santa Cruz, CA) and processed according to standard procedures. Negative controls by omitting the primary antibody were included in the assay. Cases were scored as positive when unequivocal brown staining was observed in the nuclei of tumor cells. Immunoreactivity was expressed as the percentage of positively stained target cells in four intensity categories (–, no staining; +, low/weak; ++, moderate/distinct; +++, high/intense). Twist1 score values were independently assigned by two blinded investigators (G.G.-R. and C.D.), and a consensus was reached on all scores used for computation.

## RNA extraction and expression studies

Total RNA was isolated with the RNeasy Kit (QIAGEN, Crawley, West Sussex, UK). The quality of the RNAs was verified by the 2100 Bioanalyzer (Agilent Technologies, Waldbronn, Germany); only samples with an RNA integrity number value above 7 were used for further analysis. Real-time PCR was performed as detailed in the Supplemental Data: for the calculation of expression fold changes, sample 1 represented each single tumor sample, and sample 2 was the average of all ( $n = 22$ ) NTs. Microarray methods are also reported in the Supplemental Data.

## Protein studies

Immunoblotting was carried out according to standard procedures. Anti-TWIST1 (sc-81417) and anti-p53 (Pab 240) monoclonal antibodies were from Santa Cruz Biotechnology; monoclonal anti- $\alpha$ -tubulin antibody was from Sigma-Aldrich; anti-cleaved (Asp175) caspase-3 p17 and p19 fragments polyclonal (5A1) antibody was from Cell Signaling Technology, Inc. (Beverly, MA). Secondary antimouse and antirabbit antibodies coupled to horseradish peroxidase were from Santa Cruz Biotechnology.

## RNA silencing

Small inhibitor duplex RNA targeting TWIST1 (no. 3, 5, and 7) and the scrambled control [nonspecific small interfering RNA (siRNA) duplex containing the same nucleotides but in irregular sequence] have been described previously (16) and were chemically synthesized by Sigma-Aldrich. Based on its higher silencing efficiency, TWIST1 siRNA 3 (hereafter referred to as TWIST1 siRNA) was selected and used throughout the paper. The day of transfection,  $1 \times 10^5$  cells were incubated with 50 nM siRNA and electroporated using MicroPorator (MP-100, Digital Bio; Euroclone, Milan, Italy) according to the manufacturer's instructions. Cells were harvested 24, 48, and 72 h after transfection, counted, and analyzed for protein expression. Methods used to determine cell viability, motility, and invasion are detailed in the Supplemental Data.

## TWIST1 transfection

The pcDNA 3-TWIST1 vector is described elsewhere (29). TPC-1 cells were transfected by using the Lipofectamine Reagent (Invitrogen, Carlsbad, CA) according to the instructions of the manufacturer. Two days later, G418 (Invitrogen) was added at a concentration of 1.2 mg/ml. Two mass populations of several clones and three independent cell clones were isolated, expanded, and screened for TWIST1 expression by Western blot and RT-PCR analysis. One mass population and two cell clones transfected with the control pcDNA 3 vector were expanded. To generate stable shRNA (short hairpin RNA)-expressing cell line, CAL62 cells were transfected with shTWIST1 and shLUC vectors (20) by using the Lipofectamine reagent (Invitrogen) according to the instructions of the manufacturer. Two days later, puromycin (Invitrogen) was added at a concentration of 0.5 mg/ml. Mass populations and several cell clones were isolated, expanded, and screened for TWIST1 knockdown by Western blot and RT-PCR analysis. Methods used to determine cell viability, motility, and invasion are detailed in the Supplemental Data.

## Statistical analysis

Statistical analyses were carried out using the GraphPad InStat software program (version 3.06.3; GraphPad Software, Inc., San Diego, CA). All *P* values were two-sided, and differences were significant when *P* < 0.05.

## Results

### Up-regulation of TWIST1 in ATC

We evaluated TWIST1 expression levels by immunohistochemistry in 157 human tissues including: 15 NT, 13

PTC, 88 PDC, and 41 ATC samples. Representative immunohistochemical staining is shown in Fig. 1A, and the entire dataset is reported in Table 1. TWIST1 was virtually undetectable in NT, PTC, and PDC samples. In contrast, 49% of the ATC samples (20 of 41) were positive for TWIST1 expression. Positivity ranged between at least 5 and no more than 25% (+) to at least 60% (+++) of cells (Fig. 1A and Table 1); no staining was observed in the absence of the primary antibody (data not shown). TWIST1 positivity correlated with moderate/high proliferation rate assessed by Ki67/MIB1 immunoreactivity (Freeman-Halton extension of the Fisher exact probability test, *P* = 0.048) (Supplemental Table 1). There was also a trend for a significant association with up-regulation of the cell cycle regulated minichromosome maintenance 5 protein (Freeman-Halton extension of the Fisher exact probability test, *P* = 0.11) (data not shown). TWIST1 expression correlated with the fusocellular ATC phenotype and inversely correlated with the epithelioid ATC phenotype ( $\chi^2$  test, *P* = 0.0002; Freeman-Halton extension of the Fisher exact probability test, *P* = 0.0001) (Supplemental Table 1), suggesting that TWIST1 is involved in mesenchymal transition of ATC cells. Accordingly, there was a trend toward a correlation between TWIST1 up-regulation and lack of  $\beta$ -catenin staining at the plasma membrane (Freeman-Halton extension of the Fisher exact probability test, *P* = 0.119) (data not shown). Finally, TWIST1 positivity correlated with p53 positivity (Freeman-Halton extension of the Fisher exact probability test, *P* = 0.030) (Supplemental Table 1).

To determine whether TWIST1 up-regulation also occurred at the RNA level, we examined an independent set of ATC (*n* = 15), PDC (*n* = 4), PTC (*n* = 19), and NT (*n* = 22) samples by quantitative RT-PCR. As shown in Fig. 1B, TWIST1 mRNA was up-regulated by more than 5-fold in about 50% (seven of 15) of the ATC samples, with values greater than 10-fold in 13% (two of 15) of them. NT, PTC, and PDC samples expressed lower TWIST1 levels compared with ATC (*P* < 0.001) (Fig. 1B).

In vertebrates, there are two TWIST genes, TWIST1 and TWIST2 (also known as Dermo1), and their encoded proteins show an identity in the basic helix-loop-helix domain of more than 90% (20). Therefore, we also measured TWIST2 expression by quantitative RT-PCR in thyroid tissue samples. TWIST2 was overexpressed in some cases, but at a lower extent with respect to TWIST1 (Supplemental Fig. 1). Indeed, TWIST2 was up-regulated by more than 2-fold in only about half of the ATC samples (four of nine), with values greater than 5-fold in only one of nine ATC samples. No PTC sample up-regulated TWIST2 (Supplemental Fig. 1A).

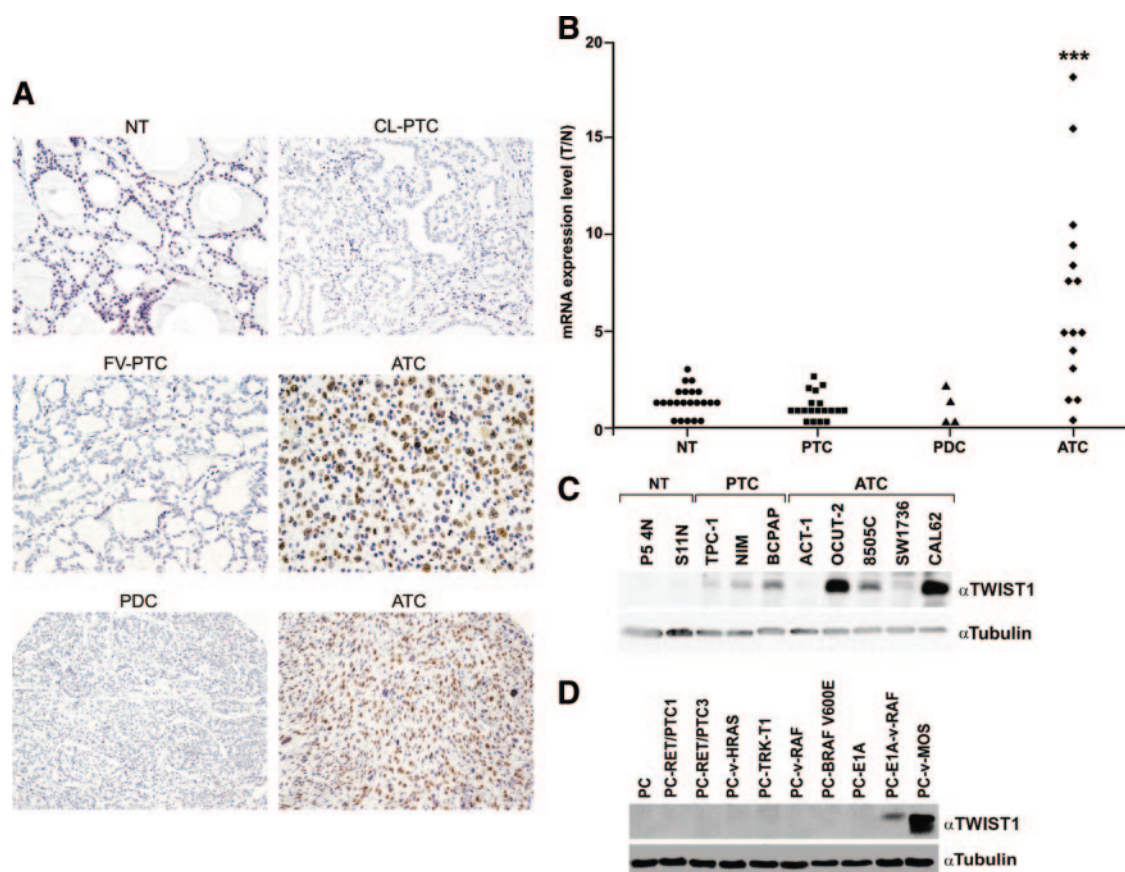


**FIG. 1.** Expression of TWIST1 in thyroid tissue samples and in cell lines. A, Immunohistochemical analysis of TWIST1 protein expression in normal and malignant thyroid tissues. Representative histological sections from NT (20× magnification), classical PTC (CL-PTC; 10× magnification), follicular variant PTC (FV-PTC; 20× magnification), PDC (4× magnification), and ATC (20× and 4× magnification) stained with a mouse monoclonal anti-TWIST1 antibody are shown. The NT, CL-PTC, FV-PTC, and PDC sections were negative for TWIST1, whereas the two ATC cases featured high/intense immunoreactivity levels (+++, e.g. ≥60% of cells); in particular, the ATC sample at 20× magnification showed 65% of positive cells, whereas the ATC at 4× magnification showed 85% of positive cells. B, Quantitative RT-PCR of TWIST1 mRNA in NT (n = 22), PTC (n = 19), PDC (n = 4) and ATC (n = 15) snap-frozen tissue samples. The level of TWIST1 expression in each sample was measured by comparing its fluorescence threshold with the average fluorescence threshold of the NT samples. The average results of triplicate samples are plotted. C, NT follicular cells (P5 4N and S11N), PTC (TPC-1, NIM, and BCPAP), and ATC (ACT-1, OCUT-2, 8505C, SW1736, and CAL62) cell lines were analyzed by immunoblot using a mouse monoclonal anti-TWIST1 antibody. Anti  $\alpha$ -tubulin monoclonal antibody was used as a control for equal protein loading. D, Immunoblot of TWIST1 expression in rat thyroid PC cells expressing the indicated oncogenes. \*\*\*,  $P < 0.001$ .

**Up-regulation of TWIST1 in thyroid cancer cell lines**

We analyzed TWIST1 expression in cultured human thyroid cells. To this aim, we used primary cultures of NT follicular cells (P5 4N and S11N) and a panel of PTC

**TABLE 1.** TWIST1 expression in thyroid samples (n = 157)

Tissue	TWIST1 positivity, % of positive samples (positive/total samples)		
NT	0% (0/15)		
PTC	0% (0/13)		
PDC	0% (0/88)		
ATC	49% (20/41)	+	17% (7/41)
		++	15% (6/41)
		+++	17% (7/41)

+, ≥5 to ≤25% of positive cells; ++, >25 to <60% of positive cells; +++, ≥60% of positive cells.

(TPC-1, NIM, BCPAP) and ATC (ACT-1, OCUT-2, 8505C, SW1736, CAL62) cell lines. Western blot analysis showed up-regulation of a band at approximately 26 kDa, which corresponded to the TWIST1 protein only in the ATC cell lines OCUT-2, 8505C, and CAL62 (Fig. 1C). TWIST1 expression was lower in the other ATC cells and in all the PTC cell lines analyzed, whereas it was undetectable in NT cells (Fig. 1C). RT-PCR analysis confirmed the Western blot results (data not shown). Finally, CAL62 and BCPAP also up-regulated TWIST2 mRNA by more than 2-fold with respect to NT cells (Supplemental Fig. 1B).

To confirm TWIST1 expression in a model cell system and to start exploring whether TWIST1 up-regulation correlated with loss of differentiation or with an aggressive tumor phenotype, we used a panel of rat thyroid follicular Fischer rat-derived thyroid follicular cell

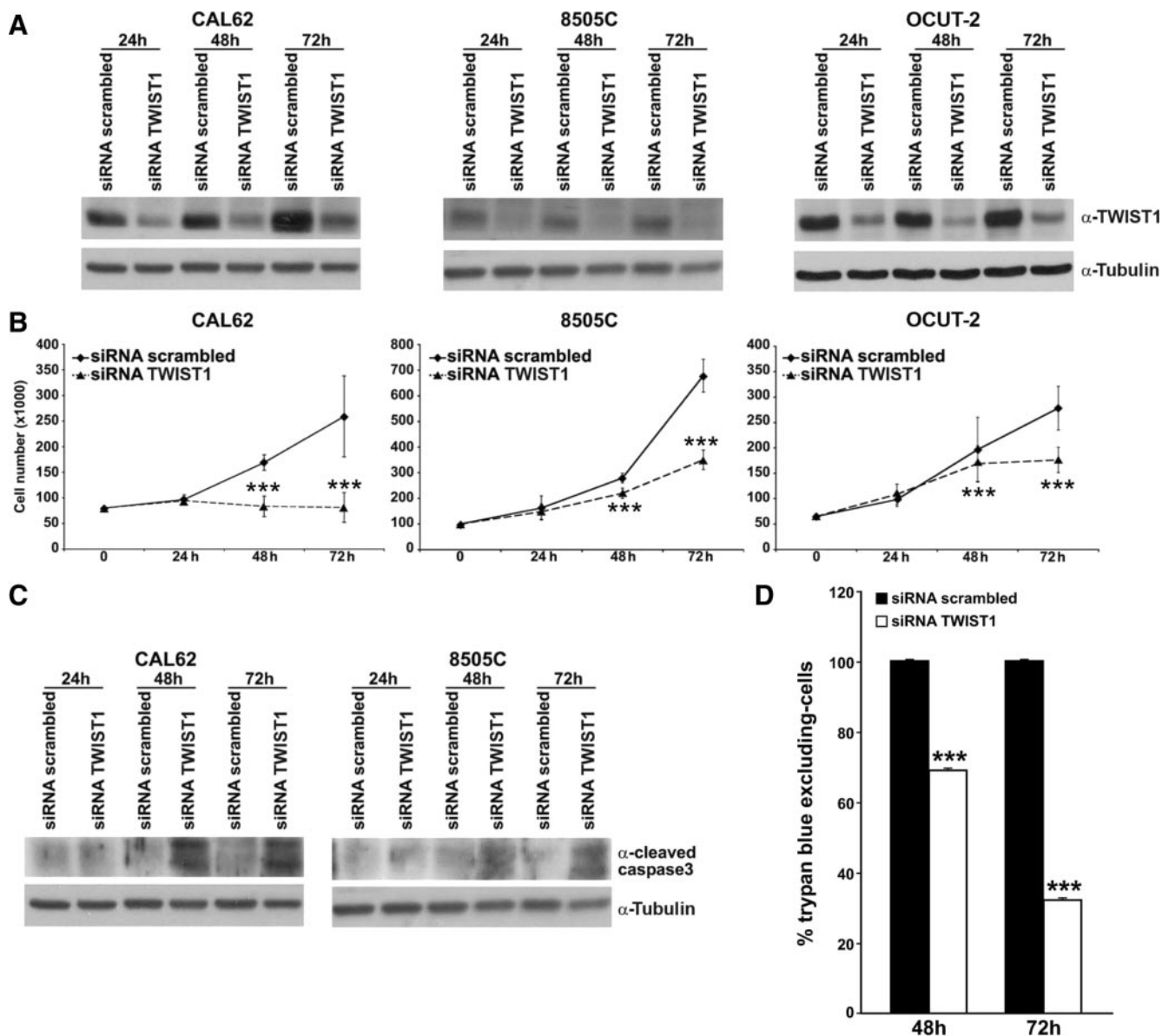


**FIG. 2.** Effects of TWIST1 knockdown in ATC cells. A, CAL62, 8505C, and OCUT-2 cells were transfected with TWIST1 siRNA or with scrambled siRNA. Cells were harvested at different time points, and protein lysates were subjected to immunoblotting with the indicated antibodies. B, CAL62, 8505C, and OCUT-2 cells were transfected with TWIST1 siRNA or with scrambled siRNA and counted at different time points. Values represent the average of triplicate experiments  $\pm$  95% confidence intervals. C, CAL62 and 8505C cells were transfected with TWIST1 siRNA or with scrambled siRNA. Cells were harvested at different time points, and protein lysates were subjected to immunoblotting with the indicated antibodies. D, The indicated cell lines were transfected with TWIST1 siRNA or scrambled siRNA; after 48 and 72 h, cells were collected by trypsinization, stained for 10 min with trypan blue, and counted in triplicate. The percentage of trypan blue excluding cells compared with cells transfected with siRNA scrambled is reported  $\pm$  sd. \*\*\*,  $P < 0.001$ .

line PC CI 3 (PC) cells adoptively expressing various oncogenes (PC-RET/PTC1, PC-RET/PTC3, PC-v-HRAS, PC-TRK-T1, PC-v-RAF, PC-BRAF V600E, PC-E1A, PC-E1A-v-RAF, and PC-v-MOS). Although the expression of v-MOS and of the E1A/v-RAF combination enabled PC cells to grow in semisolid medium and to induce tumors in athymic mice, the expression of the RET/PTC1/3, HRAS, TRK, RAF (v-RAF and BRAF) and E1A oncogenes only caused loss of differentiation without fostering a tumorigenic phenotype (24, 25). Figure 1D shows that TWIST1 was only expressed in the PC cells

transformed by v-MOS, and at lower levels by E1A + v-RAF. Therefore, TWIST1 up-regulation correlated with malignant phenotype rather than loss of differentiation of rat thyroid cells.

### Knockdown of TWIST1 induces apoptosis of ATC cells

We evaluated the effects of TWIST1 ablation in ATC cells by RNA interference. We initially tested, by Western blot in CAL62 cells, the efficiency of TWIST1 ablation using three different siRNA (no. 3, 5, and 7) (16). TWIST1

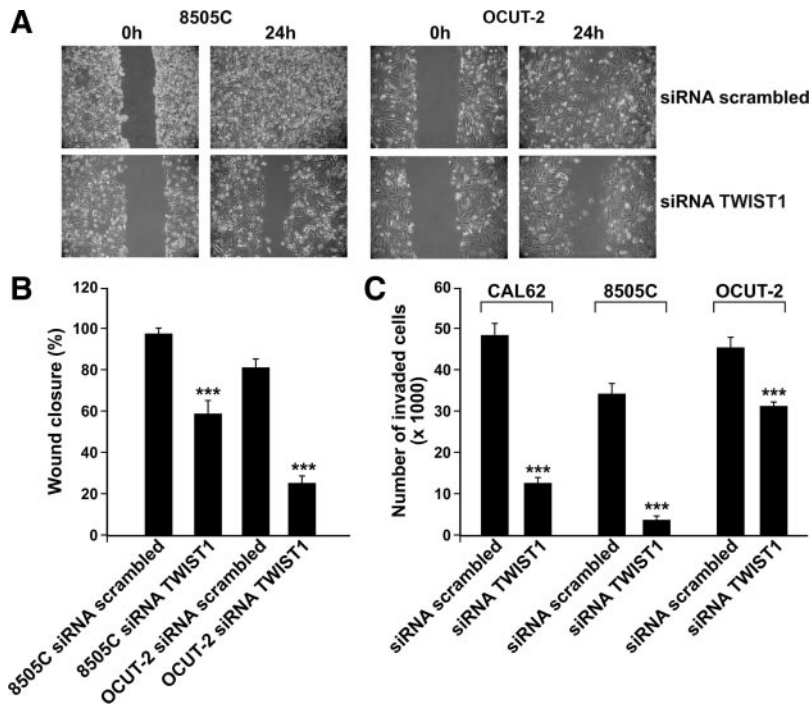


**FIG. 3.** Effects of TWIST1 knockdown on ATC cell migration and invasion. A, Cells were transfected with TWIST1 siRNA or scrambled siRNA; a scraped wound was introduced, and cell migration into the wound was monitored at 24 h. B, Wound closure was measured by calculating pixel densities in the wound area and expressed as percentage of wound closure of triplicate areas  $\pm$  SD. C, Cells were transfected with TWIST1 siRNA or scrambled siRNA; after transfection, cells were seeded in the upper chamber of transwells and incubated for 12 h; the upper surface of the filter was wiped clean, and cells on the lower surface were stained and counted. Invasive ability was expressed as number of invaded cells. Values represent the average of triplicate experiments  $\pm$  SD. \*\*\*,  $P < 0.001$ .

siRNA 3 (hereafter named TWIST1 siRNA) reduced TWIST1 protein levels of about 60% (Fig. 2A) and therefore was selected for further experiments, whereas the other two siRNAs (5 and 7) were less effective, with siRNA 5 being practically devoid of any effect and siRNA 7 depleting TWIST1 protein by less than 30% (Supplemental Fig. 2).

We knocked down TWIST1 by transient siRNA TWIST1 transfection in CAL62, 8505C, and OCUT-2 cells. As shown in Fig. 2A, a TWIST siRNA silenced the TWIST1 protein starting at 24 h after transfection, and the effect lasted up to 72 h, whereas a scrambled siRNA control had no effect (Fig. 2A). Thus, cells were transfected with TWIST1 siRNA or with scrambled siRNA and counted at different time points (24, 48, and 72 h) (Fig. 2B). Seventy-two hours after transfection, CAL62 cells transfected with scrambled siRNA numbered  $259 \times 10^3$ , whereas those transfected with TWIST1 siRNA numbered  $81 \times 10^3$  ( $P = 0.0008$ ); 8505C cells transfected with scrambled siRNA numbered  $679 \times 10^3$ , whereas those transfected with TWIST1 siRNA numbered  $351 \times 10^3$  ( $P < 0.0001$ ); OCUT-2 cells transfected with scrambled siRNA numbered  $278 \times 10^3$ , and those transfected with

TWIST1 siRNA numbered  $176 \times 10^3$  ( $P = 0.0009$ ) (Fig. 2B). It should be noted that CAL62, but not 8505C and OCUT-2, expressed detectable levels of TWIST2 (Supplemental Fig. 1B). Thus, it is feasible, because of the high degree of homology between TWIST1 and TWIST2, that the effects of TWIST1 siRNA observed in CAL62 cells were due to the combined inhibition of TWIST1 and TWIST2. Accordingly, at 24 h after siRNA transfection, TWIST2 mRNA was down-regulated by 1.8-fold in CAL62 (data not shown).

At 48 and 72 h, siRNA TWIST1 induced cell apoptosis of CAL62 and 8505C cells as measured by immunoblot with an antibody for the cleaved products of caspase 3 (Fig. 2C). Accordingly, the percentages of trypan blue excluding (viable) cells, of CAL62 transfected with TWIST1 siRNA 48 and 72 h after transfection, were of 69 and 32%, respectively, with respect to scrambled control, confirming that TWIST1 depletion reduced thyroid cancer cell viability ( $P < 0.001$ ) (Fig. 2D).

Because TWIST1 has been associated with premature senescence of cancer cells (20), we performed a senescence-associated  $\beta$ -galactosidase (SA- $\beta$ -gal) staining assay on siRNA TWIST1-treated cells. Seventy-two hours after transfection with TWIST1 siRNA, the percentage of SA- $\beta$ -gal-positive cells was 1.3%, whereas it was 0.7% in scrambled siRNA transfected cells. As a positive control, the percentage of SA- $\beta$ -gal-positive cells was 38% in normal human diploid fibroblasts treated with Etoposide (Sigma-Aldrich) (data not shown). Thus, although significant, senescence induced by TWIST1 knockdown involved only a minor fraction of ATC cells.

### Knockdown of TWIST1 impairs cell migration and invasion of ATC cells

We evaluated the migration (by a wound-healing assay) and invasion (by a Matrigel invasion assay) ability of TWIST1 siRNA-transfected cells compared with scrambled siRNA-transfected cells. As shown in Fig. 3A, 8505C and OCUT-2 cells transfected with the scrambled control efficiently migrated into the wound; in contrast, cells transfected with TWIST1 siRNA had a greatly reduced migrating ability ( $P < 0.001$ ). Furthermore, cells transfected with TWIST1 siRNA had a reduced ability to invade Matrigel compared with control cells ( $P < 0.001$ ) (Fig. 3B).

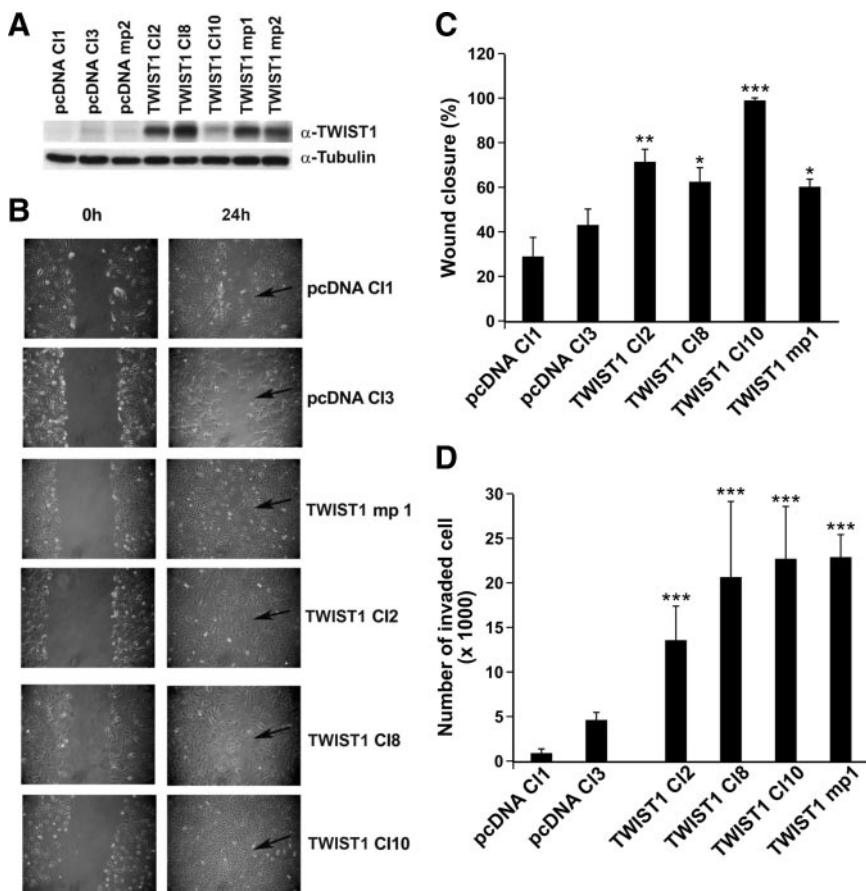


**FIG. 4.** Effects of TWIST1 overexpression on TPC-1 cell migration and invasion. A, Expression levels of TWIST1 in TPC-1-transfected cells. After G418 selection, cells were lysed and blotted with the indicated antibodies. B, A scraped wound was placed on the confluent monolayer of TPC-1 transfected with TWIST1 or the empty vector, and the cell migration into the wound was monitored at 24 h. Arrows indicate the site of wound closure. C, Wound closure was measured by calculating pixel densities in the wound area and expressed as percentage of wound closure of triplicate areas  $\pm$  SD. D, Cells were seeded in the upper chamber of transwells and incubated for 12 h; the upper surface of the filter was wiped clean, and cells on the lower surface were stained and counted. Invasive ability was expressed as number of invaded cells. Values represent the average of triplicate experiments  $\pm$  SD. \*,  $P < 0.05$ ; \*\*,  $P < 0.01$ ; and \*\*\*,  $P < 0.001$ .

#### Effects of stable silencing of TWIST1 in CAL62 cells

We stably transfected CAL62 cells with an shTWIST1 plasmid or with shLUC control (20). After antibiotic selection, cells were screened by Western blot for TWIST1 expression. A mass population (mp) (shTWIST1 mp) with a TWIST1 knockdown of approximately 52% was used for further study (Supplemental Fig. 3A). Consistent with data obtained upon transient TWIST1 silencing (Fig. 2), shTWIST1 mp cells showed decreased migration and invasion ability with respect to shLUC-transfected cells ( $P < 0.001$ ) (Supplemental Fig. 3, B–D). To address effects of TWIST1 knockdown on chemosensitivity, cells were treated with cisplatin (200 or 1000 nM) or staurosporine (300 or 500 nM) and counted at 24 h. Upon treatment with cisplatin (1000 nM) or staurosporine (300–500 nM), shTWIST1 mp cells had a decreased viability compared with control cells ( $P < 0.001$ ) (Supplemental Fig. 3E).

Finally, the number of colonies formed in semisolid medium (soft agar) was also reduced by 2-fold compared with the shLUC mp control ( $P < 0.05$ ) (Supplemental Fig. 3F). Thus, TWIST1 ablation *in vitro* affected several hallmarks of malignancy of CAL62 cells, including anchorage-independent proliferation, survival, and invasion.

#### Ectopic TWIST1 promotes cell migration and invasion of PTC cells

PTC cells, TPC-1, which have low endogenous levels of TWIST1, were transfected with a TWIST1-expressing plasmid (pcDNA-TWIST1) or with the empty vector (pcDNA). Mass populations and cell clones were selected in G418 (1.2 mg/ml). TWIST1 expression was increased (~4- to 13-fold) in all the cell lines transfected with TWIST1 compared with the controls (Fig. 4A). Growth rate was similar in TWIST1- and vector-transfected control cell lines (data not shown). Therefore, we studied cell migration using the wound closure assay. As shown in Fig. 4, B and C, migration rate was higher in TWIST1-transfected cells than in control cells ( $P < 0.05$ ). We next seeded TWIST1-transfected and control cells into the top chamber of transwells and evaluated their ability to invade Matrigel.

TPC-1 cells had basal levels of invasiveness, and TWIST1 overexpression further increased this ability by 4- to 6-fold ( $P < 0.001$ ) (Fig. 4D). Thus, TWIST1 stimulated cell motility and invasion, although wound closure and Matrigel invasion extent were not directly proportional to the TWIST1 expression levels (Fig. 4). These findings suggest that the TWIST1 expression level is not the only molecular determinant of thyroid cancer cell invasive phenotype.

#### Ectopic TWIST1 protects PTC cells from apoptosis

We treated TPC-1 cells transfected with TWIST1 or control vector with different concentrations of cisplatin (200, 1000, and 2000 nM) and counted cell number at 24 h. As shown in Fig. 5A, cell viability was higher in TWIST1-transfected than in control cells upon treatment with the highest drug dose ( $P < 0.05$ ). Moreover,

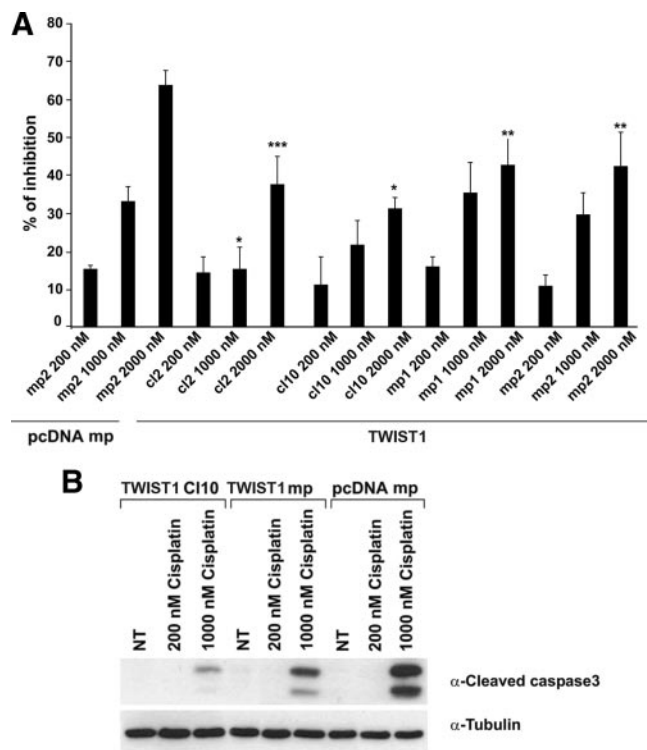


**FIG. 5.** Effects of TWIST1 overexpression on TPC-1 cell apoptosis. A, The cells were treated with increasing doses of cisplatin and counted 24 h after treatment. Data are shown as percentage of inhibition of cell viability. Values represent the average of three independent experiments  $\pm$  SD. \*,  $P < 0.05$ ; \*\*,  $P < 0.01$ ; and \*\*\*,  $P < 0.001$ . B, The indicated cell lines were treated with increasing doses of cisplatin, lysed, and blotted with the indicated antibodies.

the amount of caspase 3 cleaved product was lower in TWIST1-transfected than in control cells (Fig. 5B).

Finally, we searched an Affymetrix microarray-based data set for genes that were previously reported to be TWIST1 targets and related to cell cycle and apoptosis control (30). TWIST1-overexpressing cells (TPC-1 TWIST1 mp1, TWIST1 mp2, and TWIST1 Cl2) up-regulated ( $P < 0.05$ ), with respect to pcDNAmp control, the expression of AKT2 (average fold change  $\pm$  SD,  $2 \pm 0.5$ ) and BCL-2 (average fold change  $\pm$  SD,  $1.67 \pm 0.2$ ), whereas they down-regulated the expression of p21CIP/WAF1 (average fold change  $\pm$  SD,  $0.7 \pm 0.3$ ). TWIST1 overexpression, instead, did not significantly change the expression of p14ARF, BAX, and TIMP1 in our system (data not shown).

## Discussion

Thyroid cancer includes tumor types as different as well-differentiated carcinomas that have a very good prognosis and undifferentiated carcinomas or ATC that are among the most aggressive human cancers. As yet, the molecular players sustaining such different behavior are largely un-

known. Here, we demonstrate that TWIST1 is up-regulated in ATC samples. Overall TWIST1 up-regulation in ATC is more prominent at the RNA than at the protein level. It is possible that TWIST1 overexpression is affected not only at the transcriptional level but also at the post-transcriptional level. TWIST1 up-regulation was associated with mitotic index, as determined by Ki67/MIB1. However, the fact that TWIST1 did not influence cell proliferation in cultured cells suggests that it is not directly involved in controlling cell proliferation. In ATC samples, TWIST1 positivity also correlated with markers of mesenchymal transition (fusocellular phenotype) and malignancy (p53 positivity); however, correlation with p53 expression was not demonstrated in cultured thyroid cancer cells because TWIST1-positive (OCUT-2, 8505C, and CAL62) and TWIST1-negative (TPC-1, BCPAP, NIM, ACT-1, SW1736) cells both had either high (8505C, ACT-1) or low/undetectable (CAL62, OCUT-2, TPC-1, BCPAP, NIM, SW1736) p53 expression (Supplemental Fig. 4).

*In vitro* cellular models confirmed the role of TWIST1 in determining the ATC phenotype and identified the ATC features that were sustained by TWIST1 up-regulation. TWIST1 up-regulation did not correlate with loss of differentiation; indeed, it did not occur in PC cells that lost differentiation secondary to the expression of various oncogenes. Rather, TWIST1 overexpression correlated with a malignant phenotype being present in tumorigenic PC-v-MOS and PC-E1A+v-RAF cells (24). Moreover, TWIST1 expression was necessary to counteract spontaneous ATC cell apoptosis and to sustain the invasive and motile phenotype of ATC cells. Accordingly, when overexpressed in PTC cells, TWIST1 promoted cell migration and protected cells from apoptosis. Given the high homology between TWIST1 and -2, the TWIST siRNA also targeted TWIST2 (1.8-fold), albeit at lower levels than TWIST1 (2.5-fold). Thus, it is possible that at least in CAL62 cells effects were due to the combined inhibition of TWIST1 and TWIST2.

TWIST1 expression is responsive to Wnt-1 (31), IGF-I (32), and nuclear factor  $\kappa$ B (NF- $\kappa$ B) signaling (33). Elements of the Wnt pathway, particularly CTNNB1 (the gene coding  $\beta$ -catenin), were found to be mutated in PDC and ATC (34). Moreover, NF- $\kappa$ B is activated in human thyroid cancer cells, in particular in ATC (35). Therefore, both the Wnt-1/ $\beta$ -catenin and NF- $\kappa$ B pathways are good candidates as mediators of TWIST1 up-regulation in ATC.

Up-regulation of TWIST1 is associated with cellular resistance to anticancer drugs such as cisplatin, taxol, and vincristine in various types of cancers (18, 19, 36). Here, we show that TWIST1 overexpression protected thyroid

cancer cells from cell death induced by cisplatin and staurosporine. This suggests that TWIST1 may be exploited as a molecular marker of the response of thyroid cancer to chemotherapy.

## Acknowledgments

We thank G. Vecchio for continuous support. We thank F. Curcio for the P5 4N cells, H. Zitzelsberger for the S11N cells, C. H. Heldin for the SW1736 cells, N. Onoda for the OCUT-2 and ACT-1 cells, and Drs. J. Cameselle-Teijeiro, A. Herrero, and M. Fresno-Forcelledo for providing human ATC samples. We are grateful to Jean Ann Gilder for text editing.

Address all correspondence and requests for reprints to: Giuliana Salvatore, Dipartimento di Studi delle Istituzioni e dei Sistemi Territoriali, Università “Parthenope,” Via Medina 40, 80133 Naples, Italy. E-mail: giuliana.salvatore@uniparthenope.it.

This work was supported by the Associazione Italiana per la Ricerca sul Cancro, the Istituto Superiore di Oncologia, the Italian Ministero della Salute, the Ministero dell’Università e della Ricerca, the European Community Contract FP6-36495, and the Programa Ramón y Cajal–Ministerio de Ciencia e Innovación, Social EU Funds, Universidad de Valladolid, Spain.

Disclosure Summary: The authors have nothing to declare.

## References

- Kondo T, Ezzat S, Asa SL 2006 Pathogenetic mechanisms in thyroid follicular-cell neoplasia. *Nat Rev Cancer* 6:292–306
- Fagin JA, Mitsiades N 2008 Molecular pathology of thyroid cancer: diagnostic and clinical implications. *Best Pract Res Clin Endocrinol Metab* 22:955–969
- Smallridge RC, Marlow LA, Copland JA 2009 Anaplastic thyroid cancer: molecular pathogenesis and emerging therapies. *Endocr Relat Cancer* 16:17–44
- Ringel MD 2009 Molecular markers of aggressiveness of thyroid cancer. *Curr Opin Endocrinol Diabetes Obes* 16:361–366
- Nikiforov YE 2004 Genetic alterations involved in the transition from well-differentiated to poorly differentiated and anaplastic thyroid carcinomas. *Endocr Pathol* 15:319–327
- García-Rostán G, Costa AM, Pereira-Castro I, Salvatore G, Hernandez R, Hermsem MJ, Herrero A, Fusco A, Cameselle-Teijeiro J, Santoro M 2005 Mutation of the PIK3CA gene in anaplastic thyroid cancer. *Cancer Res* 65:10199–10207
- Wu G, Mambo E, Guo Z, Hu S, Huang X, Gollin SM, Trink B, Ladenson PW, Sidransky D, Xing M 2005 Uncommon mutation, but common amplifications, of the PIK3CA gene in thyroid tumors. *J Clin Endocrinol Metab* 90:4688–4693
- Malaguarnera R, Vella V, Vigneri R, Frasca F 2007 p53 family proteins in thyroid cancer. *Endocr Relat Cancer* 14:43–60
- Salvatore G, Nappi TC, Salerno P, Jiang Y, Garbi C, Ugolini C, Miccoli P, Basolo F, Castellone MD, Cirafici AM, Melillo RM, Fusco A, Bittner ML, Santoro M 2007 A cell proliferation and chromosomal instability signature in anaplastic thyroid carcinoma. *Cancer Res* 67:10148–10158
- Chen ZF, Behringer RR 1995 Twist is required in head mesenchyme for cranial neural tube morphogenesis. *Genes Dev* 9:686–699
- Thisse B, el Ghouzzi V, Perrin-Schmitt F 1987 The twist gene: isolation of a *Drosophila* zygotic gene necessary for the establishment of dorsoventral pattern. *Nucleic Acids Res* 15:3439–3453
- el Ghouzzi V, Le Merrer M, Perrin-Schmitt F, Lajeunie E, Benit P, Renier D, Bourgeois P, Bolcato-Bellemin AL, Munnich A, Bonaventure J 1997 Mutations of the TWIST gene in the Saethre-Chotzen syndrome. *Nat Genet* 15:42–46
- Maestro R, Dei Tos AP, Hamamori Y, Krasnokutsky S, Sartorelli V, Kedes L, Doglioni C, Beach DH, Hannon GJ 1999 Twist is a potential oncogene that inhibits apoptosis. *Genes Dev* 13:2207–2217
- Puisieux A, Valsesia-Wittmann S, Ansieau S 2006 A twist for survival and cancer progression. *Br J Cancer* 94:13–17
- Valsesia-Wittmann S, Magdeleine M, Dupasquier S, Garin E, Jallas AC, Combaret V, Krause A, Leissner P, Puisieux A 2004 Oncogenic cooperation between H-Twist and N-Myc overrides failsafe programs in cancer cells. *Cancer Cell* 6:625–630
- Yang J, Mani SA, Donaher JL, Ramaswamy S, Itzykson RA, Come C, Savagner P, Gitelman I, Richardson A, Weinberg RA 2004 Twist, a master regulator of morphogenesis, plays an essential role in tumor metastasis. *Cell* 117:927–939
- Kalluri R, Weinberg RA 2009 The basics of epithelial-mesenchymal transition. *J Clin Invest* 119:1420–1428
- Wang X, Ling MT, Guan XY, Tsao SW, Cheung HW, Lee DT, Wong YC 2004 Identification of a novel function of TWIST, a bHLH protein, in the development of acquired taxol resistance in human cancer cells. *Oncogene* 23:474–482
- Li J, Wood 3rd WH, Becker KG, Weeraratna AT, Morin PJ 2007 Gene expression response to cisplatin treatment in drug-sensitive and drug-resistant ovarian cancer cells. *Oncogene* 26:2860–2872
- Ansieau S, Bastid J, Doreau A, Morel AP, Bouchet BP, Thomas C, Fauvet F, Puisieux I, Doglioni C, Piccinin S, Maestro R, Voeltzel T, Selmi A, Valsesia-Wittmann S, Caron de Fromental C, Puisieux A 2008 Induction of EMT by twist proteins as a collateral effect of tumor-promoting inactivation of premature senescence. *Cancer Cell* 14:79–89
- Schweppe RE, Klopper JP, Korch C, Pugazhenti U, Benezra M, Knauf JA, Fagin JA, Marlow LA, Copland JA, Smallridge RC, Haugen BR 2008 Deoxyribonucleic acid profiling analysis of 40 human thyroid cancer cell lines reveals cross-contamination resulting in cell line redundancy and misidentification. *J Clin Endocrinol Metab* 93:4331–4341
- Salerno P, De Falco V, Tamburrino A, Nappi TC, Vecchio G, Schweppe RE, Bollag G, Santoro M, Salvatore G 2010 Cytostatic activity of adenosine triphosphate-competitive kinase inhibitors in BRAF mutant thyroid carcinoma cells. *J Clin Endocrinol Metab* 95:450–455
- Curcio F, Ambesi-Impombato FS, Perrella G, Coon HG 1994 Long-term culture and functional characterization of follicular cells from adult normal human thyroids. *Proc Natl Acad Sci USA* 91:9004–9008
- Fusco A, Berlingieri MT, Di Fiore PP, Portella G, Grieco M, Vecchio G 1987 One- and two-step transformations of rat thyroid epithelial cells by retroviral oncogenes. *Mol Cell Biol* 7:3365–3370
- Melillo RM, Castellone MD, Guarino V, De Falco V, Cirafici AM, Salvatore G, Caiazzo F, Basolo F, Giannini R, Kruhoffer M, Orntoft T, Fusco A, Santoro M 2005 The RET/PTC-RAS-BRAF linear signaling cascade mediates the motile and mitogenic phenotype of thyroid cancer cells. *J Clin Invest* 115:1068–1081
- Hedinger C, Williams ED, Sobin LH 1989 The WHO histological classification of thyroid tumors: a commentary on the second edition. *Cancer* 63:908–911
- DeLellis RA, Lloyd R, Heitz PU 2004 WHO classification of tumors: pathology and genetics of tumors of endocrine organs. Lyon, France: IARC Press
- Volante M, Collini P, Nikiforov YE, Sakamoto A, Kakudo K, Kato R, Lloyd RV, Li Volsi VA, Papotti M, Sobrinho-Simoes M, Bussolati G, Rosai J 2007 Poorly differentiated thyroid carcinoma: the Turin proposal for the use of uniform diagnostic criteria and an algorithmic diagnostic approach. *Am J Surg Pathol* 31:1256–1264
- Demontis S, Rigo C, Piccinin S, Mizzau M, Sonogo M, Fabris M, Brancolini C, Maestro R 2006 Twist is substrate for caspase cleav-

- age and proteasome-mediated degradation. *Cell Death Differ* 13:335–345
30. **Ansieau S, Morel AP, Hinkal G, Bastid J, Puisieux A** 2010 TWISTing an embryonic transcription factor into an oncoprotein. *Oncogene* 29:3173–3184
  31. **Reinhold MI, Kapadia RM, Liao Z, Naski MC** 2006 The Wnt-inducible transcription factor TWIST1 inhibits chondrogenesis. *J Biol Chem* 281:1381–1388
  32. **Dupont J, Fernandez AM, Glackin CA, Helman L, LeRoith D** 2001 Insulin-like growth factor 1 (IGF-1)-induced twist expression is involved in the anti-apoptotic effects of the IGF-1 receptor. *J Biol Chem* 276:26699–26707
  33. **Pham CG, Bubici C, Zazzeroni F, Knabb JR, Papa S, Kuntzen C, Franzoso G** 2007 Upregulation of Twist-1 by NF- $\kappa$ B blocks cytotoxicity induced by chemotherapeutic drugs. *Mol Cell Biol* 27:3920–3935
  34. **Garcia-Rostan G, Tallini G, Herrero A, D'Aquila TG, Carcangiu ML, Rimm DL** 1999 Frequent mutation and nuclear localization of  $\beta$ -catenin in anaplastic thyroid carcinoma. *Cancer Res* 59:1811–1815
  35. **Pacifico F, Leonardi A** 2010 Role of NF- $\kappa$ B in thyroid cancer. *Mol Cell Endocrinol* 321:29–35
  36. **Zhang X, Wang Q, Ling MT, Wong YC, Leung SC, Wang X** 2007 Anti-apoptotic role of TWIST and its association with Akt pathway in mediating taxol resistance in nasopharyngeal carcinoma cells. *Int J Cancer* 120:1891–1898

## **TWIST1 plays a pleiotropic role in determining the anaplastic thyroid cancer phenotype**

Paolo Salerno, Ginesa Garcia-Rostan, Sara Piccinin, Tammaro Claudio Bencivenga, Gennaro Di Maro, Claudio Doglioni, Fulvio Basolo, Roberta Maestro, Alfredo Fusco, Massimo Santoro, Giuliana Salvatore

### **Supplemental Methods**

*Cell cultures*-Normal thyroid primary S11N cells were provided by H. Zitzelsberger (Department of Radiation Cytogenetics, Neuherberg, Germany) and P5 4N cells were provided by F. Curcio (Università di Udine, Udine, Italia) in 2003. 8505C and CAL62 cells were purchased from DSMZ (Deutsche Sammlung von Mikroorganismen und Zellkulturen GmbH, Braunschweig, Germany) in 2006. SW1736 cells were obtained from N.E. Heldin (University Hospital, Uppsala, Sweden) in 2005. OCUT-2 and ACT-1 cells were provided by N. Onoda (Osaka University of Medicine, Osaka, Japan) in 2005. TPC-1 cells were obtained from M. Nagao (Carcinogenesis Division, National Cancer Center Research Institute, Tokyo, Japan) in 1990. NIM cells were obtained from J. Fagin (Memorial Sloan Kettering Cancer Center, New York, NY) in 1993. BCPAP cells were obtained from N. Fabien (CNRS, Oullins, France) in 1994. 8505C, SW1736 and CAL62 cells were DNA profiled by short tandem repeat analysis in 2009 and shown to be unique and identical to those reported in Schweppe *et al.*, 2008 (1, 2). The BCPAP cell line was genotyped as reported elsewhere Schweppe *et al.*, 2008 (1). The TPC-1 cell line was identified based on the unique presence of the RET/PTC1 rearrangement. S11N cells were grown in RPMI (Invitrogen, Groningen, The Netherlands) containing 20% fetal bovine serum; P5 4N were grown as previously described (3). The thyroid cancer cell lines were grown in Dulbecco's modified Eagle's medium (DMEM) (Invitrogen) containing 10% fetal bovine serum.

The Fischer rat-derived differentiated thyroid follicular cell line PC Cl 3 (hereafter named “PC”) was grown in Coon’s modified Ham F12 medium supplemented with 5% calf serum and a mixture of six hormones (6H): thyrotropin (10mU/ml), hydrocortisone (10nM), insulin (10µg/ml), apo-transferrin (5µg/ml), somatostatin (10ng/ml), and glycyl-histidyl-lysine (10ng/ml) (Sigma-Aldrich, St. Louis, MO). PC adoptively expressing several oncogenes (PC RET/PTC1, PC RET/PTC3, PC v-HRAS, PC-BRAF-V600E, PC-TRK-T1, PC v-RAF, PC v-MOS, PC E1A and PC E1A-v-RAF) have been described previously and cultured in the same medium as PC but without the 6H (4, 5).

*Cell culture methods-* For cell viability determination, cells were collected by trypsinization, stained for 10 min with 0.4% trypan-blue (Sigma) according to manufacturer’s instructions, and counted in triplicate.

For senescence-Associated-β-galactosidase staining, CAL62 ( $2 \times 10^5$ ) cells were transfected with TWIST1 siRNA or with scrambled control. Seventy-two h after transfection, the cells were washed twice with PBS, fixed with 2% formaldehyde and 0.2% glutaraldehyde in PBS, and washed twice in PBS. Then, cells were stained overnight in X-gal staining solution [1 mg/ml X-gal, 40 mM citric acid/sodium phosphate (pH 6.0), 5 mM potassium ferricyanide, 5 mM potassium ferrocyanide, 150 mM NaCl, 2 mM MgCl<sub>2</sub>] and stained cells were counted. Positive control was represented by normal human diploid fibroblasts IMR-90 treated with Etoposide 20 µM for 24 h.

Cell invasion was examined using a reconstituted extracellular matrix (Matrigel, BD Biosciences, San Jose, CA). The cell suspension ( $1 \times 10^5$  cells per well) was added to the upper chamber of transwell cell culture chambers on a prehydrated polycarbonate membrane filter of 8-µm pore size (Costar, Cambridge, MA) coated with 35 µg of Matrigel (BD Biosciences). The lower chamber was filled with 2.5% medium. After 12-h incubation at 37°C, non-migrating cells on the upper side of the filter were wiped-off. Invading cells were mounted on glass slides

using mounting medium and stained with Hoechst (Sigma). Cell migration was quantified by counting the number of stained nuclei in five individual fields in each Transwell membrane, by fluorescence microscopy, in triplicate.

For wound closure, a wound was induced on the confluent monolayer cells by scraping a gap using a micropipette tip. Photographs were taken at 100 X magnification using phase-contrast microscopy immediately after wound incision and 24 h later. Pixel densities in the wound areas were measured using the Cell<sup>a</sup> software (Olympus Biosystem Gmb) and expressed as percentage of wound closure where 100% is the value obtained at 10h for control cells.

For growth in semisolid medium, colony formation ability of CAL62 shLUC mp and CAL62 shTWIST1 mp cells was examined by soft agar assay. Briefly, 7 ml of FBS supplemented medium containing 0.5% noble agar were added to 60-mm cell culture dish and allowed to solidify (base agar). Next,  $2 \times 10^4$  cells were mixed with 1.5 ml of FBS supplemented medium containing 0.83% noble agar and added to the top of base agar. The cells were then cultured for 14 days at 37°C under 5% carbon dioxide and colonies were counted.

*RNA extraction and expression studies* - Total RNA was isolated with the RNeasy Kit (Qiagen, Crawley, West Sussex, UK). The quality of the RNAs was verified by the 2100 Bioanalyzer (Agilent Technologies, Waldbronn, Germany); only samples with RNA integrity number (RIN) value > 7 were used for further analysis. One µg of RNA from each sample was reverse-transcribed with the QuantiTect<sup>®</sup> Reverse Transcription (Qiagen). For quantitative RT-PCR, we used the Human ProbeLibray<sup>™</sup> system (Exiqon, Denmark). TWIST1 primer sequences were:

TWIST1 -F: 5'-GGC TCA GCT ACG CCT TCT C-3'

TWIST1 -R: 5'- CCT TCT CTG GAA ACA ATG ACA TCT-3'

PCR reactions were performed in triplicate and fold changes were calculated with the formula:

$2^{-(\text{sample 1 } \Delta\text{Ct} - \text{sample 2 } \Delta\text{Ct})}$ , where  $\Delta\text{Ct}$  is the difference between the amplification fluorescent

thresholds of the mRNA of interest and the mRNA of RNA polymerase 2 used as an internal

reference. Sample 1 represented each single tumor sample and sample 2 was the average of all (n. 22) normal thyroids.

For microarrays, 10 µg purified total RNA from 3 TWIST1 TPC-1 transfectants (TWIST1 mp1, TWIST1 mp2, TWIST1 C12) and pcDNAmp2 control was transcribed into cDNA using Superscript RT (Invitrogen), in the presence of T7-oligo(dT)24 primer, deoxyribonucleoside triphosphates (dNTPs), and T7 RNA polymerase promoter (Invitrogen). An *in vitro* transcription reaction was then performed to generate biotinylated cRNA which, after fragmentation, was used in a hybridization assay on Affymetrix U133 plus 2.0 GeneChip microarrays, according to manufacturer's protocol (GeneChip 3' IVT Express Kit, Affymetrix). Normalization was performed by global scaling and analysis of differential expression was performed by Microarray Suite software 5.0 (Affymetrix). The final results were imported into Microsoft Excel (Microsoft).

## Supplemental Results

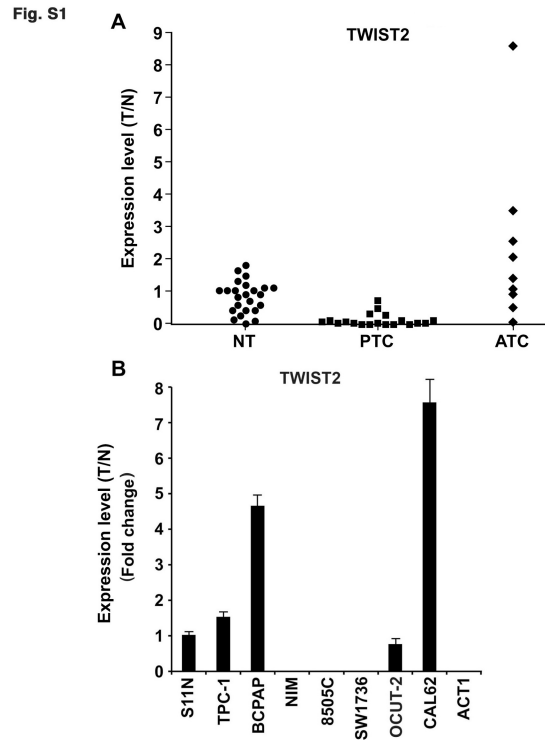


**Figure 1: A:** Quantitative RT-PCR of TWIST2 mRNA in NT (n=22), PTC (n= 19), and ATC (n=9) snap-frozen tissue samples. The level of TWIST2 expression in each sample was measured by comparing its fluorescence threshold with the average fluorescence threshold of the 22 NT samples. The average results of triplicate samples are plotted. **B:** Quantitative RT-PCR of TWIST2 mRNA in normal human thyroid follicular cells (S11N), PTC (TPC-1, BCPAP and NIM) and ATC (8505C, SW1736, OCUT-2 CAL62, ACT- 1) cell lines. The level of TWIST2 expression in each sample was measured by comparing its fluorescence threshold with the fluorescence threshold of the human thyroid follicular cells (S11N). The average results of triplicate samples  $\pm$  SD are plotted.

Fig. S2

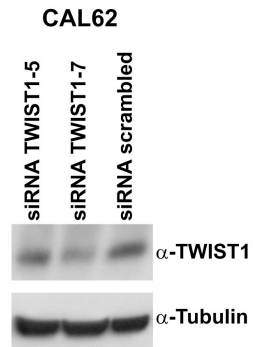


**Figure 2:** CAL62 were transfected with two different small inhibitor duplex RNA targeting TWIST1 (#5, #7) and the scrambled control. Cells were harvested 48 h after transfection, and analyzed for TWIST1 protein expression. Tubulin was used for normalization.

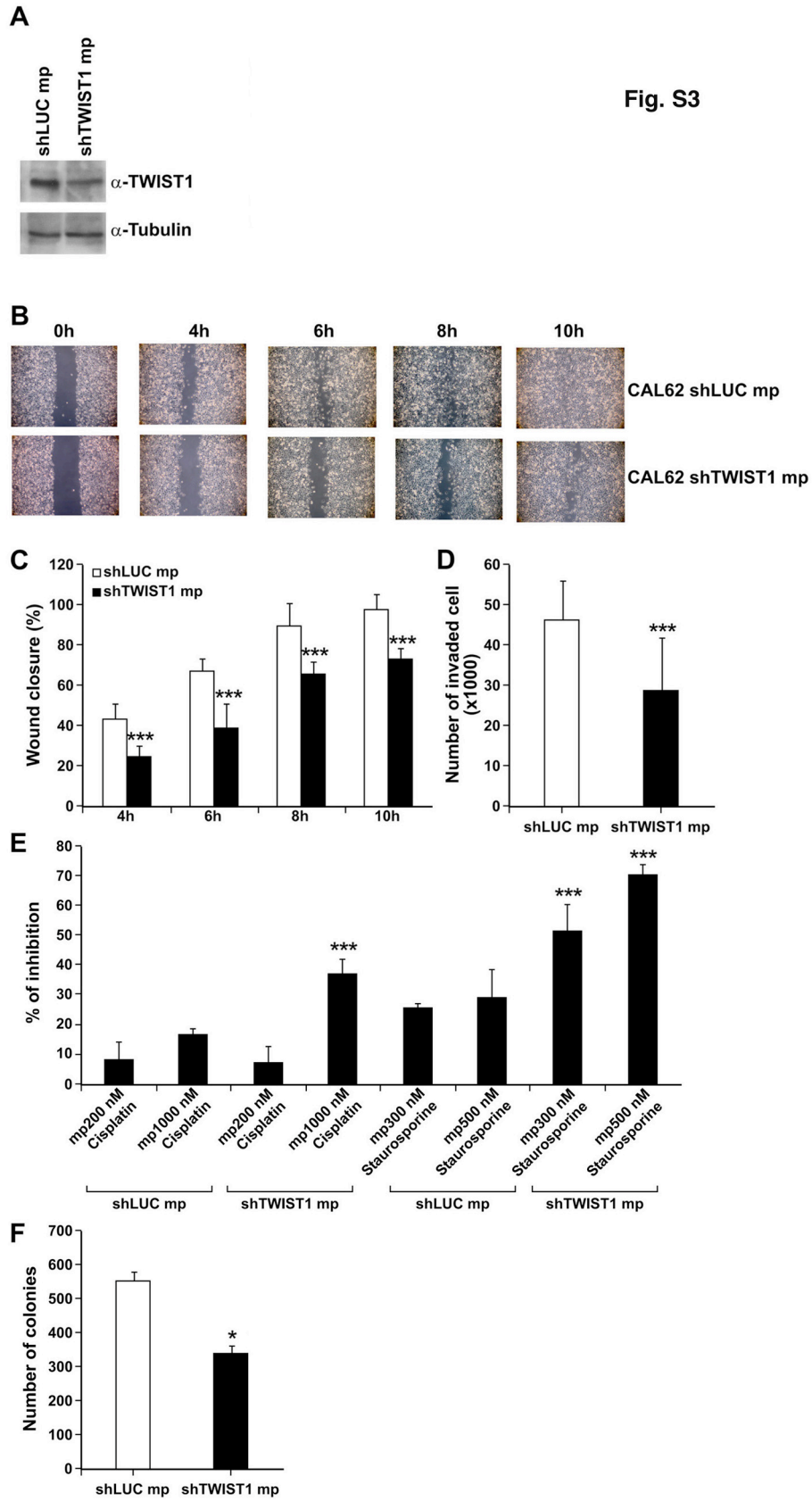
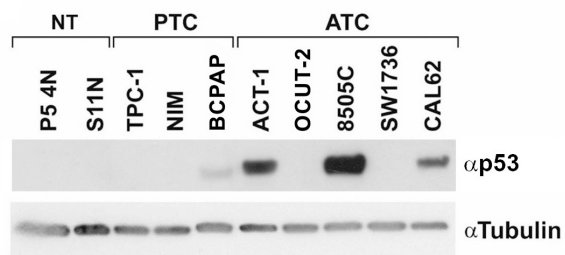


Fig. S3

**Figure 3:** **A** Expression levels of TWIST1 and Tubulin in CAL62 cells transfected with shLUC or shTWIST1; **B:** A scraped wound was placed on the confluent monolayer of CAL62 transfected with shTWIST1 or shLUC and the cell migration into the wound was monitored at the indicated time points. **C:** Wound closure was measured by calculating pixel densities in the wound area and expressed as percentage of wound closure of triplicate areas  $\pm$  SD. **D:** CAL62 transfected with shTWIST1 or shLUC ( $1 \times 10^5$ ) were seeded in the upper chamber of transwells and incubated for 12 h; the upper surface of the filter was wiped clean and cells on the lower surface were stained and counted. Invasive ability is expressed as number of invaded cells. Values represent the average of triplicate experiments  $\pm$  SD. **E:** The cells were treated with increasing doses of Cisplatin or Staurosporine and counted after 24 h. The percentage of viability inhibition is shown: values represent the average of three independent experiments  $\pm$  SD. **F:** CAL62 shLUC mp and CAL62 shTWIST1 mp cells were seeded in soft agar. Total number of colonies were counted after 14 days: values represent the average of three independent experiments  $\pm$  SD. Asterisks indicate  $p < 0.05$  (\*),  $p < 0.01$  (\*\*) and  $p < 0.001$  (\*\*\*)).

Fig. S4



**Figure 4:** Expression levels of p53 in human thyroid cell lines. Cells were lysed and blotted with the indicated antibodies.

### Supplemental References

1. **Schweppe RE, Klopper JP, Korch C, Pugazhenti U, Benezra M, Knauf JA, Fagin JA, Marlow LA, Copland JA, Smallridge RC, Haugen BR** 2008 Deoxyribonucleic acid profiling analysis of 40 human thyroid cancer cell lines reveals cross-contamination resulting in cell line redundancy and misidentification. *J Clin Endocrinol Metab* 93:4331-4341
2. **Salerno P, De Falco V, Tamburrino A, Nappi TC, Vecchio G, Schweppe RE, Bollag G, Santoro M, Salvatore G** 2010 Cytostatic activity of adenosine triphosphate-competitive kinase inhibitors in BRAF mutant thyroid carcinoma cells. *J Clin Endocrinol Metab* 95:450-455
3. **Curcio F, Ambesi-Impiombato FS, Perrella G, Coon HG** 1994 Long-term culture and functional characterization of follicular cells from adult normal human thyroids. *Proc Natl Acad Sci U S A* 91:9004–9008
4. **Fusco A, Berlingieri MT, Di Fiore PP, Portella G, Grieco M, Vecchio G** 1987 One- and two-step transformations of rat thyroid epithelial cells by retroviral oncogenes. *Mol Cell Biol* 7:3365-3370
5. **Melillo RM, Castellone MD, Guarino V, De Falco V, Cirafici AM, Salvatore G, Caiazzo F, Basolo F, Giannini R, Kruhoffer M, Orntoft T, Fusco A, Santoro M** 2005 The RET/PTC-RAS-BRAF linear signaling cascade mediates the motile and mitogenic phenotype of thyroid cancer cells. *J Clin Invest* 115: 1068-1081

**Table 1:** Clinico-pathological features of anaplastic thyroid carcinoma and TWIST1 expression.

Features	TWIST1 negative (n=21)	TWIST1 positive (n=20)	p-value
<b>Phenotype</b>			
Epithelioid (n=19)	76% (16/21)	15% (3/20)	0.0001
Mixed (n=7)	9% (2/21)	25% (5/20)	
Fusocellular (n=15)	15% (3/21)	60% (12/20)	
<b>Ki67/MIB1 expression</b>			
+++ (n=9)	10% (2/21)	35% (7/20)	0.048
++ (n=16)	33% (7/21)	45% (9/20)	
+ (n=15)	52% (11/21)	20% (4/20)	
Negative (n=1)	5% (1/21)	0% (0/20)	
<b>p53 expression</b>			
+++ (n=14)	19% (4/21)	50% (10/20)	0.030
++ (n=10)	33% (7/21)	15% (3/20)	
+ (n=5)	5% (1/21)	20% (4/20)	
Negative (n=12)	43% (9/21)	15% (3/20)	

+: ≥5–≤25% of positive cells

++: >25–<60% of positive cells

+++ : ≥60% of positive cells

# **Attached Manuscript # III**

**Gennaro Di Maro et al.**

Anterior gradient protein 2 promotes survival, migration and invasion of papillary thyroid carcinoma cells.

Manuscript in preparation

*Anterior gradient protein 2 promotes survival, migration and invasion of papillary thyroid carcinoma cells*

Gennaro Di Maro <sup>1</sup>, et al.

<sup>1</sup> Dipartimento di Medicina Molecolare e Biotecnologie Mediche, Università “FedericoII”, Napoli, 8013, Italy.

**Abbreviated Title:** Role of AGR2 in papillary thyroid carcinoma

**Key words:** thyroid cancer, AGR2, endoplasmic reticulum stress

### **Abstract**

Papillary thyroid carcinoma (PTC) is the most common endocrine malignancy. Through a cDNA microarray analysis, we have isolated Anterior gradient protein 2 (AGR2) as a gene upregulated in PTC. AGR2 is a disulfide isomerase overexpressed in several human carcinomas and recently linked to endoplasmic reticulum (ER) stress. We demonstrated by real-time PCR and immunohistochemistry that PTC overexpressed AGR2 respect to normal thyroid tissues. Knockdown of AGR2 induced apoptosis and decreased migration and invasion of PTC cells. Ectopic expression of AGR2 in non-transformed human thyroid cells increased cell migration and invasion and protected cells from ER stress induced by Bortezomib. Thus, AGR2 is a novel marker of PTC and plays a role in thyroid cancer cell survival, migration, invasion and protection from ER stress.

## 1. Introduction

Thyroid carcinoma is the most common endocrine neoplasm and is increasing in incidence (Siegel et al., 2012). Most thyroid carcinoma arises from thyroid follicular cells. These include papillary thyroid carcinoma (PTC) (which accounts for 80% of all thyroid tumors) and follicular thyroid carcinoma (FTC) (approximately 15% of thyroid tumors) as well as the less common anaplastic thyroid carcinoma (Nikiforov and Nikiforova 2011; Kondo et al., 2006). PTC is a well-differentiated slow growing and treatable tumor. The tumor is usually removed by surgery and treated by iodine 131 radiation therapy, however, a few PTC carriers develop recurrences and distant metastases (Nikiforov and Nikiforova 2011; Kondo et al., 2006).

To look for genes potentially involved in the neoplastic transformation of the thyroid gland, we conducted a cDNA microarray screening of different thyroid tumors (Salvatore et al., 2007). Among the genes highly upregulated in PTC, we focused on Anterior gradient protein 2 (AGR2). AGR2, also known as hAG-2 or Gob-4, is the human orthologue of the *Xenopus laevis* protein, XAG-2. In the frog embryo, XAG-2 induces cement gland differentiation (Aberger et al., 1998; Komiya et al., 1999).

Subsequent studies have shown a significant function for AGR2 in a range of biological pathways including cell migration and cellular transformation (Brychtova et al., 2011). AGR2 protein is upregulated in several human carcinoma, including breast, pancreatic, ovarian, esophageal, lung and prostate cancers, and is associated with a metastatic phenotype and poor prognosis (Barraclough et al., 2009; Zhang JS et al., 2005). Many studies revealed that overexpression or suppression of AGR2, in different cancer model systems, can affect cell proliferation, invasion and survival, metastasis and tumor growth (Chevet et al, 2012).

Recently, AGR2 has been shown to have structural characteristics of the protein disulfide isomerase (PDI) family, including a carboxy-terminal endoplasmic reticulum (ER) retention signal KTEL and a single thioredoxin-like domain with a CXXS motif (Persson et al., 2005). PDI proteins catalyze formation, reduction, and isomerization of disulfide bonds, thereby facilitating the maturation of proteins in the ER and ensure correct folding and multimerization of proteins targeted for the secretory pathway. During tumorigenesis, the high proliferation rate of cancer cells requires increased activities of ER protein folding, assembly, and transport, a condition that can induce ER stress. Importantly, AGR2 knock out mice had

elevated endoplasmic reticulum (ER) stress (Zhao et al., 2010). AGR2 expression is induced by ER stress, and siRNA knockdown of AGR2 increases ER stress response (Zhao et al., 2010; Higa et al., 2011). Furthermore, AGR2 localizes in the ER of normal intestinal epithelial cells and is essential for *in vivo* production of mucus (Park SW et al., 2009). Indeed, AGR2 mediates processing of the intestinal mucin MUC2 through formation of mixed disulfide bonds (Park SW et al., 2009).

In this work, we analyze the expression of AGR2 in PTC and its functional consequences.

## 2. Materials and methods

*2.1 Tissue samples* – Tumors (n= 39) and normal (n=25) thyroid tissue samples for immunohistochemical analysis were retrieved from the Pathology Department of the Istituto Pascale, Naples, Italy. In addition, RNA from frozen tissues of 10 PTC cases and 10 normal matched thyroid controls was obtained from the Chernobyl Tissue Bank (<http://www.chernobyltissuebank.com>) (Thomas, 2012). Fifty PTC and 50 normal thyroid tissues used in the DNA array were obtained from Imperial College London, London, UK. In all cases, the respective institutional review boards approved the study protocols. The samples were classified according to the diagnostic criteria required for the identification of PTC (Hedinger et al., 1989).

*2.2. Immunohistochemical staining* - Sections of paraffin-embedded samples were stained with hematoxylin and eosin for histological examination to ensure that the samples fulfilled the diagnostic criteria (Hedinger et al., 1989). For immunohistochemistry analysis, 2 µm paraffin sections were deparaffinised and then placed in a solution of absolute methanol and 0.3% hydrogen peroxide for 30 minutes and then washed in phosphate buffered saline (PBS) before immunoperoxidase staining. The slides were then incubated overnight at 4°C in a humidified chamber with mouse monoclonal antibody against AGR2 (PO1, Abnova, Taipei City, Taiwan) diluted 1:100 in PBS. The slides were subsequently incubated with biotinylated goat anti-mouse IgG for 20 minutes (Vectostain ABC kits, Vector Laboratories) and then with premixed reagent ABC (Vector) for 20 minutes. The immunostaining was performed by incubating the slides in diaminobenzidine (DAB, DAKO) solution containing 0.06 mM DAB and 2 mM hydrogen peroxide in 0.05% PBS, pH 7.6, for 5 minutes, and after chromogen development, the slides were washed, dehydrated with alcohol and xylene and mounted with coverslips using a permanent mounting medium (Permount). Micrographs were taken on Kodak Ektachrome film with a photo Zeiss system. Negative controls were performed in each case by incubating tissue slides with secondary antibody only. The expression of AGR2 was categorized as positive (staining of  $\geq 10\%$  of the tumor cells) and negative (staining of  $< 10\%$  of the tumor cells). The staining intensity of positive cells was further graded in: score 1 (10-50% of positive cells), score 2 (51-75% of positive cells) and

score 3 (76-100% of positive cells). Score values were independently assigned by two blinded investigators (G.C. and M.M.) and a consensus was reached on all scores used for computation.

*2.3. Cell cultures-* Human papillary thyroid cancer cell line TPC-1, was obtained from M. Nagao (Carcinogenesis Division, National Cancer Center Research Institute, Tokyo, Japan). The TPC-1 cell line was identified based on the unique presence of the RET/PTC1 rearrangement. Nthy-ori 3-1 cells are non transformed human thyrocytes immortalized by the Large T of SV40 and were obtained from the European Tissue Culture collection (Sigma Aldrich, St. Louis, MO, USA). Nthy-ori 3-1 cell line was grown in Roswell Park Memorial Institute (RPMI) 1640 medium supplemented with 10% fetal bovine serum (FBS), L-glutamine and penicillin/streptomycin (Invitrogen, Carlsbad, California, USA). TPC-1 cell line was grown Dulbecco's modified Eagle's medium (DMEM) (Invitrogen) supplemented with 10% fetal bovine serum (FBS), L-glutamine and penicillin/streptomycin (Invitrogen).

Bortezomib was obtained from Millenium (Cambridge, MA, USA).

*2.5 Cell viability* - For cell viability determination, cells were collected by trypsinization stained for 10 minutes with 0.4% trypan-blue (Sigma Aldrich) according to manufacturer's instructions, and counted in triplicate.

*2.6 Chemoinvasion* - Cell invasion was examined using a reconstituted extracellular matrix (Matrigel, BD Biosciences, San Jose, CA). The cell suspension ( $1 \times 10^5$  cells per well) was added to the upper chamber of transwell cell culture chambers on a prehydrated polycarbonate membrane filter of 8- $\mu$ m pore size (Costar, Cambridge, MA) coated with 35  $\mu$ g of Matrigel (BD Biosciences). The lower chamber was filled with 10% medium. After incubation at 37° C, non-migrating cells on the upper side of the filter were wiped-off. Invading cells were mounted on glass slides using mounting medium and stained with Hoechst (Sigma Aldrich). Cell migration was quantified by counting the number of stained nuclei in five individual fields in each transwell membrane, by fluorescence microscopy, in duplicate.

*2.7 Wound closure assay* - A wound was introduced on the confluent monolayer cells using a micropipette

tip. Photographs were taken at 40 X magnification using phase-contrast microscopy immediately after wound incision and at different time-points. Wound closure was measured by calculating pixel densities in the wound area by Cell<sup>a</sup> software (Olympus Biosystem Gmb, Hamburg, Germany) and expressed as percentage of wound closure of triplicate areas  $\pm$  SD.

*2.8 RNA silencing* - Pools of 4 small inhibitor duplex RNAs (ON-*TARGETplus* siRNA SMARTpool) targeting human AGR2 (# L-003626-00), and a non-targeting pool (ON-*TARGETplus* Non-Targeting Pool) control (#D 001810-10-20) were purchased from Dharmacon RNAi Technologies (Dharmacon Inc., Chicago, IL, USA). Cells were grown under standard conditions. The day before transfection,  $1 \times 10^5$  TPC-1 cells were plated in 60-mm dishes in complete medium without antibiotics and electroporated using MicroPorator (MP-100, Digital Bio, Euroclone, Milan, Italy) according to the manufacturer's instructions. Cells were harvested 48 and 72 hours after transfection, counted and analyzed for protein expression.

*2.9. Protein studies* - Immunoblotting was carried out according to standard procedures. Anti-AGR2 (PO1) monoclonal antibody was from Abnova (Taipei City, Taiwan); anti-GADD153 (B-3, sc-7351) monoclonal antibody was from Santa Cruz Biotechnology (Santa Cruz, CA, USA); anti- $\alpha$ -tubulin monoclonal antibody was from Sigma-Aldrich. Secondary anti-mouse and anti-rabbit antibodies coupled to horseradish peroxidase were from Santa Cruz Biotechnology.

*2.10. Generation of stable AGR2 transfectants* - cDNA containing the complete coding sequence of human AGR2 was produced by reverse transcription of RNA from HT29 colon adenocarcinoma cells (American Type Culture Collection, Rockville, MD, USA) using the following primers:

AGR2 Cl For.: 5'-ATCCTCGAGCGATCATGGAGAAAATTCCA-3';

AGR2 Cl Rev.: 5'-ATCGGATCCCAATTCAGTCTTCAGCAA-3' (annealing temperature: 60°C).

AGR2 cDNA was cloned into pcDNA3.1 (hereafter named pcDNA) (Invitrogen) by using BamHI and XhoI restriction enzymes and verified by sequencing.

A point mutation in AGR2 that changed the cysteine at aminoacid position 81 to serine (C→S) was introduced in the pcDNA-AGR2 plasmid by the Stratagene QuikChange site-directed mutagenesis kit

(Agilent Technologies, Inc. Life Sciences and Chemical Analysis Group, Santa Clara, CA, USA).

The following oligonucleotides were used:

AGR2 C81S For: 5'- CATCACTTGGATGAGTCCCCACACAGTCAAGC-3';

AGR2 C81S Rev: 5'- GCTTGACTGTGTGGGGACTCATCCAAGTGATG-3' (annealing temperature: 55°C).

The Nthy-ori 3-1 and TPC-1 cells were transfected with pcDNA-AGR2, pcDNA-AGR2 (C→S) or the empty vector (pcDNA) using the Lipofectamine Reagent (Invitrogen) according to the instructions of the manufacturer. Two days later, G418 (Invitrogen) was added at a concentration of 0.3 mg/ml (Nthy-ori 3-1) or at a concentration of 1.2 mg/ml (TPC-1). Several clones and mass populations of transfectants were isolated, expanded and screened for AGR2 expression by Western blot.

*2.11. RNA extraction and expression studies* - Total RNA was isolated with the RNeasy Kit (Qiagen, Crawley, West Sussex, UK). The quality of the RNAs was verified by the 2100 Bioanalyzer (Agilent Technologies, Waldbronn, Germany); only samples with RNA integrity number (RIN) value > 7 were used for further analysis. One µg of RNA from each sample was reverse-transcribed with the QuantiTect® Reverse Transcription (Qiagen).

*2.12. Semi-quantitative RT-PCR*- Semiquantitative RT-PCR was applied to study AGR2 expression in PTC samples and normal thyroid matched control; amplimers and annealing temperatures were as follows:

AGR2 F: CTG GCCAGAGATAACCACAGTC;

AGR2 R: AGTTGGTCACCCCAACCTC (annealing temperature: 60°C).

β-actin mRNA was used as housekeeping gene; β-actin amplimers and annealing temperatures were as follows:

β-Actin F: TGC GTGACATTAAGGAGAAG;

β-Actin R: GCTCGTAGCTCTTCTCCA (annealing temperature: 60°C).

PCR were performed in triplicates, PCR products were subjected to agarose gel electrophoresis and signal intensity was analyzed with the Phosphorimager (Typhoon 8600, Amersham Pharmacia Biotech) interfaced with the ImageQuant software.

2.13. *Xbp1 splicing assay*- Xbp1 splicing was measured by semi-quantitative RT-PCR using the following specific primers:

Xbp1s. For: 5'- AAACAGAGTAGCAGCTCAGACTGC-3';

Xbp1s. Rev: 5'- CCTTCTGGGTAGACCTCTGGGAG-3' (annealing temperature: 64°C); flanking the splicing site yielding PCR product sizes of 164 and 138 bp, Xbp1u (unspliced) and Xbp1s (spliced) respectively. Products were resolved on 2.5% agarose gels and band intensity was determined densitometrically with the ImageJ software.

2.14. *Statistical analysis*- Data are presented as mean  $\pm$  standard deviations. Mann–Whitney *U* test or Student *t* unpaired tests were used. *P* values were 2-sided throughout, and  $P < 0.05$  was considered statistically significant. Statistical analyses were carried out using the Graph Pad InStat software program (version 3.1a, La Jolla, CA, USA).

### 3. Results

#### 3.1. *AGR2 is upregulated in human PTC samples*

We measured AGR2 expression by immunohistochemistry with an anti-AGR2 monoclonal antibody in 64 thyroid samples including 25 normal thyroid (NT) samples and 39 PTC samples. Representative immunohistochemical staining is shown in Figure 1A, and the entire dataset is reported in Table 1. AGR2 was expressed at low levels in normal thyroid glands (Fig. 1A, inset 1). In contrast, a large fraction (~ 71%) of PTC samples (PTC classical papillary variant: 23 out of 28 samples; PTC follicular variant: 5 out of 11 samples), were positive for AGR2 expression in more than 75% (3+) of the cells, and positivity was confined to tumor cells (Table 1 and Figure 1A, inset 2). No staining was observed in the absence of the primary antibody (Figure 1A, inset 3). Normal colon mucosa was used as positive control (Figure 1A, inset 4).

To obtain an additional assessment of AGR2 upregulation and to determine whether upregulation occurred also at RNA level, we verified AGR2 expression levels in a DNA array dataset of 50 normal human thyroid (NT) samples and 50 PTC samples. As shown in Figure 1B, PTC samples showed significantly increased AGR2 levels compared to normal thyroid tissues ( $P=0.000000365$ ). The data was further confirmed by semi-quantitative RT-PCR analysis in an independent set of PTC samples. Nine out of ten PTC samples analyzed expressed elevated AGR2 mRNA levels compared to the matched normal thyroid tissues (Figure 1C).

#### 3.2. *Knockdown of AGR2 induces apoptosis of TPC-1 cells*

We evaluated the effects of AGR2 ablation in TPC-1 cells by RNA interference. TPC-1 cells were transfected with AGR2 siRNA or with scrambled siRNA, counted and lysed at different time points. At 48 and 72 hours after transfection AGR2 siRNA reduced AGR2 protein levels respectively of about 56% and 96% (Fig. 2A). Forty-eight hours after transfection TPC-1 cells transfected with scrambled siRNA numbered  $192 \times 10^3$ , whereas those transfected with AGR2 siRNA numbered  $146 \times 10^3$  ( $P=0.0492$ ). Seventy-two hours after transfection, TPC-1 cells transfected with scrambled siRNA numbered  $413 \times 10^3$ , whereas those transfected with AGR2 siRNA numbered  $279 \times 10^3$  ( $P=0.0045$ ) (Fig. 2B). Accordingly, the percentages of trypan blue excluding (viable) cells, of TPC-1 transfected with AGR2 siRNA, 48 and 72 hours post

transfection, were of 77% and 33% of scrambled control respectively, confirming that AGR2 depletion reduced thyroid cancer cell viability ( $P<0.0001$ ) (Figure 2C).

### 3.3. Knockdown of AGR2 reduces migration and invasion of TPC-1 cells

We evaluated the migration (by a wound-healing assay) and invasion (by a Matrigel invasion assay) ability of AGR2 siRNA-transfected cells. A scraped wound was introduced on the confluent monolayer of TPC-1 cells transfected with AGR2 siRNA or scrambled siRNA. Figure 2D and E shows that TPC-1 transfected with the scrambled control efficiently migrated into the wound; in contrast, cells transfected with AGR2 siRNA had a reduced migrating ability both at 12 hours ( $P<0.0001$ ) and at 24 hours ( $P<0.0001$ ). Moreover, cells transfected with AGR2 siRNA showed a reduced ability to invade Matrigel compared to control cells ( $P<0.0001$ ) (Fig. 2F and G).

### 3.4. Ectopic AGR2 promotes migration and invasion of Nthy-ori 3-1 cells

We transfected the non-transformed thyroid cells, Nthy-ori 3-1, which do not express AGR2, with an AGR2-expressing plasmid (pcDNA-AGR2), or with an AGR2-mutant plasmid (pcDNA-AGR2 C→S), or with the empty vector (pcDNA). The cysteine 81 to serine mutation (C→S) in the thioredoxin domain of AGR2 ablates the catalytic activity of AGR2 (24). Several cell clones and mass populations of Nthy-ori 3-1 cells transfected with the different plasmids, were selected in G418. One mass population of AGR2, one mass population of AGR2 (C→S) and one mass population of vector (pcDNA) control transfected cells were selected for further studies (Fig. 3A). Nthy-ori 3-1 AGR2, AGR2 (C→S) and pcDNA cells show comparable growth rates (Fig. 3B). Then, we studied cell migration using the wound closure assay. A scraped wound was introduced on the confluent monolayer of Nthy-ori 3-1 transfected with AGR2, AGR2 (C→S) or the empty vector (pcDNA), and the cell migration into the wound was monitored after 9 and 12 hours. As shown in Figure 3C and D, migration rate was higher in AGR2-transfected cells compared to control vector (pcDNA) cells at 9 hours ( $P<0.0001$ ) and at 12 hours ( $P<0.0001$ ) and compared to AGR2 (C→S) cells at 9 hours ( $P=0.0006$ ) and at 12 hours ( $P<0.0001$ ). We next seeded AGR2, AGR2 (C→S) cells and vector control (pcDNA) cells into the top chamber of transwells and evaluated their ability to invade Matrigel. AGR2

overexpression increased the invasive ability of Nthy-ori 3-1 cells in comparison to vector control (pcDNA) cells ( $P < 0.0001$ ) and in comparison to AGR2 (C→S) cells ( $P < 0.0001$ ) (Fig. 3E and F).

### 3.5. Ectopic AGR2 promotes cell migration and invasion of TPC-1 cells

To confirm these findings, we overexpressed AGR2 in TPC-1 cells. Cells were transfected with AGR2 (pcDNA-AGR2), with AGR2-mutant plasmid (pcDNA AGR2 C→S) or with the empty vector (pcDNA). Mass populations were selected in G418 (Supplemental Figure 1A). Growth rate was similar in TPC-1-AGR2, AGR2 (C→S) and control (pcDNA) cell lines (Supplemental Figure 1B). Then, we studied cell migration using the wound closure assay. As shown in Supplemental Figure 1C migration rate was higher in TPC-1 AGR2 cells compared to AGR2 (C→S) cells ( $P < 0.0001$ ) and compared to vector control (pcDNA) cells ( $P < 0.0001$ ). We next seeded TPC-1 AGR2, AGR2 (C→S) and pcDNA control cells into the top chamber of transwells and evaluated their ability to invade Matrigel. TPC-1 cells had a basal level of invasiveness, AGR2 overexpression further increased this ability in comparison to TPC-1 AGR2 (C→S) cells ( $P < 0.0001$ ) and to control vector (pcDNA) cells ( $P < 0.0001$ ) (Supplemental Figure 1D).

### 3.6. AGR2 protects non transformed thyroid Nthy-ori 3-1 cells from endoplasmic reticulum stress

AGR2 is a disulfide isomerase on the basis of its CXXS motif, and has a role in the endoplasmic reticulum (ER) stress response (Fritzsche et al., 2006 b). Thus, we studied the effects of AGR2 ectopic expression in the ER stress pathway upon treatment with Bortezomib. Bortezomib is a potent and selective inhibitor of the proteasome that causes an accumulation of unfolded proteins in the ER (Mujtaba and Dou, 2011; Mitsiades et al., 2006). Nthy-ori 3-1 cells transfected with AGR2, AGR2 (C→S) or vector (pcDNA) were treated for 24 hours with Bortezomib 100 nM. After treatment, cells were stained with trypan-blue and counted. As shown in Figure 4A overexpression of AGR2 in Nthy-ori 3-1 cells treated with Bortezomib increased cell viability in comparison to overexpression of AGR2 (C→S) ( $P = 0.0002$ ) and to control (pcDNA) ( $P = 0.0006$ ). Trypan blue excluding cells were 50%, 73% and 45% respectively in Nthy-ori 3-1 pcDNA, AGR2 and AGR2 (C→S) cells treated with Bortezomib.

Then, we examined the expression levels of members of the UPR pathways, in particular of Chop (also named GADD153) and of the spliced form of X box-binding protein 1 (Xbp1s). GADD153 and Xbp1s are

well-characterized biomarkers of ER stress (Ma and Hendershot, 2004; Moenner et al., 2007). Then, we determined by Western blot the expression level of GADD153 (Chop) in Nthy-ori 3-1 AGR2, AGR2 (C→S) or empty vector (pcDNA) cells treated with Bortezomib (100 nM) for 24 hours. As shown in Figure 4B a reduced increase in the amount of GADD153 protein upon Bortezomib treatment was detected in Nthy-ori 3-1 AGR2 cells compared to pcDNA of ~ 13 fold ( $P < 0.0001$ ) and compared to AGR2 (C→S) cells of ~ 13 fold ( $P < 0.0001$ ). These data indicate that AGR2 ectopic expression protects non-transformed thyroid cells from ER stress induced by Bortezomib.

#### 4. Discussion

AGR2 is a protein disulfide isomerase that is overexpressed in several human carcinoma and can stimulate cancer cell proliferation, invasion, survival and metastasis.

In the present study, we demonstrated that AGR2 is a novel marker of papillary thyroid carcinoma (PTC). Further, we investigated the functional role of AGR2 using gain and loss-of-function approaches. Knockdown of AGR2 in papillary thyroid carcinoma cells induced cell death, decreased cell migration and invasion. On the other hand, forced AGR2 expression in non-transformed thyroid, Nthy-ori 3-1 cells, which are endogenously deficient of AGR2, resulted in increased cell migration and invasion and protection from ER stress.

The endoplasmic reticulum (ER) is the cell organelle where secretory and membrane proteins are synthesized and folded. Proteins that fail to fold properly are retained in the ER and their accumulation may constitute a form of stress to the cell. Several signaling pathways, collectively known as unfolded protein response (UPR), have evolved to detect the accumulation of misfolded proteins in the ER and activate a cellular response that attempts to maintain homeostasis. (Ma and Hendershot 2004; Moenner et al., 2007).

Increased expression of the UPR components, including Xbp1 and GADD153 have been detected in breast cancer, gastric tumors, and esophageal adenocarcinomas (Ma and Hendershot 2004; Moenner et al., 2007).

In this context, our hypothesis is that AGR2 is a protein upregulated by PTC cells to cope with the ER stress. As shown for other ER resident proteins (Ma and Hendershot 2004; Moenner et al., 2007), increased AGR2 expression could enhance ER folding capacity and allow cancer cells to cope with increased protein production and secretion, participating in cancer aggressiveness. Further, the expression of PDI proteins and ER chaperones has also been correlated with cancer invasion and metastasis in several tumor types (Lovat et al., 2008; Goplen et al., 2006) and here we provide similar evidence for AGR2 in PTC.

**Acknowledgements**

The technical assistance of Mayakannan Manikandan is gratefully acknowledged.

## References

- Aberger F, Weidinger G, Grunz H, Richter K 1998 Anterior specification of embryonic ectoderm: the role of the *Xenopus* cement gland-specific gene XAG-2. *Mech Dev* 72: 115–130
- Barracough DL, Platt-Higgins A, de Silva Rudland S, Barracough R, Winstanley J, West CR, Rudland PS 2009 The metastasis-associated anterior gradient 2 protein is correlated with poor survival of breast cancer patients. *Am J Pathol* 175: 1848–1857
- Brychtova V, Vojtesek B, Hrstka R 2011 Anterior gradient 2: a novel player in tumor cell biology. *Cancer Lett* 304: 1-7
- Chen R, Pan S, Duan X, Nelson BH, Sahota RA, de Rham S, Kozarek RA, McIntosh M, Brentnall TA 2010 Elevated level of anterior gradient-2 in pancreatic juice from patients with pre-malignant pancreatic neoplasia. *Mol Cancer* 9: 149
- Chevet E, Fessart D, Delom F, Mulot A, Vojtesek B, Hrstka R, Murray E, Gray T, Hupp T. Emerging roles for the pro-oncogenic anterior gradient-2 in cancer development. *Oncogene*. 2012 Sep 3.
- Fletcher GC, Patel S, Tyson K, Adam PJ, Schenker M, Loader JA, Daviet L, Legrain P, Parekh R, Harris AL, Terrett JA 2003 hAG-2 and hAG-3, human homologues of genes involved in differentiation, are associated with estrogen receptor-positive breast tumours and interact with metastasis gene C4.4a and dystroglycan. *Br J Cancer* 88: 579–585
- Fritzsche FR, Dahl E, Dankof A, Burkhardt M, Pahl S, Petersen I, Dietel M, Kristiansen G 2007 Expression of AGR2 in non small cell lung cancer. *Histol Histopathol* 22:703–708
- Fritzsche FR, Dahl E, Pahl S, Burkhardt M, Luo J, Mayordomo E, Gansukh T, Dankof A, Knuechel R, Denkert C, Winzer KJ, Dietel M, Kristiansen G 2006 Prognostic relevance of AGR2 expression in breast cancer. *Clin Cancer Res* 12:1728–1734
- Goplen D, Wang J, Enger PØ, Tysnes BB, Terzis AJ, Laerum OD, Bjerkvig R 2006 Protein disulfide isomerase expression is related to the invasive properties of malignant glioma. *Cancer Res* 66:9895–9902
- Hedinger C, Williams ED, and Sobin LH 1989 The WHO histological classification of thyroid tumors: a commentary on the second edition. *Cancer* 63:908– 911

- Higa A, Mulot A, Delom F, Bouchecareilh M, Nguyễn DT, Boismenu D, Wise MJ, Chevet E 2011 Role of pro-oncogenic protein disulfide isomerase (PDI) family member anterior gradient 2 (AGR2) in the control of endoplasmic reticulum homeostasis. *J Biol Chem* 286: 44855-44868
- Komiya T, Tanigawa Y, Hirohashi S 1999 Cloning of the gene gob-4, which is expressed in intestinal goblet cells in mice. *Biochim Biophys Acta* 1444:434-438
- Kondo T, Ezzat S, Asa SL 2006 Pathogenetic mechanisms in thyroid follicular-cell neoplasia. *Nat Rev Cancer* 6: 292-306
- Liu D, Rudland PS, Sibson DR, Platt-Higgins A, Barraclough R 2005 Human homologue of cement gland protein, a novel metastasis inducer associated with breast carcinomas. *Cancer Res* 65: 3796-3805
- Lovat PE, Corazzari M, Armstrong JL, Martin S, Pagliarini V, Hill D, Brown AM, Piacentini M, Birch-Machin MA, Redfern CP 2008 Increasing melanoma cell death using inhibitors of protein disulfide isomerases to abrogate survival responses to endoplasmic reticulum stress. *Cancer Res* 68:5363-5369
- Ma Y, Hendershot LM 2004 The role of the unfolded protein response in tumour development: friend or foe? *Nat Rev Cancer*. 4: 966-977
- Mitsiades CS, McMillin D, Kotoula V, Poulaki V, McMullan C, Negri J, Fanourakis G, Tseleni-Balafouta S, Ain KB, Mitsiades N 2006 Antitumor effects of the proteasome inhibitor bortezomib in medullary and anaplastic thyroid carcinoma cells in vitro. *J Clin Endocrinol Metab* 91:4013-4021
- Moenner M, Pluquet O, Bouchecareilh M, Chevet E 2007 Integrated endoplasmic reticulum stress responses in cancer. *Cancer Res* 67:10631-10634
- Mujtaba T, Dou QP 2011 Advances in the understanding of mechanisms and therapeutic use of bortezomib. *Discov Med*. 12: 471-480
- Nikiforov YE, Nikiforova MN 2011 Molecular genetics and diagnosis of thyroid cancer. *Nat Rev Endocrinol* 7: 569-580
- Park K, Chung YJ, So H, Kim K, Park J, Oh M, Jo M, Choi K, Lee EJ, Choi YL, Song SY, Bae DS, Kim BG, Lee JH 2011 AGR2, a mucinous ovarian cancer marker, promotes cell proliferation and migration. *Exp Mol Med* 43: 91-100

- Park SW, Zhen G, Verhaeghe C, Nakagami Y, Nguyenvu LT, Barczak AJ, Killeen N, Erle DJ 2009 The protein disulfide isomerase AGR2 is essential for production of intestinal mucus. *Proc Natl Acad Sci U S A* 106: 6950–6955
- Persson S, Rosenquist M, Knoblach B, Khosravi-Far R, Sommarin M, Michalak M 2005 Diversity of the protein disulfide isomerase family: identification of breast tumor induced Hag2 and Hag3 as novel members of the protein family. *Mol Phylogenet Evol* 36: 734-740
- Pohler E, Craig AL, Cotton J, Lawrie L, Dillon JF, Ross P, Kernohan N, Hupp TR 2004 The Barrett's antigen anterior gradient-2 silences the p53 transcriptional response to DNA damage. *Mol Cell Proteomics* 3: 534–547
- Ramachandran V, Arumugam T, Wang H, Logsdon CD 2008 Anterior gradient 2 is expressed and secreted during the development of pancreatic cancer and promotes cancer cell survival. *Cancer Res* 68: 7811–7818.
- Salvatore G, Nappi TC, Salerno P, Jiang Y, Garbi C, Ugolini C, Miccoli P, Basolo F, Castellone MD, Cirafici AM, Melillo RM, Fusco A, Bittner ML, Santoro M 2007 A cell proliferation and chromosomal instability signature in anaplastic thyroid carcinoma. *Cancer Res* 67: 10148-10158
- Siegel R, Naishadham D, Jemal A 2012 Cancer statistics. *CA Cancer J Clin.* 2012 1: 10-29
- Thomas GA 2012 The Chernobyl Tissue Bank: integrating research on radiation-induced thyroid cancer. *J Radiol Prot* 32: N77-80
- Thompson DA, Weigel RJ 1998 hAG-2, the human homologue of the *Xenopus laevis* cement gland gene XAG-2, is coexpressed with estrogen receptor in breast cancer cell lines. *Biochem Biophys Res Commun* 251: 111–116
- Wang Z, Hao Y, Lowe AW 2008 The adenocarcinoma-associated antigen, AGR2, promotes tumor growth, cell migration, and cellular transformation. *Cancer Res* 68: 492–497
- Zhang JS, Gong A, Chevillie JC, Smith DI, Young CY 2005 AGR2, an androgen-inducible secretory protein overexpressed in prostate cancer. *Genes Chromosomes Cancer* 43: 249–259
- Zhang Y, Forootan SS, Liu D, Barraclough R, Foster CS, Rudland PS, Ke Y 2007 Increased expression of anterior gradient-2 is significantly associated with poor survival of prostate cancer patients. *Prostate Cancer Prostatic Dis* 10: 293–300

Zhao F, Edwards R, Dizon D, Afrasiabi K, Mastroianni JR, Geyfman M, Ouellette AJ, Andersen B, Lipkin SM 2010 Disruption of Paneth and goblet cell homeostasis and increased endoplasmic reticulum stress in *Agr2*<sup>-/-</sup> mice. *Dev Biol* 338:270–2

## Legend to Figures

### Figure 1: AGR2 expression in human thyroid tissue samples.

**A)** Representative images of normal thyroid (NT) (inset 1), papillary thyroid carcinoma (PTC) (inset 2), normal colon sample (inset 4) (used as positive control) stained with a mouse monoclonal anti-AGR2 antibody, are presented. PTC shows a strong immunoreactivity for AGR2, while NT is negative. Inset 3, shows a PTC sample incubated only with secondary antibody. Photos were taken at 200x magnification. **B)** Expression of AGR2 in DNA array of 50 normal thyroid (NT) samples and 50 PTC. The box plot for AGR2 shows a significant upregulation of this gene in tumor tissues. **C)** Semiquantitative RT-PCR showing increased levels of AGR2 in PTC samples in comparison to matched normal thyroids control. Human  $\beta$ -actin mRNA levels were used for normalization.

### Figure 2: Effects of AGR2 knockdown on TPC-1 cell growth, migration and invasion.

**A)** TPC-1 cells were transfected with AGR2 siRNA or with scrambled siRNA. Cells were harvested at different time points and protein lysates were subjected to immunoblotting with the indicated antibodies. **B)** TPC-1 cells were transfected with AGR2 siRNA or with scrambled siRNA and counted at different time points. Values represent the average of triplicate experiments  $\pm$  standard deviations. **C)** TPC-1 cells were transfected with AGR2 siRNA or with scrambled siRNA; after 48 and 72 hours cells were collected by trypsinization, stained for 10 minutes with trypan-blue and counted in triplicate. The percentage of trypan blue excluding cells compared to cells transfected with scrambled siRNA is reported  $\pm$  standard deviations. **D)** TPC-1 cells were transfected with AGR2 siRNA or with scrambled siRNA, after 48 hours a wound was introduced and cell migration into the wound was monitored at 12 and 24 hours. **E)** Wound closure was measured by calculating pixel densities in the wound area and expressed as percentage of wound closure of triplicate areas  $\pm$  standard deviations. **F)** TPC-1 cells were transfected with AGR2 siRNA or with scrambled siRNA; 48 hours after transfection, cells were seeded in the upper chamber of transwells and incubated for 24 hours; the upper surface of the filter was wiped clean and cells on the lower surface were stained with 0.1% crystal violet photographed and counted. This figure is representative of three independent

experiments. **G)** Invasive ability is expressed as number of invaded cells. Values represent the average of triplicate experiments  $\pm$  standard deviations. Asterisks indicate  $P < 0.05$  (\*),  $P < 0.01$  (\*\*) and  $P < 0.001$  (\*\*\*).

**Figure 3: Effects of AGR2 ectopic expression on non-transformed thyroid, Nthy-ori 3-1, cell growth, migration and invasion.**

**A)** Expression levels of AGR2 and AGR2 (C $\rightarrow$ S) in transfected Nthy-ori 3-1 cells: after G418 selection, cells were lysed and blotted with the indicated antibodies. **B)** Nthy-ori 3-1 cells transfected with AGR2, AGR2 (C $\rightarrow$ S) or empty vector (pcDNA) were plated and counted at different time points. Values represent the average of triplicate experiments  $\pm$  standard deviations. **C)** A wound was introduced on confluent monolayer of Nthy-ori 3-1 cells transfected with AGR2, AGR2 (C $\rightarrow$ S) and vector control (pcDNA) and wound closure was monitored at 9 and 12 hours time points. **D)** Wound closure was measured by calculating pixel densities in the wound area and expressed as percentage of wound closure of triplicate areas  $\pm$  standard deviations. **E)** Nthy-ori 3-1 cells transfected with AGR2, AGR2 (C $\rightarrow$ S) or the empty vector (pcDNA) were seeded in the upper chamber of transwells and incubated for 24 hours; the upper surface of the filter was wiped clean and cells on the lower surface were stained and counted. **F)** Invasive ability was expressed as number of invaded cells. Values represent the average of triplicate experiments  $\pm$  standard deviations. Asterisks indicate  $P < 0.001$  (\*\*\*).

**Figure 4: Effects of Bortezomib in non transformed thyroid Nthy-ori 3-1 cells ectopically expressing AGR2.**

**A)** Nthy-ori 3-1 cells transfected with AGR2, AGR2 (C $\rightarrow$ S) or with the empty vector (pcDNA) were treated for 24 hours with Bortezomib 100 nM. After treatment cells were collected by trypsinization, stained for 10 minutes with trypan-blue and counted in triplicate. The percentage of trypan blue excluding cells is reported  $\pm$  standard deviations. Asterisks indicate  $P < 0.001$  (\*\*\*). **B)** Nthy-ori 3-1 cells transfected with AGR2, AGR2 (C $\rightarrow$ S) or with the empty vector (pcDNA) were treated for 24 hours with Bortezomib 100 nM. After treatment cells were lysed, and protein lysates were subjected to immunoblotting with the indicated antibodies.

**Table 1:** AGR2 expression in thyroid samples (n=64)

Tissue*	Number of sample	AGR2 (score**)			
		Negative	Positive		
		0	1+	2+	3+
NT	25	4	21		
PTC	28 (PTC CV)	1	2	2	23
	11 (PTC FV)	2	1	3	5

\* NT= normal thyroid; PTC CV= papillary thyroid carcinoma, classical variant; PTC FV= papillary thyroid carcinoma, follicular variant

\*\*

0 = <10% of positive cells

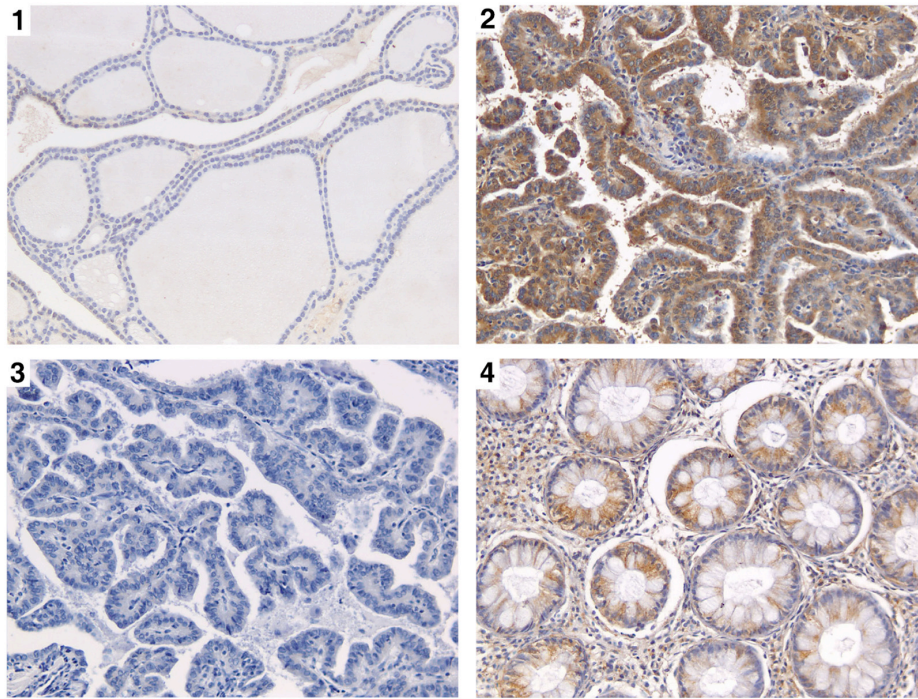
1 = 10-50% of positive cells

2 = 51-75% of positive cells

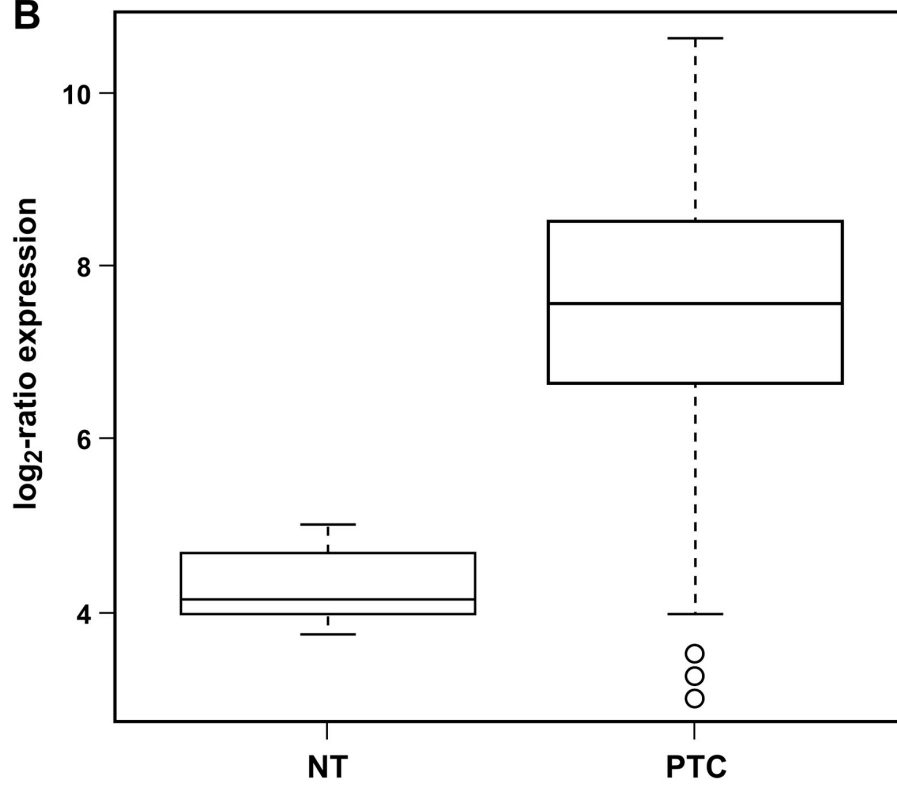
3 = 76-100% of positive cells

**Figure 1**

**A**



**B**



**C**

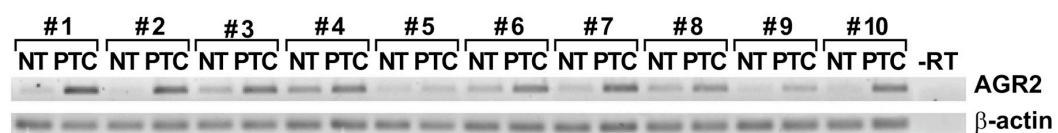


Figure 2

TPC-1

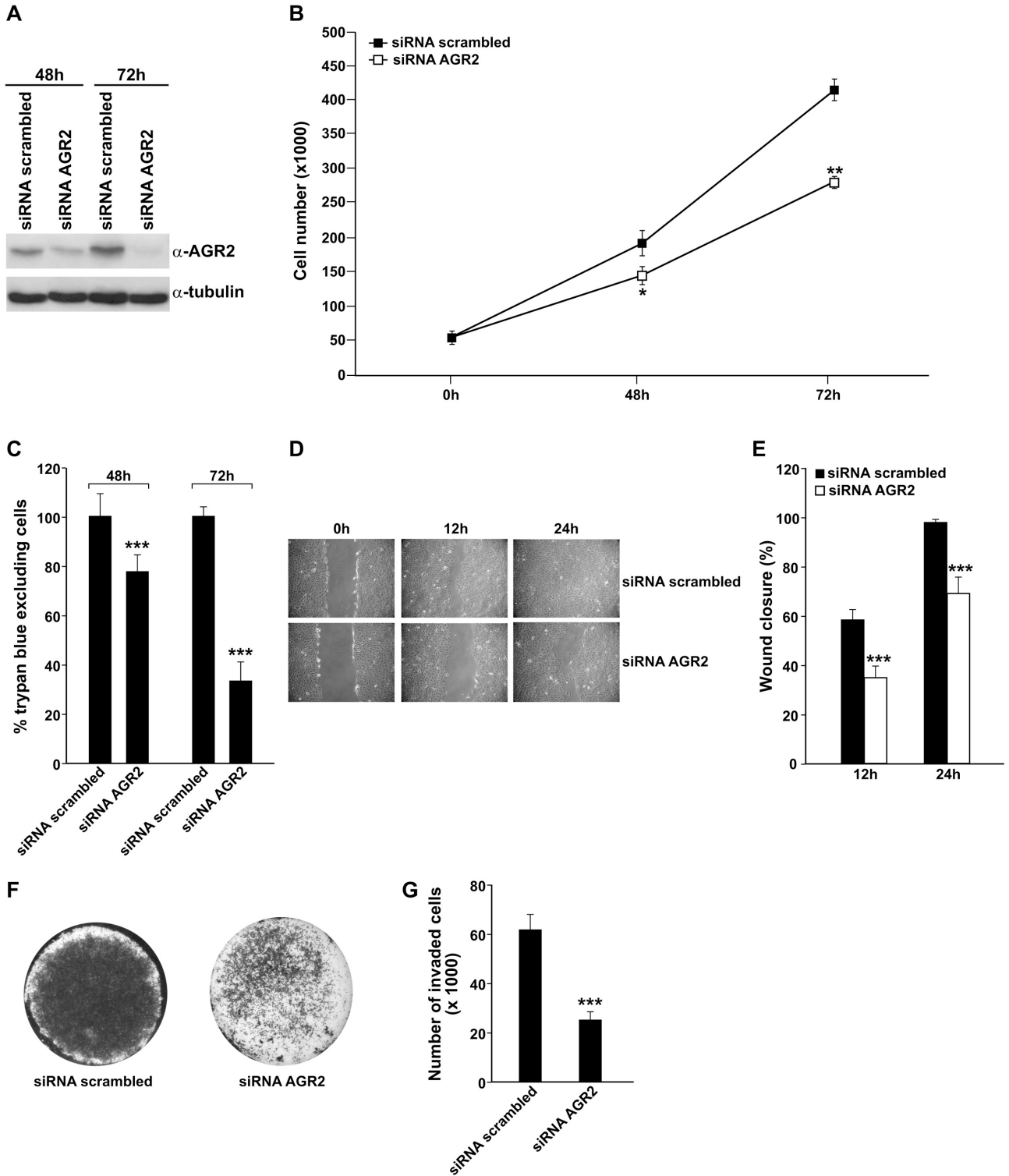


Figure 3

Nthy-ori 3-1

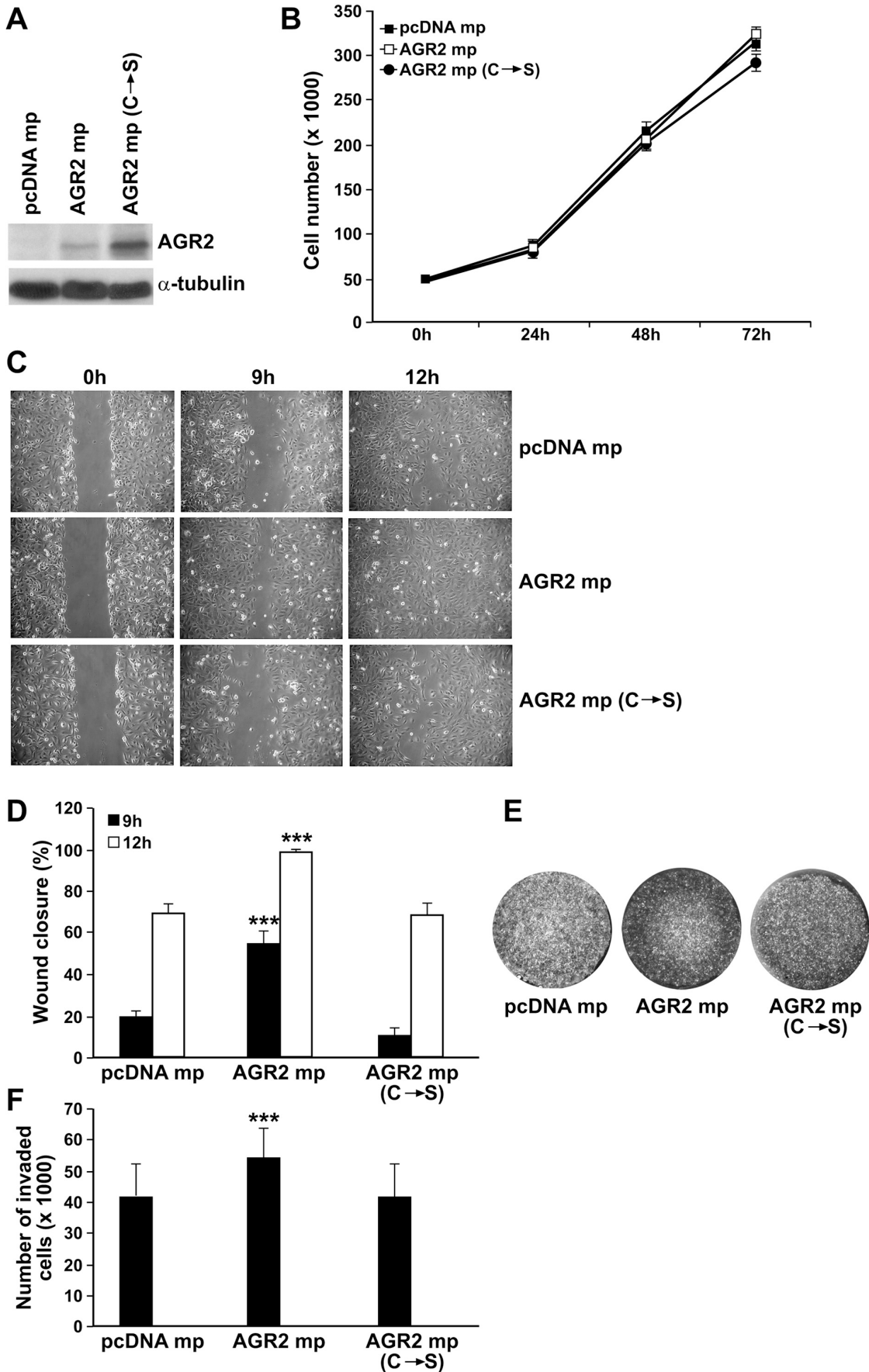
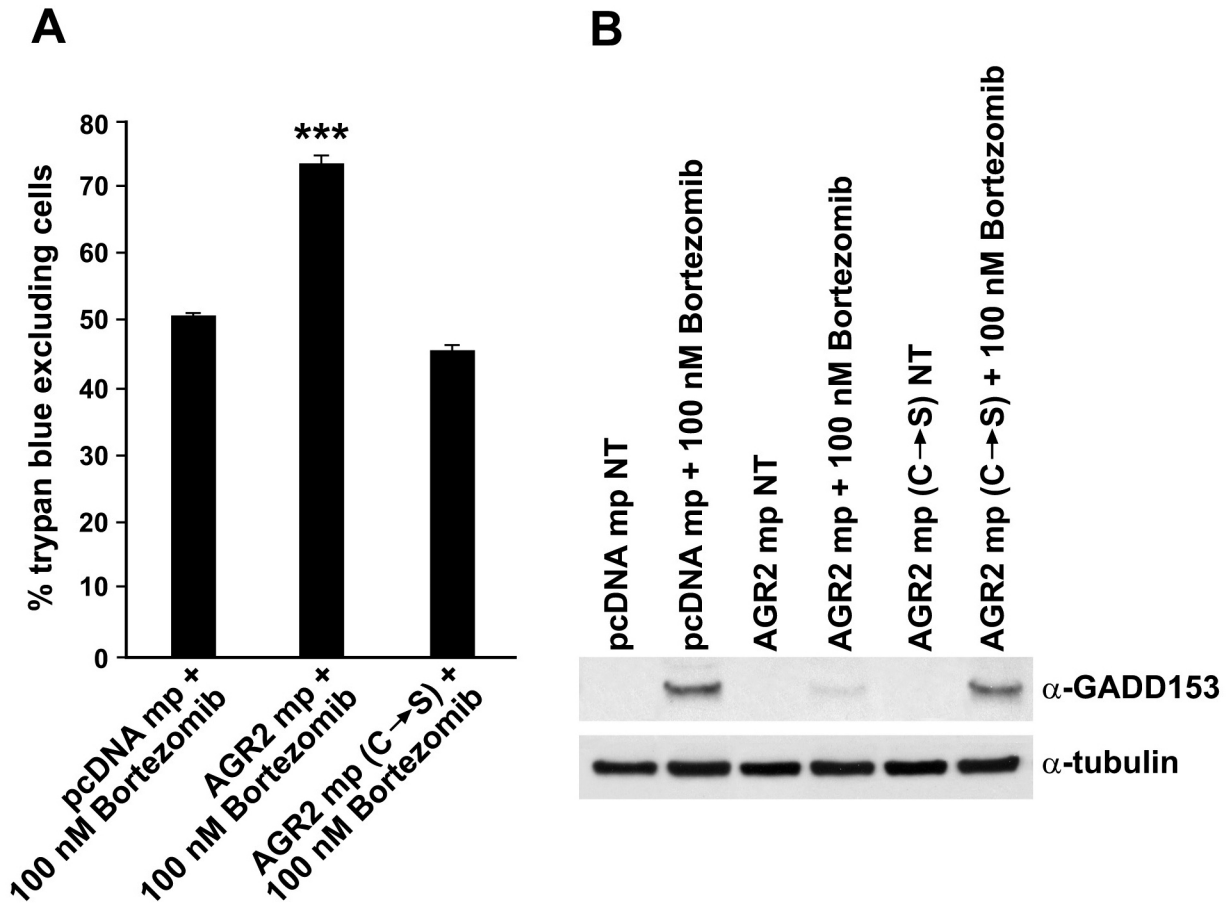
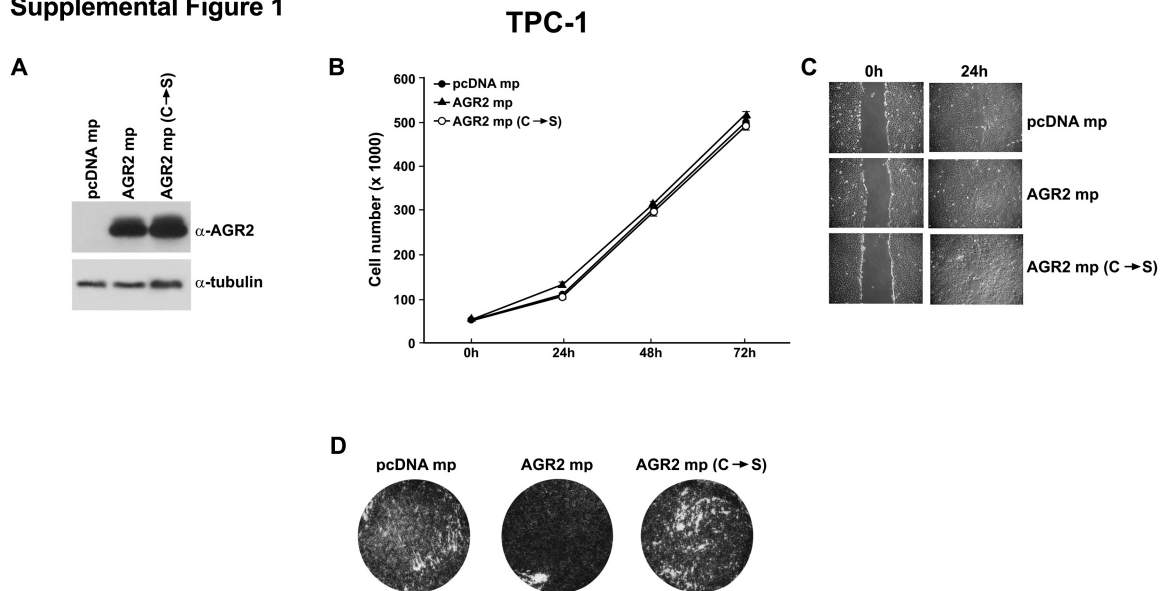


Figure 4

### Nthy-ori 3-1



## Supplemental Figure 1



### Supplemental Figure 1: Effects of AGR2 ectopic expression on TPC-1 cell growth, migration and invasion.

Expression levels of transfected AGR2 and AGR2 (C $\rightarrow$ S) in TPC-1 cells: after G418 selection, cells were lysed and blotted with the indicated antibodies. **B**) TPC-1 cells transfected with AGR2, AGR2 (C $\rightarrow$ S) or empty vector (pcDNA) were plated and counted at different time points. Values represent the average of triplicate experiments  $\pm$  standard deviations. **C**) A wound was introduced on confluent monolayer of TPC-1 cells transfected with AGR2, AGR2 (C $\rightarrow$ S) and vector control (pcDNA) and wound closure was monitored at 24 hours time point. **D**) TPC-1 cells transfected with AGR2, AGR2 (C $\rightarrow$ S) or the empty vector (pcDNA), were seeded in the upper chamber of

transwells and incubated for 24 hours; the upper surface of the filter was wiped clean and cells on the lower surface were stained and counted.

## **Attached Manuscript # IV**

Marcello Mancini, Adelaide Greco,  
Giuliana Salvatore, Raffaele Liuzzi,  
**Gennaro Di Maro**, Emilia Vergara,  
Gennaro Chiappetta, Rosa Pasquinelli,  
Arturo Brunetti, Marco Salvatore.

Ultrasound imaging of thyroid tumor  
angiogenesis with microbubbles targeted to  
vascular endothelial growth factor receptor  
type 2 in mice.

Manuscript in preparation

**ULTRASOUND IMAGING OF THYROID TUMOR ANGIOGENESIS WITH MICROBUBBLES  
TARGETED TO VASCULAR ENDOTHELIAL GROWTH FACTOR RECEPTOR TYPE 2 IN  
MICE**

**Abbreviated title ULTRASOUND IMAGING OF THYROID TUMOR ANGIOGENESIS**

Marcello Mancini MD <sup>1,2</sup>, Adelaide Greco PhD <sup>3,5</sup>, Giuliana Salvatore<sup>4</sup>, MD PhD, Raffaele Liuzzi<sup>1</sup> PhD,  
Gennaro Di Maro PhD <sup>6</sup>, Emilia Vergara MD <sup>3</sup>, Gennaro Chiappetta PhD <sup>7</sup>, Rosa Pasquinelli PhD <sup>7</sup>, Arturo  
Brunetti MD <sup>3,5</sup>, Marco Salvatore MD <sup>3</sup>

<sup>1</sup>Institute of Biostructure and Bioimaging, Italian National Research Council (CNR), Naples, Italy

<sup>2</sup>SDN Foundation IRCCS, Naples, Italy. <sup>3</sup>Department of Scienze Biomediche Avanzate. Università degli Studi di Napoli “Federico II”, 80131 Naples, Italy. <sup>4</sup>Dipartimento di Studi delle Istituzioni e dei Sistemi Territoriali, Università degli Studi di Napoli “Parthenope”, Naples, Italy. <sup>5</sup>CEINGE-Biotecnologie Avanzate s.c.a.r.l., Naples, Italy. <sup>6</sup> Dipartimento di Biologia e Patologia Cellulare e Molecolare, Università degli Studi di Napoli “Federico II”, 80131 Naples, Italy. <sup>7</sup>Functional Genomic Unit, Istituto Nazionale Tumori G.Pascale, Naples, Italy

Original article

Word count: text 3120

**Corresponding author:**

**Marcello Mancini.**  
**institute of Biostructure and Bioimaging, Italian National Research Council (CNR)**  
**Via T De Amicis 95 – 80145 Naples, Italy.**  
**Ph: +39 0812203187 Ext. 211; Fax +39 0812296117;**  
**e-mail: [marcello.mancini58@gmail.com](mailto:marcello.mancini58@gmail.com)**

**Key words: Thyroid, transgenic, high resolution ultrasound, cancer, contrast agent**

**Acknowledgements**

We thank Massimo Santoro for the TG-TRK-T1 mice.

**Disclosure Summary: The authors have nothing to disclose**

This study was supported by:

MIUR FIRB Prot. RBNE08E8CZ MERIT program.

Associazione Italiana per la Ricerca sul Cancro (AIRC).

## ABSTRACT

To evaluate whether Contrast Enhanced Ultrasound (CEUS) with microbubbles (MBs) targeted to VEGFR-2 is able to characterize *in vivo* the VEGFR-2 expression in the tumor vasculature of a mouse model of thyroid cancer (Tg-TRK-T1).

Animal protocol was approved by Institutional committee on Laboratory Animal Care. Contrast-enhanced ultrasound imaging with MBs targeted with an anti-VEGFR-2 monoclonal antibody ( $UCA_{VEGFR-2}$ ) and isotype control antibody ( $UCA_{IgG}$ ) was performed in 7 mice with thyroid carcinoma, 5 mice with hyperplasia or benign thyroid nodules and 4 mice with normal thyroid. After ultrasonography, the tumor samples were harvested for histological examination and VEGFR-2 expression was tested by immunohistochemistry.

The Video intensity difference ( $VI_D$ ) caused by backscatter of the retained  $UCA_{VEGFR-2}$  was significantly higher in mice harboring thyroid tumors compared to mice with normal thyroids ( $P < 0.01$ ) and to mice harboring benign nodules ( $P < 0.01$ ). No statistically significant differences of  $VI_D$  were observed in the group of mice carrying benign nodules compared to mice with normal thyroids. Moreover in thyroid tumors  $VI_D$  of retained VEGFR-2-targeted UCA was significantly higher than that of control  $UCA_{IgG}$  ( $p < 0.05$ ).

Results of immunohistochemical analysis confirmed VEGFR-2 overexpression. The magnitude of the molecular ultrasonographic signal from a VEGFR-2-targeted UCA retained by tissue correlates with VEGFR-2 expression determined by immunohistochemistry ( $\rho = 0.793$ ,  $P = 0.0003$ ).

We demonstrated that CEUS with  $UCA_{VEGFR-2}$  might be used for *in vivo* non invasive detection and quantification of VEGFR-2 expression in thyroid cancer in mice, and to differentiate benign from malignant thyroid nodules.

## INTRODUCTION

Angiogenesis is a critical determinant of tumor growth and invasion (1,2) and successful application of novel therapies that target tumor vasculature will require selection of susceptible tumors and precise evaluation of early treatment response. Vascular endothelial growth factor and its main receptor vascular endothelial growth factor receptor 2 (VEGFR-2), are overexpressed on tumor vascular endothelial cells and have been identified as targets for antiangiogenic drugs (3-6).

Endocrine glands are well vascularised and the structure of their vessels (fenestration of epithelium) facilitates the exchange of various substances, including hormones (7). The amount of VEGFR-2 in the thyroid gland is greater in the parenchymal and nodular goiter compared to healthy subjects (8). In patients with Graves' s disease (9-10), the constant stimulation of thyroid tissue by TSH receptor (TRAb), not only increased the production of thyroid hormones, but also enhanced angiogenesis, leading to an increase in thyroid vascularity (7).

Papillary thyroid carcinoma (PTC) is the most common malignancy of the thyroid gland. At the molecular level PTC is characterized by genetic alterations of components of the mitogen-activated protein kinase (MAPK) pathway (11). These include structural chromosome rearrangements affecting NTRK1 (TRK-T1) tyrosine kinase receptor that undergo in-frame recombination with various partner genes (12). Specifically, the TRK-T1 oncogene results from a paracentric inversion of chromosome 1q25 that fuses the 5' end of the TPR (Translocated Promoter Region) to the 3' end of NTRK1 genes generating the constitutively active and oncogenic kinase NTRK1 (12). Transgenic mice featuring the thyroid-specific expression of TRK-T1 under the transcriptional control of the thyroid-specific bovine thyroglobulin (Tg) promoter were generated previously (13). Twenty-three % of TRK-T1 mice of age  $\leq 7$  months and 78% of mice  $> 7$  months developed thyroid nodules characterized by malignant features, such as the proliferation of follicular epithelial cells containing scant cytoplasm, mitotic figures and papillae with fibrovascular stalks (13,14).

In papillary thyroid carcinoma, increased VEGFR-2 expression correlates with an increased cancer cell proliferation assessed by Ki-67 index, with increased thyroid tumor size (15-16) and with poor prognosis (16-19). The thyroid cancer cells of primary tumors taken from patients with metastases had an higher VEGFR-2 expression compared to cells taken from primary tumors of patients without metastases (15-16).

These observations have been suggested to be clinically useful in identifying patients who are more prone to develop metastases.

Recently, tumor angiogenesis imaging *in vivo* has been noninvasively explored using contrast enhanced ultrasound (CEUS) with microbubbles (MBs) targeted to  $\alpha_v\beta_3$  integrin, endoglin, and VEGFR2 (20-24). This technique is rapidly emerging as a noninvasive and quantitative molecular imaging modality that combines the advantages of high spatial resolution, real-time imaging, and lack of ionizing radiation and may be particularly advantageous in clinical oncology because VEGFR-2 has been implicated as marker of metastatic potential and poor prognosis in certain tumors (25-27).

Microbubbles are gas-filled echogenic US contrast agents that can be targeted to specific molecular markers by means of the attachment of appropriate ligands to the surface of the MBs. A specific characteristic of MBs is their relatively large size, which prevents them from leaking into the extravascular space. This property can be exploited for imaging by targeting the MBs to disease processes reflected on the vascular endothelial cells lining the luminal surface of capillaries and vessels, such as inflammation and angiogenesis. When these functionalized MBs are injected intravenously, they distribute throughout the whole body and attach at tissue sites expressing the targeted molecular marker, leading to a local increase of the US imaging signal. This approach allows the exclusive visualization of molecular markers of angiogenesis expressed on tumor vascular endothelial cells, have a potential clinical translation in future and should improve the ability to detect, diagnose stage, select appropriate treatments, and determine prognosis in patients with thyroid pathologies.

To our knowledge, no study has addressed the potential of targeted CEUS imaging for assessment of thyroid tumor angiogenesis *in vivo* by using MBs targeted to VEGFR-2.

This study aimed to investigate whether targeted CEUS allows noninvasive assessment of VEGFR-2 expression on tumor vascular endothelium in Tg-TRK-T1 mice, a murine model of thyroid cancer. We also investigated whether the evaluation of expression levels of VEGFR2 *in vivo* can differentiate benign from malignant nodules of the thyroid.

## **MATERIALS AND METHODS**

### ***Animal Model***

Animal studies were performed in accordance with National Institutes of Health (NIH) recommendations and Animal Research Advisory Committee (ARAC) procedure (27) and the approval of the Italian Institutional animal research committee (Institutional Animal and Care Committee of the University of Naples “Federico II” and the Italian Ministry of Health). All animal procedures in this study were conducted by a veterinarian and conformed to all regulations protecting animals used for research purposes, including national guidelines (D.L. 27 Gennaio 1992, 116 Suppl. G.U 40 18 Febbraio 1992. Direttiva CEE n.609/86) as well as the protocols recommended by Workamn et al. (28).

Tg-TRK-T1 transgenic mice have been previously described (13). From 2010 to 2011, thyroid Ultrasound was performed in 16 Tg-TRK-T1 transgenic mice model of thyroid carcinogenesis (26). Body weight range of animals was 29-32 gr, equally distributed among male (n=9) and female (n=7). Mice were examined every six months and were sacrificed immediately after the last ultrasound scanning. At the time of the necroscopy, the age range of mice was 12-15 months.

### **High frequency ultrasound with targeted contrast enhanced imaging**

A Vevo 770 microimaging system (Visualsonics, Toronto, Ontario, Canada) with a single element probe, center frequency of 40-MHz was used for all the examinations. The transducer has an active face of 3 mm, a lateral resolution of 68.2  $\mu\text{m}$ , axial resolution of 38.5  $\mu\text{m}$ , focal length of 6 mm, mechanical index 0.14, transmit power 50%, and a dynamic range 52 dB (29-30). Precise and repeatable control over the position of the two-dimensional image plane was obtained with a rail system (Vevo Integrated Rail System II; Visualsonics). Mice were anesthetized using 1.5–2% isoflurane vaporized in oxygen (2Lt/min) on a heated stage, with constant monitoring of their body temperature, using physiological monitoring platform (31). Hairs were removed from the area of interest (neck and the high thorax) with a depilatory cream to obtain a direct contact of the ultrasound gel to the skin of the animal minimizing ultrasound attenuation. A prewarmed gel was used to provide a coupling medium for the transducer. Real-time imaging was performed as previously described (32). The transducer focal zone was placed at the center of the thyroid gland and nodules, when they were present. All nodules were measured in three planes, and images were recorded to document nodule location and orientation. Each examination lasted for about 30 min. All ultrasonographic

assessments were performed by the same trained sonographer (A.G.) that was not aware of the tumor type and of type of MBs administered to mice.

#### *Contrast-enhanced Agent Preparation and Injection*

The Ultrasound Contrast Agent (UCA) MicroMarker (VisualSonics, Inc, Toronto, Ontario, Canada), specifically designed for high frequency ultrasonography, was prepared and targeted according to manufacturer guidelines. These MBs have a mean diameter of 1.5  $\mu\text{m}$  (range, 1–2  $\mu\text{m}$ ) and contain approximately 7600 molecules of streptavidin per square micrometer chemically attached to the phospholipid shell of the MBs via a polyethylene glycol spacer. (22). The contrast agent preparation protocol was designed to achieve optimal saturation of the microbubble surface with a maximal amount of antibodies while minimizing the amount of free non conjugated antibodies in the solution. A vial of the dry UCA containing  $9.2 \times 10^8$  dry streptavidin-coated MBs was re-suspended in 1.2 mL of sterile saline. Then, either 30  $\mu\text{g}$  of biotinylated anti-mouse VEGFR-2 antibodies (clone Avas12a1; eBioscience, San Diego,) or a biotinylated immunoglobulin G (IgG) isotype control (eBioscience, Inc, San Diego, CA) were added per vial of contrast agent to produce either a VEGFR-2-targeted ( $UCA_{\text{VEGFR-2}}$ ) and a control UCA ( $UCA_{\text{IgG}}$ ) by using biotin-streptavidin interactions, resulting in approximately 6000 ligands per square micrometer of surface area (22). All mice were injected with two boluses of both the  $UCA_{\text{VEGFR-2}}$  and  $UCA_{\text{IgG}}$  via a tail vein (injection time, 2 seconds). Each bolus containing  $3.8 \times 10^7$  MBs in 0.02 mL of saline and was followed by a 0.02 mL saline flush.

To allow MBs to clear from previous injections, we waited at least 30 minutes between different bolus injections.

#### *Image Acquisition and Quantification*

The system was set at 50% transmit power, resulting in a mechanical index of 0.14 (manufacturer specification). Images were acquired at a 20-Hz frame rate. The data were log compressed and digitized to 12 bits. Data were further compressed to 8 bits for screen display. The ultrasound probe was positioned so that the central portion of the thyroid nodule was contained within the focal zone of the ultrasound transducer. The probe position, gain settings, and midfield focus were initially optimized and maintained throughout each experiment. The goal of the ultrasonographic image acquisition and analysis protocol (Figure 1) was to differentiate the backscattered acoustic signal due to MBs retained by the tumor from the

background signal of the tumor itself and MBs still freely circulating in the bloodstream. CEUS imaging was paused for 4 minutes after injection. This time allowed binding and retention of targeted MBs while awaiting wash-out of the unbound contrast agent.

After the 4-minute waiting period, approximately 300 ultrasonographic frames of the tumor were acquired at a temporal resolution of 10 seconds. A high-power ultrasound destruction sequence was then applied (20 cycles with a frequency of 10 MHz and a mechanical index of 0.59). After the destruction pulse, the system was reset with identical imaging parameters as before the destruction event, and another set of images ( $\approx 300$  frames) was acquired. Image processing and quantification were performed with the software implemented in the ultrasound scanner. Image processing used in the Vevo770 system relies on 2 sets of images: a predestruction set and a postdestruction data set. The received log compressed signals were expressed in an arbitrary scale unit called Video Intensity (VI). The average VI of predestruction and postdestruction (background) sonograms was measured in a region of interest encompassing the centre of examined tumor. The difference in VI between predestruction and postdestruction ultrasonographic frames was calculated and expressed as VI difference ( $VI_D$ ) that provided a relative measure of the amount of the UCA retained by the tumor and was considered to represent MBs adherent to molecular endothelial markers.

### ***Histology and Immunohistochemistry***

After CEUS imaging, mice were euthanized and thyroids were immediately fixed in buffered formalin for 4 h. Tissues underwent automated processing and paraffin embedding; 5 $\mu$ m sections were cut and hematoxylin and eosin stained for microscopic analysis. Thyroid tissues were classified according to the World Health Organization criteria for the evaluation of mouse thyroid tumors (33). Briefly, thyroid was considered as normal when composed by variable-sized follicles covered by flattened monolayered epithelial cells. Hyperplastic thyroid was defined by the occurrence of small follicles with scant colloid and tall epithelial cells merging with normal areas. Follicular adenoma was defined as a well demarcated nodule with a distinct papillary and/or follicular architecture. Malignant lesions were defined based on the invasion of the surrounding glandular parenchyma and stroma.

To confirm expression of VEGFR-2, immunohistochemistry analysis of tumor sections was performed. Formalin-fixed and paraffin-embedded 3–5  $\mu$ m sections were deparaffinized, placed in a solution of absolute methanol and 0.3% hydrogen peroxide for 30 min, and treated with blocking serum for 20 min. After

blocking, slides were incubated with a mouse monoclonal anti-VEGFR-2 antibody (dilution 1:200) in a moist chamber at 4 C and processed according to standard procedures. Negative controls by omitting the primary antibody were included. Cases were scored as positive when unequivocal brown staining was observed. Immunoreactivity was expressed as the average percentage of positively stained target cells [(-): no staining (< 5% positive cells); (+): low/weak ( $\geq 5\%$  -  $\leq 25\%$  positive cells); (++) : medium/moderate ( $> 25\%$  -  $< 50\%$  positive cells); (+++): high/ strong ( $\geq 50\%$  positive cells)]. Score values were independently assigned by two blinded investigators (G. C. and R.P.) and a consensus was reached on all scores used for computation. All histological and immunohistochemistry studies were performed and interpreted by pathologists, who did not know the diagnosis determined by ultrasonography.

### ***Statistical analysis***

Data were reported as median and range. Paired non parametric Wilcoxon's test was used to compare data from different  $VI_D$  ( $UCA_{IGg}$   $UCA_{VEGFR-2}$ ). ANOVA of Kruskal-Wallis was used to compare the contrast measurements of the three groups. *Post hoc* analysis was performed using the Dunn test. The correlation between the contrast signal and the VEGFR-2 expression was assessed by the Spearman coefficient. A  $P < 0.05$  was considered statistically significant. All statistical analysis were performed with MedCalc 12.0 statistical software.

## RESULTS

Examination of the thyroid gland was performed by CEUS with  $UCA_{VEGFR-2}$  and  $UCA_{IgG}$ . The UCA administration showed no notable toxicity, and all animals recovered after US imaging without any detectable signs of distress.

At the ultrasound evaluation in 16 mice examined: in 4 the thyroid showed normal size and homogeneous echotexture of parenchyma, without nodules, and therefore classified as normal, 2 mice showed features of benign diffuse hyperplasia and 10 mice had a nodular process.

At the histological examination 4 normal thyroids, 2 hyperplasias, 3 adenomas, 7 papillary thyroid carcinoma were found, confirming Ultrasound diagnosis. The benign thyroid nodules measured 0.11–0.27 mm (median 0.17 mm) while the tumors measured 0.16–5.51 mm (median 0.54 mm).

For thyroid tumors the  $VI_D$  was significantly higher when using  $UCA_{VEGFR-2}$  compared with  $UCA_{IgG}$  whereas for normal thyroids or in mice harboring benign thyroid nodules the  $VI_D$  for  $UCA_{VEGFR-2}$  was equal to the  $VI_D$  for  $UCA_{IgG}$  (Table 1 and Fig. 2). Median range  $VI_D$   $UCA_{VEGFR-2}$  thyroid tumors, 30.1 (range 25.1-35.6) versus  $VI_D$   $UCA_{IgG}$  19.4 (range 11.4-22.6) ( $P < 0.01$ ).

Benign nodules  $VI_D$   $UCA_{VEGFR-2}$  13.3 (range 10.8-15.8) versus  $VI_D$   $UCA_{IgG}$  11.82 (range 8.5-19.6) ( $P = n.s$ ).

Normal thyroids  $VI_D$   $UCA_{VEGFR-2}$  10.9 (range 10.3-14.9) versus  $VI_D$  in  $UCA_{IgG}$  11.3 (9.4-14.7); ( $P = n.s$ )

(Table 1). These values were used as relative measures of the VEGFR-2 over-expression within tumor

vasculature and the  $UCA_{IgG}$  served as a control for demonstration of the specificity of  $UCA_{VEGFR-2}$  retention.

The median difference between  $VI_D$   $UCA_{IgG}$  and  $VI_D$  of  $UCA_{VEGFR-2}$  was considered as a measure of VEGFR-2 specific binding, was 11.6 (range 9.6-19.2) VI units for thyroid carcinoma significantly higher ( $p = 0.0037$ )

than for normal thyroid (median 0.3, range -1.57-1.32) and hyperplasia/benign nodules (median 2.3 range -3.8-3.0).

Figure 2 shows representative VI curves of a thyroid malignant nodule, normal thyroid and benign nodule

imaged with the  $UCA_{VEGFR-2}$  and  $UCA_{IgG}$ . There was a moderately intense signal from the  $UCA_{VEGFR-2}$

retained by the tumor (Fig.2F). The corresponding images for the  $UCA_{IgG}$  showed no retention of MBs in the

tumor (Fig.2C). The  $UCA_{VEGFR-2}$  in the vascular bed of benign nodules and normal thyroids showed very low retention in  $UCA_{VEGFR-2}$  (Fig 2 D-E).

After CEUS imaging, mice were subjected to general anesthesia and then euthanized.

In the group of examined animals the greatest  $UCA_{VEGFR-2}$  Video Intensity for normal or benign thyroid nodules was 15.8 units while the lowest  $UCA_{VEGFR-2}$  Video Intensity for carcinomas was 25.1 units.

Therefore, we propose a cut-off value of 20 VI units to discriminate normal or benign nodules from malignant thyroid, that may be verified using a larger number of subjects.

To confirm expression of VEGFR-2, immunohistochemistry analysis of tumor sections was performed. The strength of the ultrasound signal from the  $UCA_{VEGFR-2}$  was significantly correlated with the level of actual VEGFR-2 expression ( $\rho$  0.793,  $P=0.0003$ ).

## DISCUSSION

In this study we have evaluated the expression levels of a well-described tumor angiogenic marker i.e. VEGFR-2 in a mouse model of thyroid tumor (Tg-TRK-T1) compared with normal or benign tumors and whether targeted CEUS allows assessment of this marker noninvasively. The *in vivo* binding of the VEGFR-2 targeted UCA in thyroid tumors was substantially higher compared with control UCA. This difference in retention affirmed the specificity of a VEGFR-2- conjugated UCA for endothelial targeting.

Vascular endothelial growth factor receptor 2 (VEGFR-2) is one of the best-characterized molecular marker of tumor angiogenesis (34-37). It is overexpressed on tumor vascular endothelial cells in several solid tumors, including breast (38,39), ovarian (40-41), pancreatic (42) and thyroid cancer (19) and it is considered an important factor in tumor angiogenesis. VEGFR-2 is an endothelium-specific receptor tyrosine kinase that is activated by VEGF A. Activation of the VEGF/VEGFR-2 pathway triggers multiple signaling networks that result in endothelial cell survival, mitogenesis, migration, differentiation, and vascular permeability (43). Insights into the expression levels of tumor angiogenic markers during the progression of cancer, could be of great importance in developing novel molecular imaging strategies aimed at visualization of tumor angiogenesis markers that are overexpressed in particular in early stage cancer for screening purposes.

The *in vivo* US imaging signals of the injected targeted UCA was correlated with results from immunochemistry analysis of VEGFR-2 expression and this positive correlation suggested that targeted contrast-enhanced US imaging could be used to monitor expression levels of angiogenic markers noninvasively. Thus retention of a VEGFR-2-targeted UCA is a more specific as *in vivo* marker for the level of VEGFR-2 expression than for the quantification of tumor vascularity.

The ability to visualize and quantify tumor angiogenesis may allow screening and detecting cancer at an early stage and antiangiogenic treatment monitoring in patients (34).

Targeted-CEUS is a promising non invasive molecular imaging approach that allows *in vivo* assessment of molecular markers of tumor angiogenesis (44-46). The number of attached MBs depends on various factors, including the extent of tumor vascularization, physical forces that translate the freely circulating contrast MBs to the vessel wall, and the affinity of the binding ligand to the molecular targets, as well as the expression level of the molecular targets on tumor vessels (47-50).

Our study has several limitations. Molecular imaging of VEGFR-2 expression was performed in developed tumors (0.16–5.51 mm in diameter) in which it is very likely that the receptor is expressed at more. Thus, the usefulness and accuracy of VEGFR-2-targeted UCA imaging at earlier stages of tumor development needs to be evaluated.

A 2-dimensional image acquisition method was used, and it is very difficult to know whether ultrasound scans perfectly correspond with the region subjected to histological examination. Studies carried out in 3D mode could ensure greater correspondence between quantitative ultrasonographic assessment of VEGFR-2 expression and results of immunochemical analysis.

The small animal Vevo770 US system for dedicated small-animal imaging used in our study for MBs detection operates on received signals that undergo log-compression prior to image display. Log-compressed gray scale image values referred as “Video Intensity” can produce inaccurate estimation of perfusion user and instrument-dependent.

In conclusion the results of our study suggests that targeted CEUS imaging allows a non-invasive assessment of VEGFR-2 expression levels in thyroid *in vivo*. The results provide further insights into the biology of angiogenesis in thyroid tumors and may help in defining promising imaging targets for both early cancer detection and antitumor therapies.

## REFERENCES

1. Klener P. Angiogenesis as part of the tumor "ecosystem" and possibilities to influence it 2010. *Klin Onkol* 23(1):14-20
2. Pandya NM, Dhalla NS, Santani DD. Angiogenesis--a new target for future therapy 2006 *Vascul Pharmacol* 44(5):265-74
3. Sato Y. Molecular diagnosis of tumor angiogenesis and anti-angiogenic cancer therapy 2003 *Int J Clin Oncol* 8(4):200-6
4. Sitohy B, Nagy JA, Dvorak HF. Anti-VEGF/VEGFR therapy for cancer: reassessing the target 2012 *Cancer Res* 72(8):1909-14
5. Kojic KL, Kojic SL, Wiseman SM. Differentiated thyroid cancers: a comprehensive review of novel targeted therapies 2012 *Expert Rev Anticancer Ther* 12(3):345-57
6. Bertolini F, Marighetti P, Martin-Padura I, Mancuso P, Hu-Lowe DD, Shaked Y, D'Onofrio A 2011 Anti-VEGF and beyond: shaping a new generation of anti-angiogenic therapies for cancer. *Drug Discov Today* 16(23-24):1052-60
7. Turner HE, Harris AL, Melmed S, Wass JA. Angiogenesis in endocrine tumors 2003 *Endocr Rev.* 24(5):600-3
8. Sato K, Miyakawa M, Onoda N, Demura H, Yamashita T, Miura M, Kasajima T, Yamazaki K & Obara T Increased concentration of vascular endothelial growth factor/vascular factor in cyst fluid of enlarging and recurrent thyroid nodules 1997 *Journal of Clinical Endocrinology and Metabolism* 82: 1968–1973
9. Ramsden JD, Buchanan MA, Egginton S, Watkinson JC, Mautner V, Eggo MC. Complete inhibition of goiter in mice requires combined gene therapy modification of angiopoietin, vascular endothelial growth factor, and fibroblast growth factor signaling 2005 *Endocrinology* 146(7):2895-902
10. Nagura S, Katoh R, Miyagi E, Shibuya M, Kawaoi A 2001 Expression of vascular endothelial growth factor (VEGF) and VEGF receptor-1 (Flt-1) in Graves disease possibly correlated with increased vascular density. *Hum Pathol* 32(1):10-7

11. Nikiforov YE, Nikiforova MN 2011 Molecular genetics and diagnosis of thyroid cancer. *Nat Rev Endocrinol* 7(10):569-80
12. Greco A, Miranda C & Pierotti MA 2010 Rearrangements of NTRK1 gene in papillary thyroid carcinoma. *Molecular and cellular endocrinology* 321:44-49.
13. Russell JP, Powell DJ, Cunnane M, Greco A, Portella G, Santoro M, Fusco A, Rothstein JL 2000 The TRK-T1 fusion protein induces neoplastic transformation of thyroid epithelium. *Oncogene* 19:5729–5735
14. Kim CS & Zhu X 2009 Lessons from mouse models of thyroid cancer. *Thyroid* 19:1317- 1331.
15. Klein M, Catargi B 2007 VEGF in physiological process and thyroid disease. *Ann Endocrinol* 68(6):438-48
16. Góth MI, Hubina E, Raptis S, Nagy GM, Tóth BE 2003 Physiological and pathological angiogenesis in the endocrine system. *Microsc Res Tech* 60(1):98-106.
17. Salajegheh A, Smith RA, Kasem K, Gopalan V, Nassiri MR, William R, Lam AK 2011 Single nucleotide polymorphisms and mRNA expression of VEGF-A in papillary thyroid carcinoma: potential markers for aggressive phenotypes *Eur J Surg Oncol* 37(1):93-9
18. Turner HE, Nagy Z, Gatter KC, Esiri MM, Harris AL, Wass JA 2000 Angiogenesis in pituitary adenomas and the normal pituitary gland. *J Clin Endocrinol Metab* 85(3):1159-62
19. Risau W. Angiogenic growth factors 1990 *Prog Growth Factor Res* 2(1):71-9
20. Ellegala DB, Leong-Poi H, Carpenter JE, et al. 2003 Imaging tumor angiogenesis with contrast ultrasound and microbubbles targeted to alpha(v)beta3 *Circulation* 108:336–341.
21. Korpanty G, Carbon JG, Grayburn PA, Fleming JB, Brekken RA 2007 Monitoring response to anticancer therapy by targeting microbubbles to tumor vasculature *Clin Cancer Res* 13:323–330.
22. Willmann JK, Paulmurugan R, Chen K, Gheysens O, Rodriguez-Porcel M, Lutz AM, Chen IY, Chen X, Gambhir SS 2008 US Imaging of Tumor Angiogenesis with Microbubbles Targeted to Vascular Endothelial Growth Factor Receptor Type 2 in Mice. *Radiology* 2:508-518

23. Lee DJ, Lyshchik A, Huamani J, Hallahan DE, Fleischer AC 2008 Relationship between retention of a vascular endothelial growth factor receptor 2 (VEGFR2)-targeted ultrasonographic contrast agent and the level of VEGFR2 expression in an in vivo breast cancer model. *J Ultrasound Med* 27(6):855–866.
24. Delorme S, Krix M 2006. Contrast-enhanced ultrasound for examining tumor biology. *Cancer Imaging* 6:148–152
25. Klasa-Mazurkiewicz D, Jarzab M, Milczek T, Lipińska B, Emerich J 2011 Clinical significance of VEGFR-2 and VEGFR-3 expression in ovarian cancer patients *Pol J Pathol* 62(1):31-40
26. Büchler P, Reber HA, Büchler MW, Friess H, Hines OJ 2002 VEGF-RII influences the prognosis of pancreatic cancer. *Ann Surg* 236(6):738-49.
27. <http://oacu.od.nih.gov/ARAC/index.htm>
28. P Workman, EO Aboagye, F Balkwill, A Balmain, G Bruder, DJ Chaplin, JA Double, J Everitt, DAH Farningham, MJ Glennie, LR Kelland, V Robinson, IJ Stratford, GM Tozer, S Watson, SR Wedge, SA Eccles 2010 An ad hoc committee of the National Cancer Research Institute. Guidelines for the welfare and use of animals in cancer research. *British Journal of Cancer* 102: 1555–1577
29. Zhou YQ, Foster FS, Qu DW, Zhang M, Harasiewicz KA, Adamson SL 2002 Applications for multifrequency ultrasound biomicroscopy in mice from implantation to adulthood *Physiol Genomics*. 10(2):113-26
30. Adelaide Greco A, Mancini M, Gargiulo S, Gramanzini M, Claudio PP, Brunetti A, Salvatore M 2012 Ultrasound Biomicroscopy in small animal research: applications in molecular and pre-clinical imaging *Journal of Biomedicine and Biotechnology* Article ID 519238, 14 pages
31. <http://www.adelaide.edu.au/ANZCCART/publications>
32. Mancini M, Vergara E, Salvatore G, Greco A, Troncone G, Affuso A, Liuzzi R, Salerno P, Scotto di Santolo M, Santoro M, Brunetti A, Salvatore M 2009 Morphological ultrasound micro-imaging of thyroid in living mice *Endocrinology* 150(10):4810-5
33. Jokinen MP, Botts S 1994 WHO International Agency for Research on Cancer. In: Turusob VS, Mohr U, eds. *Pathology of tumours in laboratory animals: tumours of the mouse*. 2nd ed. Vol 2. Lyon, France: IARC Scientific Publication 565–594.

34. Palmowski M, Huppert J, Ladewig G, Hauff P, Reinhardt M, Mueller MM, Woenne EC, Jenne JW, Maurer M, Kauffmann GW, Semmler W, Kiessling F 2008 Molecular profiling of angiogenesis with targeted ultrasound imaging: early assessment of antiangiogenic therapy effects. *Mol Cancer Ther* 7(1):101-9
35. Hodivala-Dilke K. alphavbeta3 integrin and angiogenesis: a moody integrin in a changing environment 2008 *Curr Opin Cell Biol* 20(5):514-9
36. Ferrara N 2004 Vascular endothelial growth factor: basic science and clinical progress. *Endocr Rev* 25(4):581-611
37. ten Dijke P, Goumans MJ, Pardali E 2008 Endoglin in angiogenesis and vascular diseases. *Angiogenesis* 11(1):79-89
38. Sledge GW Jr, Rugo HS, Burstein HJ 2006 The role of angiogenesis inhibition in the treatment of breast cancer. *Clin Adv Hematol Oncol* 4(10 Suppl 21):1-10
39. Khosravi Shahi P, Soria Lovelle A, Pérez Manga G 2009 Tumoral angiogenesis and breast cancer. *Clin Transl Oncol* 11(3):138-42
40. Gómez-Raposo C, Mendiola M, Barriuso J, Casado E, Hardisson D, Redondo A 2009 Angiogenesis and ovarian cancer. *Clin Transl Oncol* 11(9):564-71
41. Bednarek W, Mazurek M, Cwiklińska A, Barczyński B 2009 Expression of selected angiogenesis markers and modulators in pre-, peri- and postmenopausal women with ovarian cancer *Ginekol Pol* 80(2):93-8
42. Saif MW 2006 Primary pancreatic lymphomas. *JOP* 7(3):262-73
43. Hicklin DJ, Ellis LM 2005 Role of the vascular endothelial growth factor pathway in tumor growth and angiogenesis. *J Clin Oncol* 23(5):1011-27
44. Lindner JR 2004 Microbubbles in medical imaging: current applications and future directions. *Nat Rev Drug Discov* 3(6):527-32
45. Willmann JK, van Bruggen N, Dinkelborg LM, Gambhir SS 2008 Molecular imaging in drug development. *Nat Rev Drug Discov* 7(7):591-607

46. Pysz MA, Foygel K, Rosenberg J, Gambhir SS, Schneider M, Willmann JK 2010 Antiangiogenic cancer therapy: monitoring with molecular US and a clinically translatable contrast agent (BR55). *Radiology* 256(2):519-27
47. Willmann JK, Kimura RH, Deshpande N, Lutz AM, Cochran JR, Gambhir SS 2010 Targeted contrast-enhanced ultrasound imaging of tumor angiogenesis with contrast microbubbles conjugated to integrin-binding knottin peptides. *J Nucl Med* 51(3):433-40
48. Lindner JR, Song J, Xu F, Klibanov AL, Singbartl K, Ley K, Kaul S 2000 Noninvasive ultrasound imaging of inflammation using microbubbles targeted to activated leukocytes. *Circulation* 102(22):2745-50
49. Klibanov AL, Rasche PT, Hughes MS, Wojdyla JK, Galen KP, Wible JH Jr, Brandenburger GH 2004 Detection of individual microbubbles of ultrasound contrast agents: imaging of free-floating and targeted bubbles. *Invest Radiol* 39(3):187-95.
50. Lucidarme O, Kono Y, Corbeil J, Choi SH, Golmard JL, Varner J, Mattrey RF 2006 Angiogenesis: noninvasive quantitative assessment with contrast-enhanced functional US in murine model. *Radiology* 239(3):730-9

**Table 1: Quantitative Video Intensity for Ultrasound Contrast agent targeted with isotype control antibody (UCA<sub>IgG</sub>) and anti-VEGFR2 monoclonal antibody (UCA<sub>VEGFR2</sub>)**

	Normal Thyroid (n.4)	Hyperplasia/Benign Nodules (n.5)	Thyroid Carcinoma (n.7)
Video Intensity UCA <sub>IgG</sub>			
Video Intensity Difference	11.3 (9.4-14.7)	12.2 (8.5-19.6)	19.4 (11.4-22.6)
Video Intensity UCA <sub>VEGFR2</sub>			
Video Intensity Difference	10.9 (10.3-14.9)	13.3 (10.8-15.8)	30.1 (25.1-35.6)* §

\*Statistical significant difference between Thyroid carcinoma and normal thyroid or Hyperplasia/benign nodules  $p < 0.05$

§ Statistical significant difference between UCA targeted with anti-VEGFR2 monoclonal antibody and isotype control antibody  $p = 0.0156$

### Figure captions

#### **Fig 1 Targeted US of endothelial antigens in vessels of a tumor tissue.**

Endothelial cells of vessels (red) of tumor tissues expresses specific antigens. After intravenous administration targeted microbubbles (blue) float in vessels and remaining exclusively in the vascular compartment. Many of them bind to antigens of endothelial cells, whereas others remains in the vessel lumen freely circulating. After high-power destructive pulse, all microbubbles are destroyed (bound + circulating), following circulating microbubbles, that arrives from outside of scan plane, remain freely circulating for several seconds. On the top of the figure time/video intensity curve analysis before and after high-power destructive pulse and bottom a diagram representation of destructive methodology. Contrast intensity is the sum of the intensity from tissue, intensity from microbubbles not bound to receptors (circulating microbubbles), and intensity from microbubbles bound to receptors on endothelial cells. After digital subtraction of 300 predestruction frames from 300 postdestruction frames, resulting video intensity is due only to bound microbubbles.

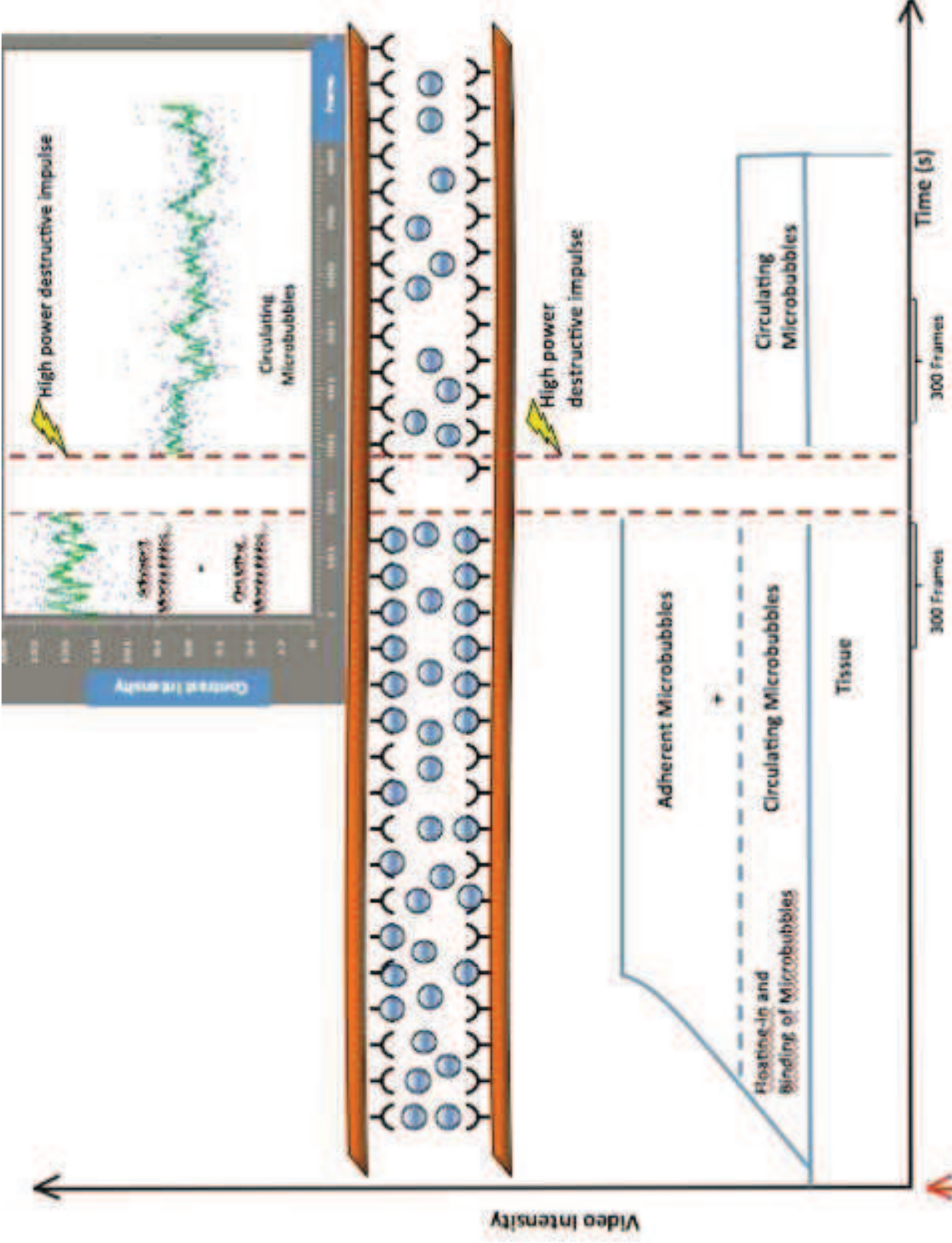
### **Fig.2 video intensities curves**

Predestruction and postdestruction video intensities curves for the control UCA (A–C) and the VEGFR2-targeted UCA (D–F). The average video intensity of predestruction and postdestruction sonograms was measured and the difference in video intensity between the predestruction and postdestruction ultrasonographic frames was calculated and expressed as video intensity difference ( $VI_D$ ). This value provided a relative measure of the amount of targeted microbubbles retained by the tumor. Video Intensities curves of a normal thyroid parenchyma (A,D), adenoma (B,E) and a thyroid tumor (C,F). These images show a significant difference between retention of the control and VEGFR2-targeted UCAs in a thyroid tumor.

**Figure 3:** Representative microphotographs of immunohistochemistry analysis of murine thyroid stained with antibodies against VEGFR type 2 receptor. Brown color indicate presence of VEGFR2  
Low grade expression of VEGFR-2 in normal thyroid (A) and in thyroid adenoma (B) and high grade expression in thyroid carcinoma (C).

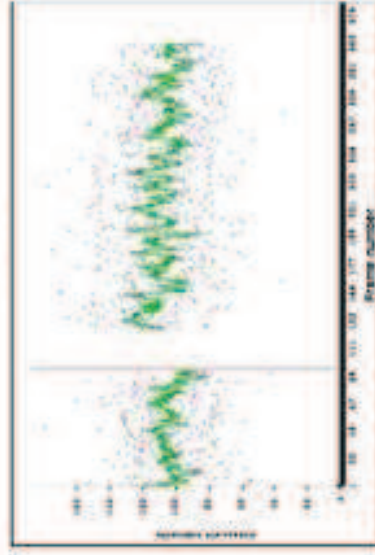
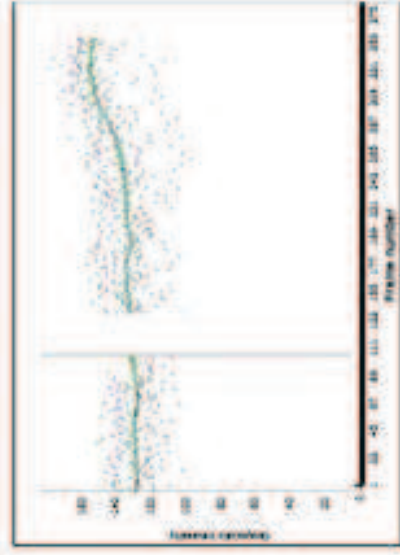
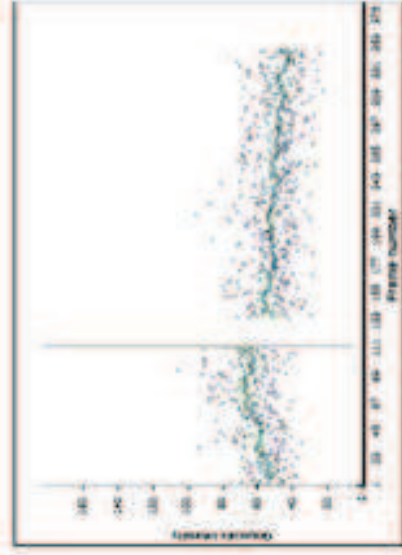
### **Fig. 4:**

Correlation between Video Intensity Difference of VEGFR-2 targeted microbubbles and expression of VEGFR-2 determined by Immunohistochemistry expressed as the average percentage of positively stained cells in normal thyroids, in hyperplasia/adenoma and in carcinomas [white dot: no staining (< 5% positive cells); orange square: low/weak ( $\geq 5\%$  -  $\leq 25\%$  positive cells); blue dot: medium/moderate ( $> 25\%$  -  $< 50\%$  positive cells); triangle: high/ strong ( $\geq 50\%$  positive cells)].

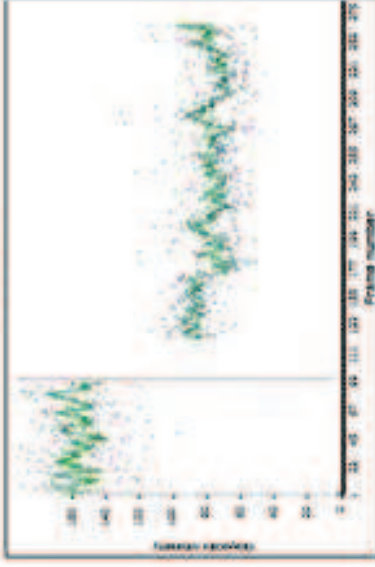
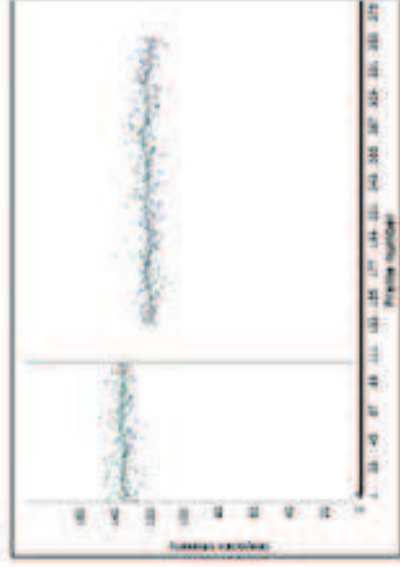
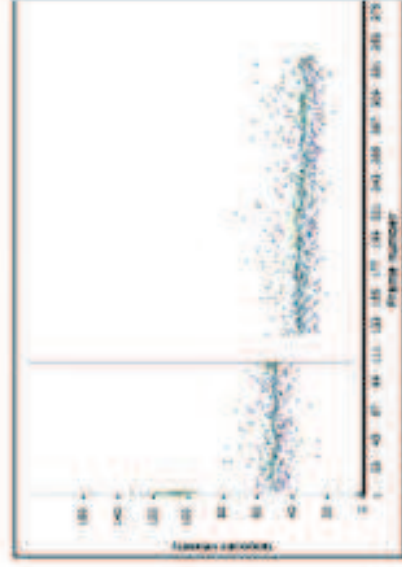


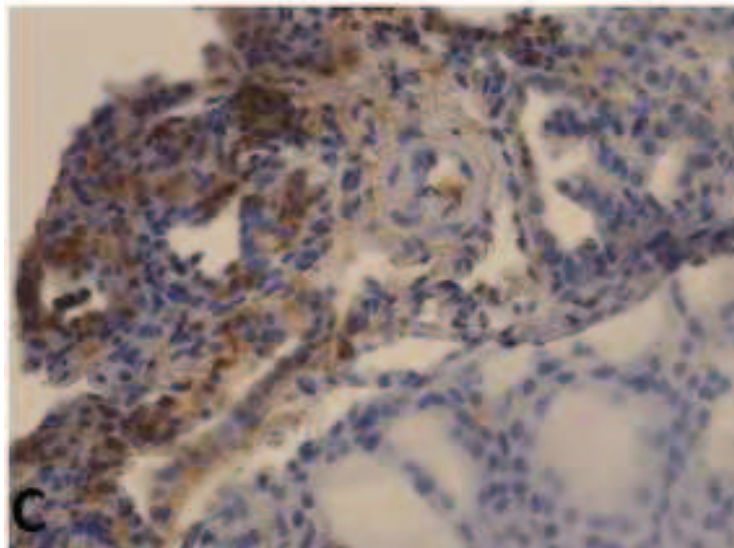
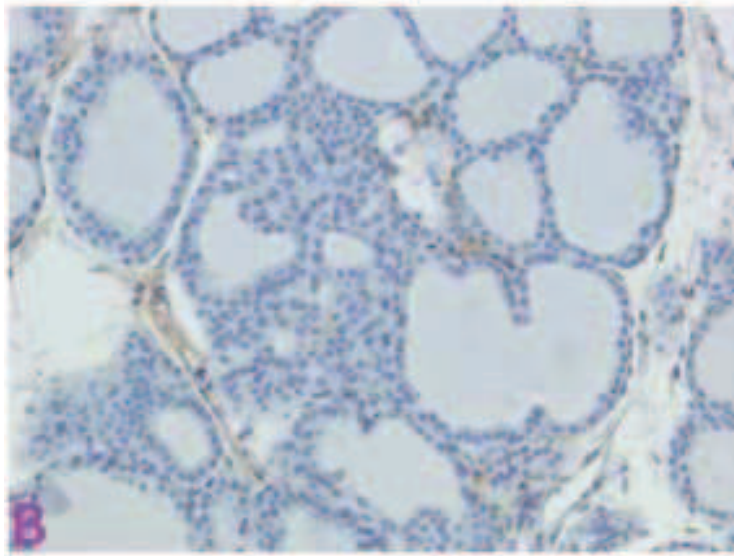
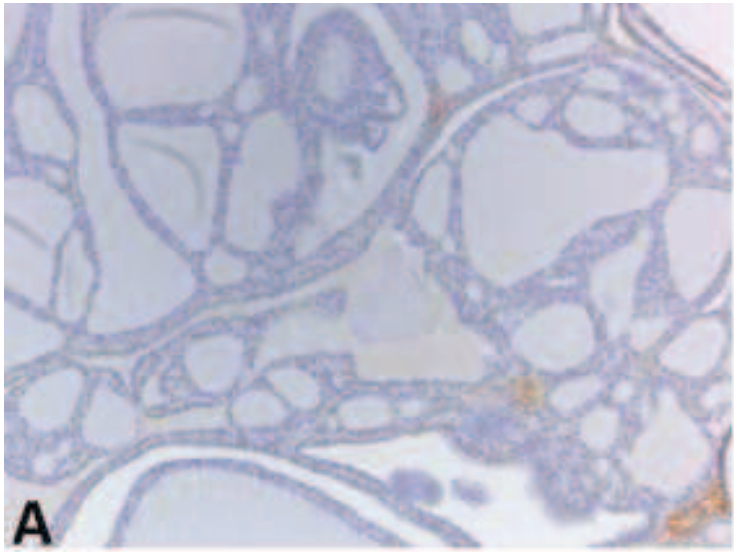
Bolus injection of Microbubbles

UCA<sub>IgG</sub>



UCA<sub>VEGFR2</sub>





Ultrasound contrast agent with microbubbles VEGFR<sub>2</sub> targeted, thyroid immunohistochemistry and VEGFR<sub>2</sub> analysis

